이학박사 학위논문

Quantitative evaluation of factors controlling groundwater contamination in Jeju Island

제주도 지역 지하수 오염에 관여하는 인자에 대한 정량적 평가 연구

2017년 8월

서울대학교 대학원

지구환경과학부

고 은 희

이학박사 학위논문

Quantitative evaluation of factors controlling groundwater contamination in Jeju Island

제주도 지역 지하수 오염에 관여하는 인자에 대한 정량적 평가 연구

2017년 8월

서울대학교 대학원

지구환경과학부

고 은 희

Abstract

Among various types of groundwater contamination, nitrate has been a major threat with regard to the deterioration of groundwater resources in many countries. The potential vulnerability of aquifers to nitrate pollution can intensify as human activities increase. Therefore, it is essential to protect water quality levels by establishing proper management plans which consider dominant factors that can be used to control the nitrate dynamics in subsurface aquifer systems.

On Jeju Island, as groundwater is the sole water resource, severe nitrate contamination of groundwater is a major concern. The island is characterized by complex hydrogeological systems and various anthropogenic activities; therefore, a systematic assessment that characterizes the complex nitrate dynamics of the island is necessary prior to the formulation of any water quality protection plan. In this study, through a combination of investigative approaches, factors controlling the nitrate dynamics are quantified in an effort to identify the mechanisms of nitrate contamination on Jeju Island.

First, the overall spatio-temporal distributions of NO_3-N concentrations along with Cl in groundwater throughout Jeju Island were identified to evaluate ongoing and continuing harmful impacts on the water quality. The determined temporal trends of these two elements were then used to assess the effects of land usage changes and groundwater management actions on groundwater quality levels. The results indicated that upward trends in NO_3-N were associated with expansions of agricultural lands,

whereas the Cl trends were considered to be affected by regulations on groundwater extraction to reduce seawater intrusion. The deterioration of the quality of groundwater by nitrate is a continuous problem on Jeju Island, especially in the western part of the island.

Based on the results of the trend analyses conducted as part of the present study, a focused study related to the continuous threat of NO_3-N as a contaminant on Jeju Island was conducted in the Gosan agricultural area in the western part of the island. This was done using a combined approach involving a numerical simulation and age-dating methods. In the Gosan study area, which contains a layered aquifer system penetrated by leaky wells, the quantification of well leakage effects was undertaken by utilizing a leaky-well module and a double-domain integration method to compute the degree of nitrate cross-contamination through the layered aquifer system. The numerical results demonstrated that the well leakage flux rapidly degraded the water quality of the underlying regional aquifer by acting as a direct pathway for nitrate-rich shallow perched groundwater. Based on predictions by the developed model with regard to decreases in the NO_3-N concentration at regional groundwater wells, the maximum allowable fertilizer amount for Gosan would be 45%–65% of the currently applied fertilizer level, whereas sealing of the regional groundwater wells would rapidly decrease the NO_3-N concentration while also mitigating the need to reduce fertilizer usage levels.

Given the complex hydrogeological features of the Gosan area, mixing of

groundwater ages is expected due to migration through various flow pathways. Therefore, three age-estimation methods were used to interpret groundwater ages (environmental tracer age dating, a lumped parameter model and a numerical model) so as to characterize the nitrate input history and determine which major pathways influence the quality of the groundwater. The results of the three age-estimation methods were compared to establish suitable groundwater management strategies. These results showed that using different age estimation methods leads to variations in the estimated contaminant loading history and, accordingly, different groundwater management strategies. The discrepancies in the age estimations produced by the different models were more prominent in the complex hydrogeological system. For this reason, it is necessary to apply multiple age estimation methods and compare the results based on an interpretation of the full age distributions.

Keywords: Groundwater; Nitrate contamination; Jeju Island; agricultural activities; Trend analysis; numerical model; leaky well; groundwater age

Student number: 2011-30113

Table of Contents

List of Figures

List of Tables

Chapter 1. Introduction

1.1 Backgrounds of this study

Globally, groundwater contamination has been a critical issue due to interference with the sustainable use of groundwater resources. Given the increases in human activities since the 1950s, the use of anthropogenic contaminants has raised deterioration levels and thus affected water quality by the various substances and occurrence pathways associated with such contaminants. Among the numerous contaminants, nitrate frequently deteriorates water quality in many countries (Postma et al., 1991; Chen and Liu, 2003; Babiker et al., 2004; Widory et al., 2004; Stadler et al., 2008; Kaown et al., 2009). The major sources of nitrate contamination are as follows: 1) diffusive sources such as fertilizer use in agricultural areas, septic waste, landfills, dairy farms; and 2) point sources such as septic tanks and sewage systems (Tilman et al., 2001; Böhlke, 2002; Tziritis, 2010). Because a high concentration of nitrate in drinking water can cause health problems, such as methemoglobinemia in infants and stomach cancer, nitrate contamination of groundwater is recognized as a critical public health problem (Wolfe and Patz, 2002).

When nitrate enters a subsurface saturated zone, these contaminants migrate along with ambient groundwater, as they are highly soluble in water and are scarcely adsorbed or precipitated in an aquifer medium. Therefore, once groundwater is polluted by nitrate, elevated concentrations of nitrate tend to remain in the subsurface

environment for long periods of time, except in cases of denitrification reduction. Moreover, due to population increases and industrial development, both of which cause contamination more often and more seriously (Tilman et al., 2001; Smith et al., 2010), many countries have made efforts to mitigate groundwater contamination or to prevent degradation of their water quality levels by applying various techniques based on research (Stites and Kraft, 2001; Almasri and Kaluarachchi, 2005; Peñe-Haro, 2010; Bonton et al., 2011).

To establish a proper management plan to address nitrate pollution, a quantitative assessment should be implemented in advance to evaluate factors controlling the fate and transport of nitrate in groundwater (Almasri and Kaluarachchi, 2005; Gheysari et al., 2009; Constantin et al., 2010; Kay et al., 2012; Bouraoui and Grizzetti, 2014). The quantification of impacts on deep aquifer systems by surface contaminant loading is challenging due to the complexity of nitrate dynamics in the subsurface environment. Identified factors associated with nitrate behavior are the amount of surface land use, the nitrogen loading level, groundwater recharge and soil characteristics, the thickness of unsaturated zones, the redox condition and the groundwater flow velocity (Nolan and Stoner, 2000; Böhlke, 2002; Green et al., 2010; Liao et al., 2012). Furthermore, certain characteristics of the aquifer geometry, such as the heterogeneity, geological layering structure, and any conduit system present also play important roles in the determination of travel pathways of nitrate plumes (Santi et al., 2006; McMahon et al., 2008a). Therefore, to evaluate nitrate contamination properly, it is essential to undertake a systematic assessment which identifies the sources, pathways and

magnitudes associated with the contamination dynamics.

Jeju Island, which is the largest island of the Republic of Korea, also faces severe nitrate contamination. Especially in the agricultural lands of the western part of the island, the excessive application of fertilizer at levels roughly 3 times the normal rate used on the island as a whole has been reported (Koh et al., 2012; Jeju Special Self-Governing Province, 2013a). Therefore, groundwater contamination by nitrate is a great concern in this area (Song et al., 2003; Jeong et al., 2004; Koh et al., 2005; Koh et al., 2012). Along with nitrate contamination, areas of saline groundwater with elevated levels of chloride (mean: 415 mg/L) have been found in the eastern part of the island due to highly permeable aquifer features in combination with excessive pumping. The anthropogenic impacts (land use changes, population increases and sea level rises due to climate change) are expected to increase on Jeju Island. All of these factors increase the vulnerability of the aquifer with regard to its future use. Site-specific hydrogeological characteristics (porous volcanic rocks, a high precipitation rate, and a relatively thin surface soil layer) on the island also have negative impacts on the groundwater resources. When precipitation easily passes through an unsaturated zone into the subsurface, it increases the potential for surface contaminants mixing and being transported with the infiltrated water. It is also important to note that Jeju Island was formed by multiple volcanic eruptions; therefore, geological layers with different hydrologic features are distributed across the island (Koh, 1997). This increases the complexity of the nitrate transport pathways in the aquifer systems on the island. Increasing exposure of these systems to combined anthropogenic and natural factors

has threatened the sustainable use of groundwater resources, which is virtually the sole water resource of the island. Therefore, it is necessary to prepare long-term plans for managing the groundwater resources of the island based on a complete understanding of the complex contamination dynamics based on an integrated approach.

To evaluate the recharge processes, origin and fate of contaminants, and the geochemical evolution of the aquatic systems, the combined use of hydrogeochemical and multiple environmental isotopes has been described in numerous studies (Böhlke and Denver, 1995; Widory et al., 2004; Koh et al., 2005; Han et al., 2014). Statistical analysis is another powerful tool used in a number of hydrogeochemical studies for classifying and identifying major mechanisms which influence the groundwater chemistry (Steinhorst and Williams, 1985; Melloul and Collin, 1992; Schot and Van der Wal, 1992; Helena et al., 2000; Cloutier et al., 2008) and predicting water quality levels based on certain relationships between variables (Benson et al., 2006; Aguilar et al., 2007; Burow et al., 2007; Kaown et al., 2007; Kent and Landon, 2013). Numerical simulation approaches can provide an alternative tool with which to measure water and solute quantities, especially considering that these factors are rarely measured in the field (Weiss and Gvirtzman, 2007; Li et al., 2008; Dragon et al., 2009; Peleg and Gvirtzman, 2010). These methods can also be used to predict the long-term impacts of adjustable flow and solute transport conditions in various scenarios (Molénat and Gascuel-Odoux, 2002; Peña-Haro et al., 2010; Pokhrel et al., 2012; Lee et al., 2013).

While the abovementioned approaches enable the characterization of nitrate

contamination conditions in an aquifer system, on Jeju Island, only individual analyses involving qualitative assessments of contamination were conducted in earlier work. However, these qualitative evaluations are limited in their ability to provide precise information (the magnitude and timing of the effects of factors) related to the nitrate dynamics on the island. Therefore, to establish proper and efficient management plans to protect the groundwater resources against nitrate contamination on Jeju Island, the implementation of quantitative approaches combining various assessment techniques is necessary to understand the nitrate contamination dynamics of the island fully in consideration of the hydrogeological characteristics.

1.2 Objectives of this study

The objectives of this study are to evaluate groundwater nitrate contamination by applying systematic investigation approaches which quantify impacts of factors affecting the nitrate dynamics in a complex aquifer system. This is described below,

In Chapter 2, the trends associated with long-term changes of nitrate and chloride concentrations that induce groundwater contamination throughout Jeju Island are identified by analytical methods. The effect of land use changes over 15 years on the transition in the quality of groundwater, and the links between trends associated with the two factors (NO_3-N and Cl concentrations) are also presented in this chapter. Based on this study, it is possible to identify a specific region of Jeju Island where is

necessary to control land development in order to protect groundwater resources.

In Chapter 3, a focused study related to the continuous deteriorating contaminants of nitrate on Jeju Island is implemented in the Gosan agricultural area to suggest efficient management plans to protect the aquifer environment. A numerical simulation is developed while applying a hydrogeochemical method from previous research which demonstrated that improperly sealed walls of groundwater wells could act as direct pathways for groundwater contamination by nitrate. In this chapter, a leaky-well module is introduced in relation to the numerical simulation to compute nitrate cross-contamination levels through the layered aquifer system on the island.

In Chapter 4, the nitrate input history and the major pathways which influence the quality of the groundwater in the Gosan complex aquifer system are evaluated using groundwater age-dating methods. To quantify the different water flow dynamics, different age-estimation models are applied to characterize the age of the groundwater at the Gosan site. The results from the different models are compared and the groundwater age distribution is evaluated in consideration of the complexity of the hydrogeological setting.

Chapter 2. Long-term groundwater NO_3-N and Cl trends in Jeju Island

Abstract

In this chapter, major contaminants of NO_3-N and Cl in groundwater of Jeju Island were targeted to evaluate continuous harmful impacts on the water quality for the future. Long-term temporal trend from 1993 to 2012 in the concentrations of NO_3-N and Cl from more than 3,900 wells was conducted using the Mann-Kendall trend test and Sen's slope analysis. Also, impacts of land use changes and groundwater management actions on groundwater quality were evaluated at the island scale with determined spatiotemporal trends of NO_3-N and Cl concentrations in groundwater of Jeju Island. The results indicate that the upward trends in NO_3-N were associated with the expansion of agricultural lands whereas Cl trends were considered to be affected by other factors in addition to the land use changes. In the mid-mountainous region, the deterioration in the groundwater quality by the both NO_3-N and Cl were

expected due to the continuous expansion of agricultural lands. In the coastal area, the NO_3-N and Cl components showed different trends depending on the regions. In the eastern area, increasing trends in NO_3-N were observed due to the development of new agricultural areas, while the Cl concentration was observed to decrease as a result of the regulation on groundwater extraction to reduce seawater intrusion. This study highlights that a comprehensive interpretation of trends in NO_3-N and Cl, and land use changes for long-term periods can provide useful insights to prepare for suitable groundwater management plans in the whole island perspective.

2.1 Introduction

Nitrate-nitrogen (NO_3-N) contamination of groundwater is a major concern in maintaining sustainable use of groundwater resources in many countries (Spalding and Exner, 1993; Nolan and Stoner, 2000; Stites and Kraft, 2001; Chen and Liu, 2003; Babiker et al., 2004; Erisman et al., 2008; Kurtzman et al., 2013). Nitrate-nitrogen contamination of groundwater has long been recognized as a public health issue because a high concentration of NO_3-N in drinking water can cause health problems, such as methemoglobinemia in infants and stomach cancer (Wolfe and Patz, 2002). Nitrate concentration in drinking water is regulated to be lower than 50 mg/L as NO_3^- or 10 mg/L as NO_3-N from many countries (Goodchild, 1998; EPA, 2010; WHO, 2011). Elevated NO_3-N levels in groundwater are known to be associated with anthropogenic sources such as synthetic fertilizers, manure, septic waste, and livestock wastewater (Böhlke, 2002; Kaown et al., 2009; Tziritis, 2010).

Contamination of groundwater by chloride (Cl) is another global issue in terms of groundwater quality (Mtoni et al., 2013; Baram et al., 2014; O'Leary et al., 2015). Potential sources of Cl contamination in groundwater are derived from agricultural fertilizers, septic effluent, animal waste, landfill leachate, road deicers, and seawater (Panno et al., 2006). High levels of Cl in groundwater are frequently observed in islands or coastal areas affected by seawater intrusion (Vengosh et al., 1999; Kim et al., 2003; Bakari et al., 2012; Han et al., 2014). Elevated amounts of the Cl component in groundwater can be also resulted from the extensive use of chemical fertilizers in

agricultural areas (Saffigna and Keeney, 1977). The maximum level of the Cl concentration for drinking water is regulated less than 250 mg/L for preventing the corrosion of water pipe, secondary health issues, and aesthetic objectives (WHO, 2002).

Jeju Island in South Korea suffers from contamination of groundwater in relation to both NO_3-N and Cl (Choi and Kim, 1989; Ko et al., 2005; Koh et al., 2007). High levels of NO_3-N contamination have been observed in the western part of the island, where intensive agricultural activities have been practiced since the 1960s (Spalding et al., 2001; Woo et al., 2001; Choung et al., 2004; Koh et al., 2005; Hyun et al., 2010; Koh et al., 2012). In terms of Cl contamination, seawater intrusion has been known as the major cause of elevated Cl concentration in groundwater, particularly in the eastern part of the island (Han and Shin, 2000; Youn et al., 2003; Jeju Special Self-Governing Province and JDI, 2012). Recent surveys also suggest that chemical fertilizers from agricultural land partially contribute to groundwater deterioration by Cl in densely cultivated areas besides seawater intrusion (Koh et al., 2007).

The sustainable management of groundwater quality in Jeju faces new challenges caused by the continuous increases in anthropogenic activities. During the last three decades (from 1975 to 2000), the island has undergone a considerable change in its land use accompanied by an expansion in urban (5.12 km^2/yr) and agricultural areas (12.90 km^2/yr), and a reduction of forest lands (-18.43 km^2/yr) (Ha et al., 2009). With the expansion of agricultural land, groundwater extraction and the use of chemical fertilizers have increased as well, leading to continuous decreases in groundwater level,

quality deterioration, and reduction of available water resources (Koh et al., 2007; Lee et al., 2007; Song and Choi, 2012). In addition, increasing groundwater abstraction for agricultural and domestic use promoted seawater intrusion into the coastal aquifer, in which 8% increase in pumping rate induced 42% increase in Cl concentration (Booh and Jeong, 2000; Kim et al., 2003). Under these circumstances, groundwater in the island becomes to more vulnerable to contamination by NO_3-N and Cl; such contamination is expected to increase in the future. In Jeju Island, it is necessary to prepare long-term management plans for groundwater because it is the sole drinking water resource.

In order to establish an adequate groundwater management plan in Jeju, an understanding of regional and long-term temporal characteristics of NO_3-N and Cl concentrations in groundwater is needed. Given the potential impact of human-related activities on subsurface environment, the influence of land use change on groundwater quality needs to be quantitatively assessed. Trend analysis can be a useful tool to assess the spatiotemporal behavior of the surface water and groundwater pollutants as well as to analyze the relationship between history of land use change and the water quality (Eckhardt and Stackelberg, 1995; Chang, 2008; Kent and Landon, 2013; Robertson and Sharp Jr, 2013; Green et al., 2014). For example, Chang (2008) found urban land use was related to increases in water pollution from non-point source nitrogen. Kent and Landon (2013) revealed that different driving forces of the transition in the land uses and hydrological features may affect the temporal trends in the NO_3^- and total dissolved solids (TDS) constituents for a decade. When groundwater quality is affected

by chemical fertilizers from agricultural lands, NO_3-N and Cl concentrations are simultaneously enriched (Kanfi et al., 1983; Kurtzman and Scanlon, 2011) except where denitrification removes the NO_3-N component. Especially, as a specific condition for agricultural areas located near the coast, the combined impacts of highly enriched levels of Cl are predicted with elevated NO_3^- concentration when agricultural pollutant loadings and seawater simultaneously influence the groundwater quality in the area. Therefore, it is necessary to assess the NO_3^- and Cl trends together regardless of whether identical or conflicting trends are present between the two parameters.

The objective of this study is to identify the spatiotemporal changes in NO_3-N and Cl concentrations that induce groundwater contamination on the entire Jeju Island. Based on the trend relationship between the two components, the effect of 15 years of land use changes and groundwater management actions on the transition of groundwater quality is assessed from a regional perspective. The results of this study will enable identification of regions of Jeju Island in which development restriction for land use is needed to protect groundwater resources.

2.2 Site descriptions

Jeju Island is the largest Korean islands with a total area of 1,847 km^2 (Fig. 2.1a) and Mt. Halla is situated in the center of the island at an altitude of 1,950 m. The island is composed mainly of porous volcanic rock formed from

multiple eruptions that occurred from the Late Pliocene to the Quaternary period; sedimentary rock is imbedded between the volcanic rocks. Basalt is a major rock type of the volcanic rocks in the island and is known to be a highly permeable rock with hydraulic conductivity in the range 84.6 to 552.2 m/day (Hahn et al., 1994; Won et al., 2005; Won et al., 2006). Owing to the above hydrogeological characteristics, groundwater recharge rate of the island is estimated to be 38.7%–45.8% of the average precipitation (2,061 mm/yr in 1992~2011; Jeju Special Self-Governing Province, 2013b) (Hahn et al., 1994; Jejudo, 2003; Choi et al., 2011; KIGAM, 2011). The Seogwipo Formation (composed of gravelly sandstone, sandstone, sandy mudstone and mudstone with bioclastic shells) with low permeability is distributed under the volcanic rock and acts as an aquiclude (Koh, 1997; Won et al., 2006). The elevation of the Seogwipo Formation is important because it determines the location and shape of the freshwater and seawater interface, which differs from the east coast to the west (Fig. 2.1b). Underneath of the Seogwipo Formation, the U Formation (unconsolidated sediments which is composed of gray to light gray fine sand and silt) and the basement of granite/tuff are located sequentially (Won et al., 2005).

As shown in Figs. 2.1a and 2.1b, three types of groundwater exist on Jeju Island; high level, parabasal, and basal groundwater, depending on their

formation depth and the relationship with seawater intrusion (Won et al., 2006; Jeju Special Self-Governing Province, 2013b). High level groundwater occurs only at high-altitude areas and has no contact with seawater. Parabasal groundwater is also a freshwater aquifer which is not in direct contact with seawater although it is located below sea level (Fig. 2.1b). The basal groundwater is a freshwater body which affected by seawater intrusion. The basal groundwater body is usually found in the eastern part of the island because the Seogwipo Formation which acts as a barrier against seawater intrusion is located deeply at a depth of −95 m to −158 m below sea level in this region (Fig. 2.1b) (Koh, 2006a).

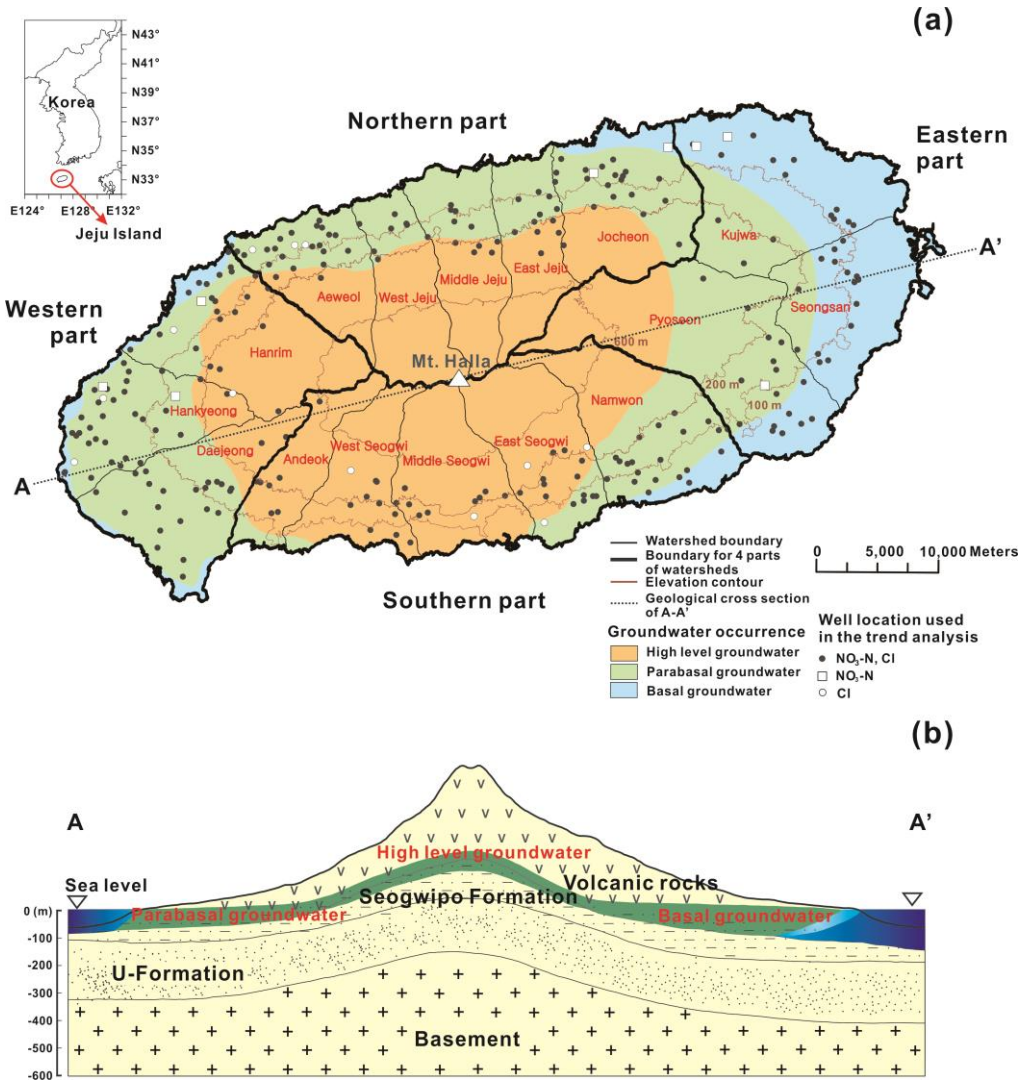

Fig.2.1 Location map of the study area showing: (a) the location of wells used for the trend analysis, and the types of groundwater found in the area; (b) schematic hydrogeologic structures along A-A' line (modified from Koh, 2006a).

2.3 Methods

Groundwater quality data collection

NO_3-N and Cl concentrations in groundwater throughout the entire island were collected by the Institute of Water Resources of the Jeju Special Self-Governing Province from 1993 until 2012; 16,366 water quality datasets were obtained from 3,983 wells. Because at least eight points are recommended for trend analysis (Grath et al., 2001), only wells for which water quality data were obtained more than eight times for both NO_3-N and Cl were selected. In addition, wells for which more than one water quality dataset was obtained between both 1993–1997 and 2007–2011 were chosen for analyzing the impact of land use changes using land use maps of 1995 and 2009.

In most cases, the water quality of the wells exhibited seasonal fluctuation according to seasonal precipitation patterns, which likely caused inaccuracies in the trend analysis for water quality data collected non-periodically (Helsel and Hirsch, 2002; Stuart et al., 2007; Pejman et al., 2009; Kent and Landon, 2013). A distinct seasonal variation such as higher concentration of NO_3-N in wet season and lower concentration in dry season in groundwater quality was observed on Jeju Island (Woo et al., 2001; Oh et al., 2010). Two factors are identified to be responsible for the observed seasonal variation. First, on Jeju Island, 75% of the annual precipitation is concentrated during the rainy season between April and September (KIGAM, 2011). Second, the surface of the island is largely covered by porous volcanic rocks. Because water quality data used for trend analysis in this study were obtained at random time periods, any differences in the

water quality data obtained between wet season (April–September) and the dry season (October– March) were evaluated prior to the trend analysis. Seasonal differences in NO_3-N and Cl concentrations were confirmed by the Mann–Whitney U test (Mann and Whitney, 1947), which is a nonparametric test used to determine whether two independent samples are different. The Mann-Whitney U test showed that 23 wells (8.3%) for NO_3-N and 19 wells (6.8%) for Cl had significant differences between wet and dry seasons. Even if significant differences existed in the water quality data between the two seasons at one well, the data was used when the following conditions were met. If more than two measurements for NO_3-N or Cl existed in both the wet and dry seasons for all three periods, 1993–1997, 1998–2006, and 2007–2011, the relevant well was included for the trend analysis based on the judgment that they are sufficient to draw long-term trend. In total, 260 wells were chosen for analysis of NO_3-N concentration trends, and 264 wells were selected to examine Cl concentration trends. Both NO_3-N and Cl data were obtained from 252 wells, 8 wells delivered NO_3-N data only, and 12 wells gave Cl data only. The locations of wells selected for the trend analysis are shown in Fig. 2.1a.

Trend analysis

In this study, the nonparametric Mann–Kendall trend test method that permits missing data (Mann, 1945; Kendall, 1948) was used to evaluate the tendency of changes in NO_3-N and Cl concentrations over time. The Mann–Kendall test computes the Mann–

Kendall statistic, S, by using two variables x_j, x_k (j > k) in the following equations:

$$S = \sum_{k=1}^{n-1}\sum_{j=k+1}^{n} sign(x_j - x_k) \quad \textbf{[Eq. 2.1]}$$

$$sign(x_j - x_k) = \begin{cases} +1 & if\ x_j - x_k > 0 \\ 0 & if\ x_j - x_k = 0 \\ -1 & if\ x_j - x_k < 0 \end{cases} \quad \textbf{[Eq. 2.2]}$$

where *n* is the number of data. To consider possible comparisons ($n(n-1)/2$) of *n* numbers of data, Kendall's tau is generated by dividing S by $n(n-1)/2$. The test for significance of Kendall's tau was performed by using the confidence level, which was set at 90% in this study.

Wells showing significant upward and downward trends in NO_3-N and Cl concentrations in the Mann–Kendall test were additionally used to calculate the magnitude of trends by using the Sen slope estimator (Hirsch et al., 1991), which is a median value (Q′) among slopes of trends (Q) in the *n* numbers of data (Eqs. [2.3] and [2.4]):

$$Q = \frac{x_j - x_k}{t_j - t_k} \qquad j>k \quad \textbf{[Eq. 2.3]}$$

$$N' = \frac{n(n-1)}{2}, \quad Q' = \begin{cases} Q_{\frac{N'+1}{2}} & if\ N' = odd \\ \frac{1}{2}\left[Q_{\frac{N'}{2}} + Q_{\frac{N'+2}{2}}\right] & if\ N' = even \end{cases} \quad \textbf{[Eq. 2.4]}$$

Calculation of land use change ratio

Land use data for 1995 (Jejudo, 1997) and 2009 (KIGAM, 2011) were used to compute the rate of change in land use on Jeju Island over 15 years; the land was divided into three major categories comprising urban, agricultural, and natural land. Residential areas and industrial facilities were classified as urban land use, and crop fields, orchards, and greenhouses were classified as agricultural land use. Natural land use included grass land, forest, and wetland. Before calculating the change rate of each land use category, the areas of the three categories were calculated for the 1995 and 2009 in each of the 16 watersheds by using ArcGIS 10.0 (ESRI, 2011). The change ratio of each land use category within the individual watershed through time was then computed by dividing the area of each land use category in 2009 by the area of relevant land use in 1995. If the calculated ratio was greater than 1.0, the land use was considered to have expanded since 1995. When the ratio was less than 1.0, the land use was reduced in relation to conversion to a different land use category.

2.4 Results and discussions

Spatial and temporal distributions of NO_3-N and Cl concentrations

The spatial distribution of averaged groundwater NO_3-N and Cl concentrations (1993~2012) used for trend analysis is shown in Fig. 2.2. Wells with average NO_3-N concentrations of more than 10 mg/L, which is the maximum contaminant level (MCL) for NO_3-N in drinking water, are mainly located in the western region of the island

with a few wells scattered in the northern and southern regions (wells exceeding MCL of NO_3-N for drinking water: 280 for western region; 77 for northern region; 54 for southern region in Table 2.1). Also, average groundwater Cl concentrations are highly distributed together with the NO_3-N component in those regions (mean concentrations of Cl: 20.47 mg/L for western region; 12.46 mg/L for northern region; 8.44 mg/L for southern region). For the eastern region of the island, although groundwater pollution by NO_3-N was rarely occurred, the MCL of drinking water was exceeded only seven times (0.53%) among the total 1,333 datasets, relatively high values of averaged Cl concentrations over 50 mg/L were distributed along the coastal area (Fig. 2.2).

Through a relationship between NO_3-N and Cl concentrations in groundwater, a source of those components could be estimated. In Fig.2.3, two major sources which elevate NO_3-N and Cl concentrations in the island are presented, which are agricultural inputs which add two components together into groundwater of the island (Koh et al., 2007), and seawater mixing which enriches Cl concentration only. Average concentrations of NO_3-N and Cl in groundwater are plotted in Fig.2.3 according to a major land use at the each well (land use type having greater than 60% of a circle area with radius of 250 m) and the groundwater types (basal, parabasal and high level groundwater). Increasing average NO_3-N concentration with Cl is observed mostly at the wells of the agricultural lands following the trend line by Koh et al. (2007) which indicates the nitrate contamination in groundwater impacted by chemical fertilizer in the study area. Relatively higher values of averaged Cl concentrations with the low NO_3-N concentration are derived from impact by seawater mixing, reflecting the

locations of the basal groundwater.

In addition to the spatial distribution of the average NO_3-N and Cl concentrations in groundwater, diverse temporal changes of the two components were observed at the selected wells as shown in Fig. 2.2a~d. Although all wells were located in the agricultural land, temporal trends of the two components showed various shapes. The NO_3-N and Cl concentrations would be increased over time from the enriched concentrations (Fig. 2.2a) or from the natural background concentrations (Fig. 2.2b). Also, temporal decreasing trends in both the NO_3-N and Cl concentrations are shown with a seasonal fluctuation (Fig. 2.2c). Different behavior over time was observed for the well shown in Fig. 2.2d in which NO_3-N concentrations slowly increased even though fluctuating change of the highly detected Cl concentration was shown.

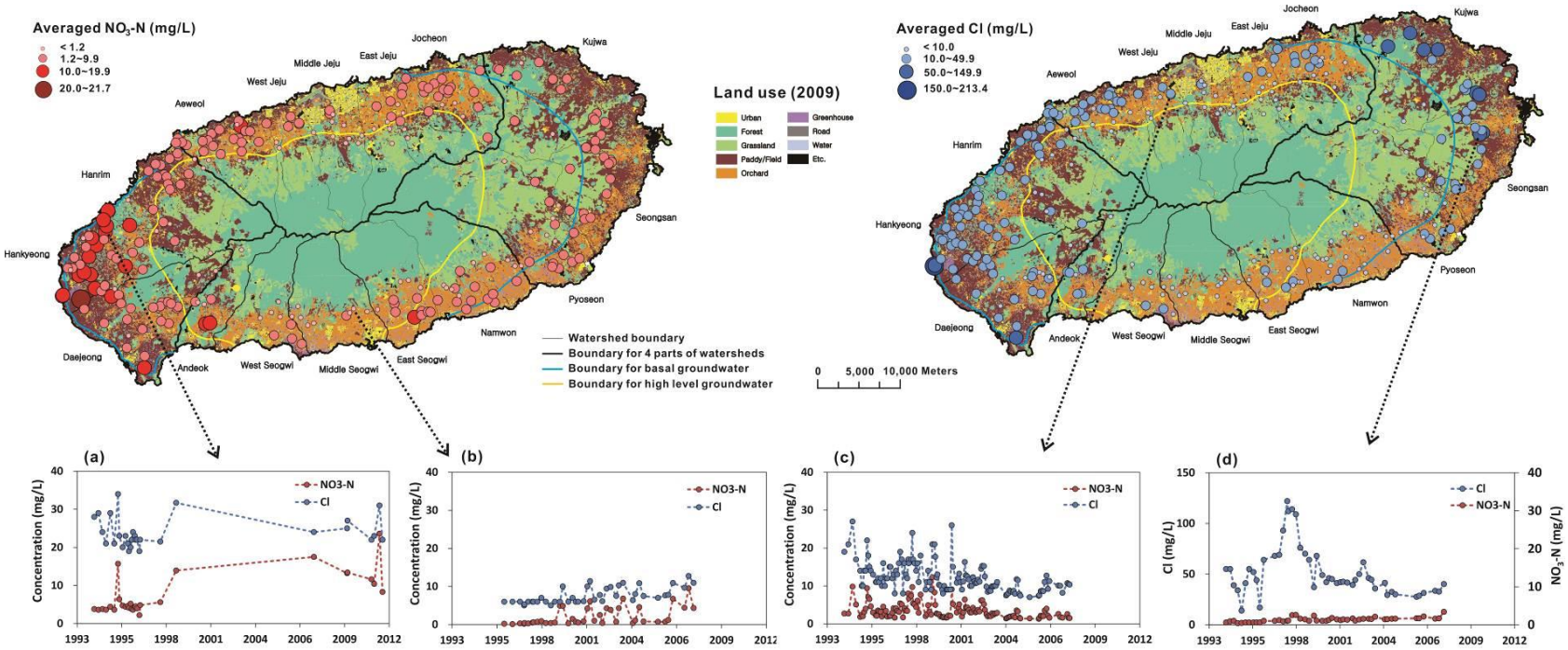

Fig.2.2 Spatial variations of averaged NO_3-N and Cl concentrations in groundwater using the land use map of 2009.

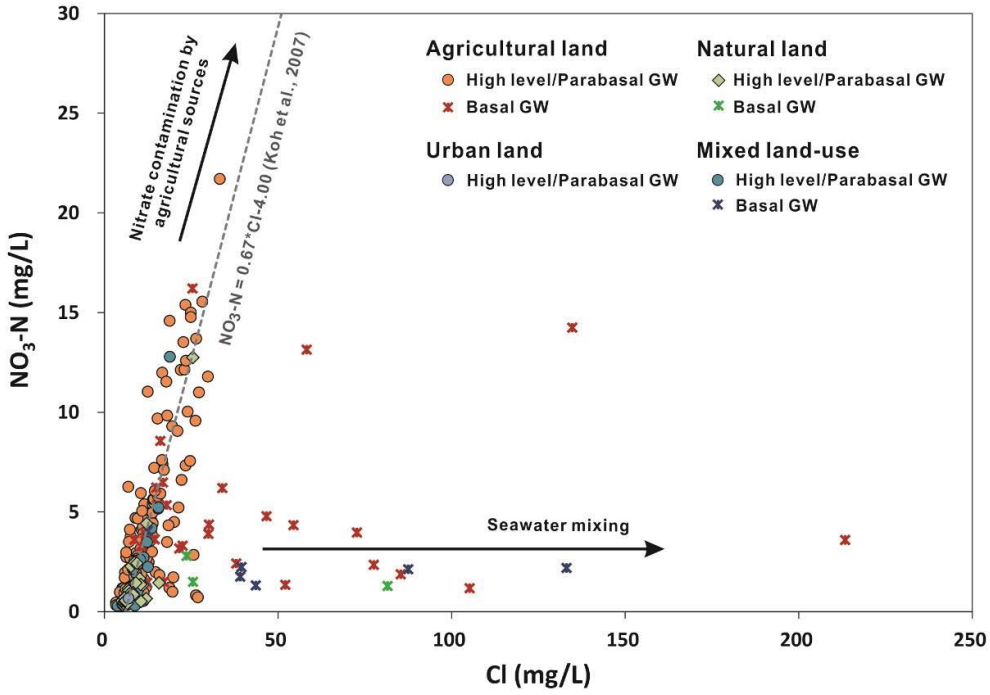

Fig.2.3. Average groundwater NO_3-N and Cl concentrations (1993-2012) at the wells classified into a major land-use of 2009 (greater than 60% of a circle area with radius of 250 m) and groundwater types.

Table 2.1 Statistical information of NO_3-N and Cl concentrations used in trend analysis

Parameter		Eastern parts	Western parts	Southern parts	Northern parts
NO_3-N	No. of datasets	1333	1398	1513	2332
	Mean	2.43	5.54	2.37	3.39
	Std. Dev.	1.76	6.00	3.94	2.98
	Minimum	0.07	0.02	0.01	0.02
	Maximum	12.00	49.00	34.20	23.20
	No. of data >10 mg/L	7	280	54	77
Cl	No. of datasets	1244	1412	1568	2216
	Mean	38.70	20.47	8.44	12.46
	Std. Dev.	45.48	39.31	5.82	11.67
	Minimum	2.90	1.00	2.00	1.00
	Maximum	348.00	763.40	54.06	177.00
	No. of data >250 mg/L	3	7	0	0

‘

Spatial changes of land use from 1995 to 2009

Natural and agricultural lands were the dominant types of the land use in the study area, covering more than 90% of the total area. From 1995 to 2009, the area of natural lands decreased from 1098.3 km^2 to 954.6 km^2, whereas the area for agricultural lands expanded from 616.6 km^2 to 750.0 km^2 (Table 2.2). The agricultural lands noticeably expanded in the eastern and western areas during the 15-year period, having a change ratio of 1.17–1.46. Agricultural land is mainly located in the lowland (<200 m elevation) of the island in 1995. However, the area covered by the agricultural land has been expended toward higher elevation in 2009. Ha et al. (2009) found that agricultural lands in the region of 200–600 m elevation (the mid-mountainous area) showed higher increasing rate than that those in the lowland (< 200 m elevation) in Jeju Island between 1995 and 2000. In the mid-mountainous area of the island, the newly located agricultural lands in 2009 were mostly the natural lands in 1995 (94.5% of the natural lands and 2.7% of the urban area) as shown in Fig. 2.4a and 2.4b.

The undeveloped natural lands have decreased in the western and eastern regions at a change ratio of 0.66–0.89 (Table 2.2) due to conversion into agricultural lands (Fig. 2.4a and b). Although the urban area occupies a minor proportion of Jeju Island (3.8% of the total area in 1995), urbanization during the 15-year period occurred over the study area of 1.04–1.74, except Kujwa and Daejeong watersheds (more than half of reduced urban land in 1995 was turned into agricultural land in 2009) (Table 2.2).

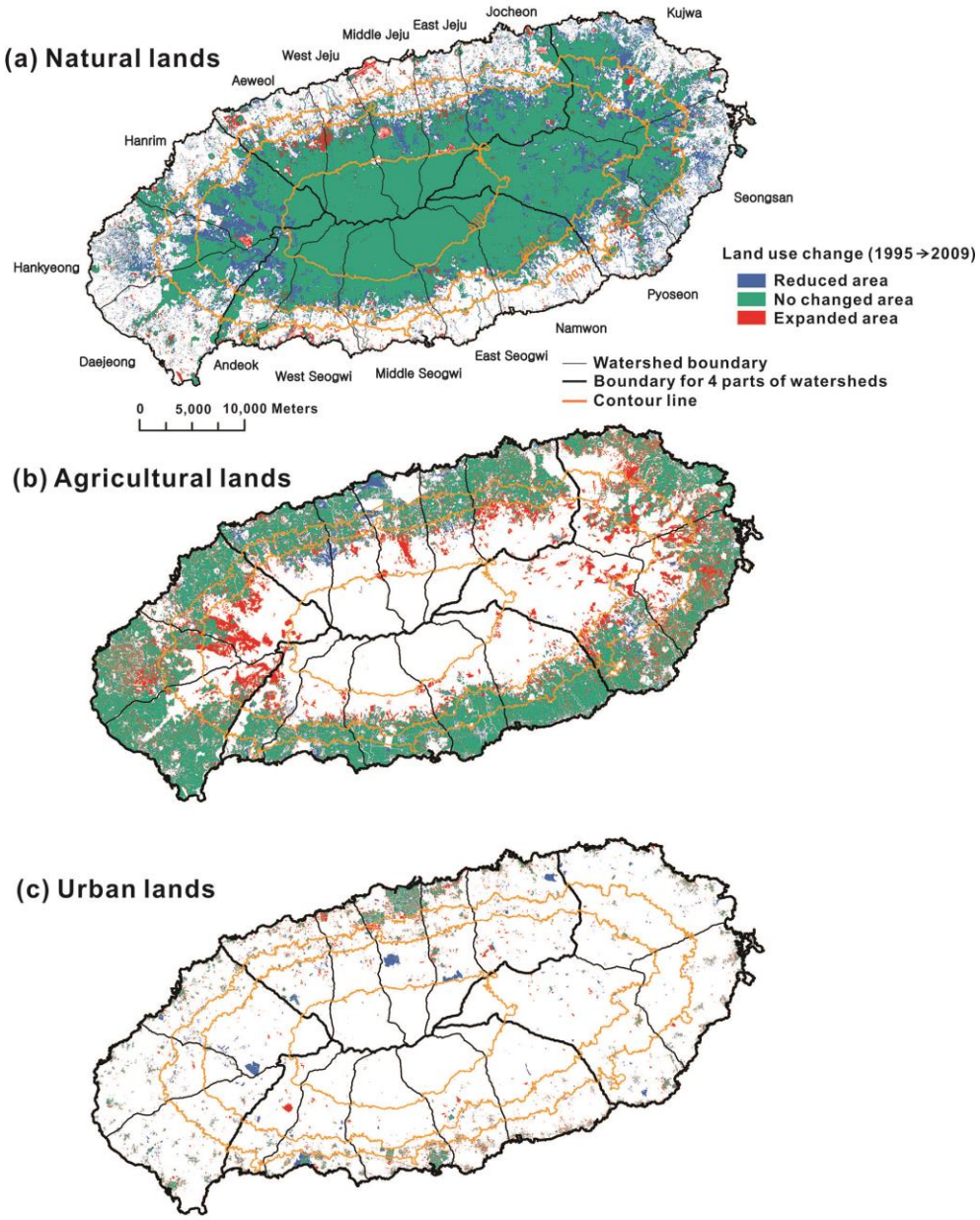

Fig.2.4. Spatial distribution of land use changes from 1995 to 2009 (a) natural lands, (b) agricultural lands and (c) urban lands.

Table 2.2 Summary of land use changes in the four major sectors (with individual watersheds).

Land uses		Urban lands			Agricultural lands			Natural lands		
Parameter		1995	2009	Change ratio†	1995	2009	Change ratio	1995	2009	Change ratio
		(km^2)			(km^2)			(km^2)		
Entire island		68.4	82.3	1.20	616.6	750.0	1.22	1098.3	954.6	0.87
Eastern part	Kujwa	4.5	4.2	0.93	53.1	77.6	1.46	109.3	85.7	0.78
	Seongsan	3.3	3.6	1.11	44.7	62.9	1.41	63.1	44.5	0.70
	Pyoseon	3.4	4.6	1.35	42.4	58.0	1.37	158.1	140.2	0.89
Western part	Hanrim	6.3	6.6	1.04	43.7	63.4	1.45	88.6	69.2	0.78
	Hankyeong	3.2	3.8	1.17	54.3	69.3	1.28	42.3	27.8	0.66
	Daejeong	5.0	4.6	0.92	70.8	82.9	1.17	50.7	40.3	0.79
Southern part	Namwon	2.2	3.6	1.63	48.3	53.0	1.10	81.0	74.7	0.92
	East Seogwi	2.1	3.0	1.46	36.0	38.0	1.05	67.1	64.6	0.96
	Middle Seogwi	4.8	5.8	1.20	33.0	35.7	1.08	65.9	62.9	0.95
	West Seogwi	4.3	4.8	1.11	27.6	29.0	1.05	49.4	47.5	0.96
	Andeok	1.4	1.8	1.30	16.1	19.7	1.22	44.1	39.6	0.90
Northern part	Jocheon	4.0	5.6	1.40	43.1	57.0	1.32	76.1	60.5	0.79
	East Jeju	5.1	6.1	1.20	23.7	24.8	1.05	44.7	42.5	0.95
	Middle Jeju	12.8	14.0	1.10	19.9	20.5	1.03	52.4	49.8	0.95
	West Jeju	2.0	3.4	1.74	19.3	18.3	0.95	66.6	65.7	0.99
	Aewoel	4.1	4.6	1.13	40.4	39.8	0.98	38.8	39.2	1.01

† Area of land use in 2009 divided by that of 1995.

NO_3-N and Cl trends and its spatial distribution

The analyzed trends in NO_3-N and Cl concentrations over time are presented in Table 2.3. In the entire island, 84 and 76 of the total monitoring wells have significant NO_3-N and Cl trends (p-value <0.1), respectively, although non-significant trends for both components constitute the majority of the results of the trend analysis (NO_3-N: 67.7% and Cl: 71.2%). The number of wells with increasing NO_3-N trends (52 wells; 20.0%) is greater than that with decreasing trends (32 wells; 12.3%). For Cl concentrations, the number of wells showing decreasing trends (47 wells; 17.8%) is greater than that showing increasing trends (29 wells; 11.0%). These results indicate that NO_3-N continue to cause deterioration in groundwater quality in comparison with Cl.

The spatial distribution of trends in NO_3-N and Cl concentrations is plotted in Fig. 2.5, which also shows with the magnitude of slopes (Sen's slope estimator) for both upward and downward trends with exception of no trends. Trends of increasing NO_3-N with Sen's slope estimators of more than 0.1 mg/L per year are mainly located in the eastern and western regions, whereas minor increments, with Sen's slope below 0.1 mg/L per year, are located in areas of relatively high elevation (Fig. 2.5a). However, decreasing trends in NO_3-N are mostly observed in the island's lowlands except the eastern region. Downward trends in Cl concentrations are distributed throughout the island, and strong decreasing slopes with magnitudes greater than −1.0 mg/L per year are observed in the eastern area where the basal groundwater is located (Fig. 2.5b). Upward trends in Cl concentrations are located mostly in areas with altitudes of 200–600 m, known as the

mid-mountainous areas, with the exception of one well which situated near the coastline in the Hankyeong watershed (Sen's slope: 2.75 mg/L per year). This result is caused by over-abstraction of groundwater during a dry season in the western area.

As previously mentioned, water pollution in the western area related to NO_3-N occurs extensively. Most of wells in the western area show no significant trends (75%) in NO_3-N concentrations (Table 2.3). Increasing trends of NO_3-N in the western area take higher percentages (17.5%) than those of decreasing trends (7.5%) as shown in Table 2.3; thus, the NO_3-N contamination of groundwater is expected to be a problem in that area, continuously. The western part of Jeju Island had higher amounts of fertilizer application in 2009, at total 628 kg-N/ha/yr (Koh et al., 2012), comparing to the average usages of fertilizer (245 kg-N/ha/yr) in the entire island (Jeju Special Self-Governing Province, 2013a). Oh et al. (2010) studied the N-excess amounts derived from synthetic fertilizers in the Gosan area of the western part and reported that 260 kg-N/ha of annual N-excess was estimated to leach into the subsurface aquatic system. They determined that the high surplus amounts of synthetic fertilizers could have caused the severe NO_3-N contamination in groundwater of the Gosan agricultural area.

Among four parts of the island, the highest percentage of increasing NO_3-N trends in groundwater appears in the eastern area (43.8% of total data for each region) (Table 2.3). As shown in Fig. 2.5a, wells located in the eastern coastal area at altitudes below 100 m have increasing trends in NO_3-N concentrations with greater Sen's slopes of 0.04–0.25 mg/L per year than those located in higher lands (Sen's slopes: 0.03–0.10

mg/L per year). Such spatial distribution of the increasing NO_3-N trends in the eastern area was also reported in the previous study by Kim et al. (2007). Even though relatively lower NO_3-N concentration is observed in the eastern area compared to that in the western area, there is a higher possibility that deterioration of the water quality by NO_3-N in that area could be appeared in the near future.

Table 2.3 Trends of NO_3-N and Cl concentration (1993~2012) in groundwater over entire island and in the four major sectors.

Parameter	NO_3-N			Cl		
Trends	Increasing	No trend	Decreasing	Increasing	No trend	Decreasing
Entire island	52† (20.0%)‡	176 (67.7%)	32 (12.3%)	29 (11.0%)	188 (71.2%)	47 (17.8%)
Eastern part	21 (43.8%)	25 (52.1%)	2 (4.2%)	4 (8.7%)	28 (60.9%)	13 (28.9%)
Western part	14 (17.5%)	60 (75.0%)	6 (7.5%)	6 (7.4%)	59 (72.8%)	16 (19.8%)
Southern part	11 (18.0%)	38 (62.3%)	10 (16.4%)	10 (15.6%)	46 (71.9%)	8 (12.5%)
Northern part	6 (8.2%)	53 (72.6%)	14 (19.2%)	9 (12.2%)	55 (74.3%)	10 (13.5%)

† The number of wells showing the relevant trend.

‡ Numbers in parentheses represent the percentage of each trend in the relevant region.

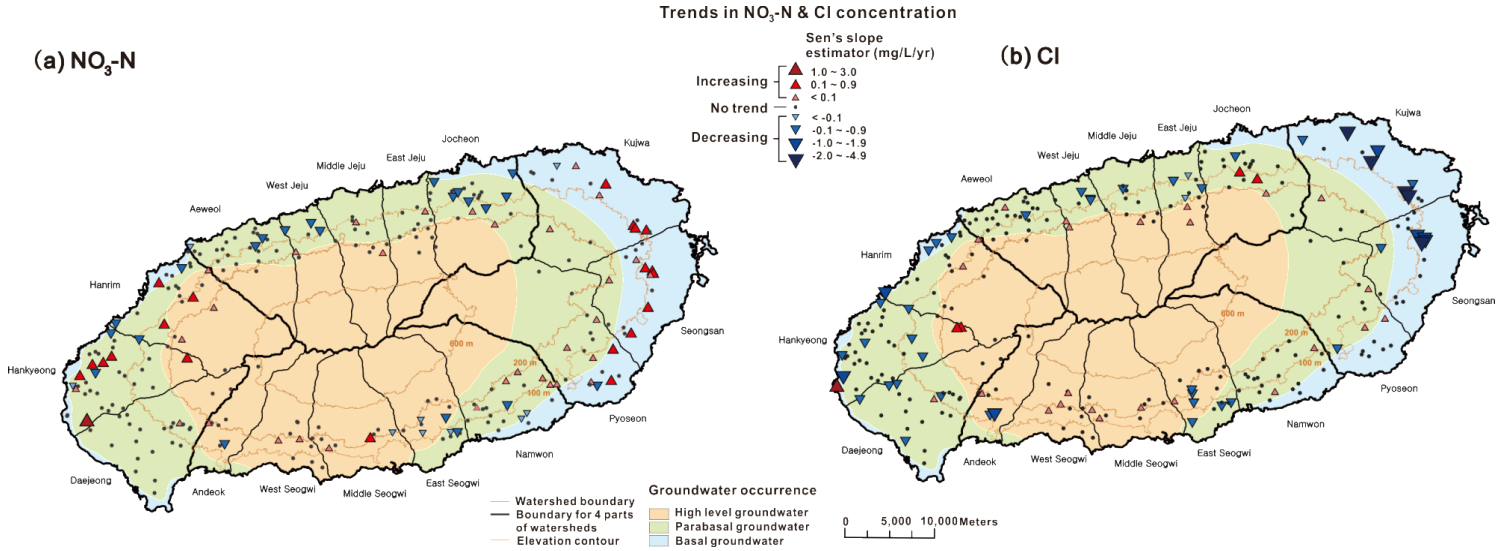

Fig.2.5. Spatial distribution of trends in: (a) NO_3-N; and (b) Cl concentrations.

Relationships between land use changes and trends

To identify effects of the land use changes on the trends of the two major pollutants on the island, the relationship between the rate of change in land use during 15 years and the percentage of three trend factors (increasing, not significant, and decreasing trend) for each 16 watersheds were investigated (Fig. 2.6). As shown in Fig. 2.6a, enlargement of the urban areas in watersheds was found to be significantly associated with decreasing trends of NO_3-N contamination (a coefficient of determination, R^2=0.56; *p*-value is less than 0.1). Because 45.5% of the developed urban area in 2009 was converted from the agricultural lands in 1995, it is therefore considered that urbanization has a positive effect on the NO_3-N concentration and thus the quality of groundwater on the island. Although it is possible that urban lands cause deterioration of the water quality in relation to leaking septic and sewer systems (Silva and Williams, 2001; Chang, 2008), past research has also confirmed that NO_3-N concentrations have declined when land use changed from agricultural land to urban landscapes from 1955 (agricultural lands: 72%, urban land: 28% of total study area) to 1995 (agricultural lands: 21%, urban land: 72% of total study area) in the Phoenix area, Arizona (Xu et al., 2007).

Areas in which agricultural lands have been expanding over time were

determined to cause a significant increasing trend of NO_3-N in the groundwater, with R^2 of 0.42 (Fig. 2.6b). Furthermore, in areas in which natural lands were reduced, NO_3-N in groundwater increased in proportion to the rate of conversion to agricultural lands (Fig. 2.6c). Positive correlations between the NO_3-N concentration and the agricultural land use have been reported in many previous studies (Eckhardt and Stackelberg, 1995; Nolan and Stoner, 2000; Gardner and Vogel, 2005; Kaown et al., 2007). Additionally, Kent and Landon (2013) suggested that increasing trends in NO_3-N concentrations (1986~2008) were related to the past agricultural land use in 1990s rather than recent urban land use in 2000s in their study area. Through this study, the impact of land use changes on the tendency of changes in the NO_3-N concentration of groundwater during the 15-year period is apparently detectable. The positive correlations were observed on the basis of the high recharge ratio of the aquifer system in the study area, where contaminant sources can easily percolate into the subsurface environment (Won et al., 2006). In contrast to the NO_3-N trends, there are no statistically significant relationships (*p*-value is greater than 0.1) between land use change and trend factors for Cl (Fig. 2.6d~f). Based on this result, the changes in the Cl concentrations of groundwater, in terms of the watershed-scale, are considered to be affected by other factors in addition to the

land use changes of the island.

As shown in Fig. 2.5, a greater number of increasing NO_3-N and Cl trends were observed in the mid-mountainous area in comparison with decreasing trends in the same area. To confirm distinct associations between trends and elevation, the trends for the two parameters were divided into three groups based on the elevation: <100 m, 100–200 m, and 200–600 m above sea level. The percentages of the trends were then calculated as shown in Fig. 2.7. A higher percentage of upward trends in NO_3-N concentration was noted in the region of 100–200 m elevation (24.0%) than that in the lower lands (<100 m elevation, 19.0%). A smaller percentage of downward trends in NO_3-N was continuously observed with elevation such as 15.5% for <100 m and 12.0% for 100–200 m. In the mid-mountainous area (200–600 m), the percentage in upward trends (16.3%) was greater than that of downward trends at 2.3%. Such relationships between trends and elevation are distinct for Cl concentrations. Greater percentages of upward trends occurred in the higher elevation region (5.6% → 13.5% → 23.4%, for <100 m, 100–200 m, and 200–600 m, respectively), whereas the proportion of downward trends continuously declines (22.4% → 18.9% → 2.1%, for <100 m, 100-200 m, and 200-600 m, respectively).

The higher number of increasing trends of both NO_3-N and Cl concentrations found in the mid-mountainous area can be attributed to the changes of land use in the region. Natural lands in the mid-mountainous area constituted 87.8% of the total land cover in 1995. In 2009, however, these lands had been reduced to 62.9%, and agricultural lands had drastically expanded from 8.8% to 17.5% of the total area, with a change ratio of 2.5 (Table 2.4). The ratios of enlarged agricultural lands in the areas of lower than 100 m and that in the 100–200 m elevation region are 1.1 and 1.2, respectively. Such abrupt expansion of the agricultural lands in the mid-mountainous area could have caused an increment of non-point sources such as chemical fertilizers (complex fertilizer, urea, fused phosphate, potassium chloride; Jeju Special Self-Governing Province, 2013a), which would have added NO_3-N and Cl components into the groundwater in that region. The mid-mountainous area is important with respect to the groundwater of Jeju Island because it is the major recharge region for the aquifer located in the coastal area (Koh et al., 2005). Therefore, if agricultural lands in the mid-mountainous area continue to expand, the water quality of the aquifer system below the area could deteriorate further. Moreover, the progress of the pollution within the groundwater could reach the aquifer located in the lower lands.

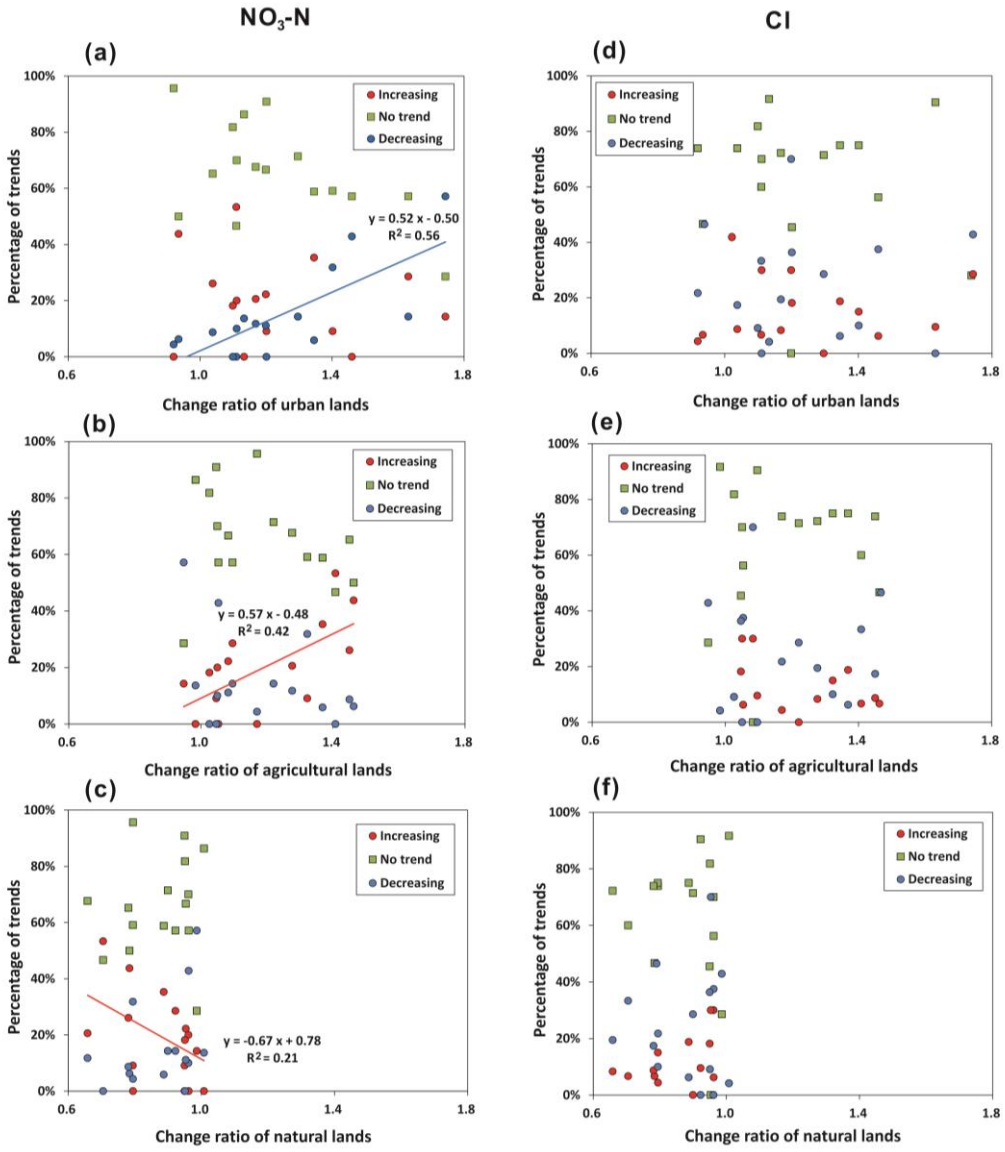

Fig.2.6. Relationship between the change ratio of land usage and trends in (a) urban lands, (b) agricultural lands, (c) natural lands versus percentage of NO_3-N trend; (d) urban lands (e) agricultural lands, (f) natural lands versus percentage of Cl trend (three points represent the percentage of three trends in each of the 16 watersheds; a trend line is added for a relation having a statistically significance of *p<0.1*).

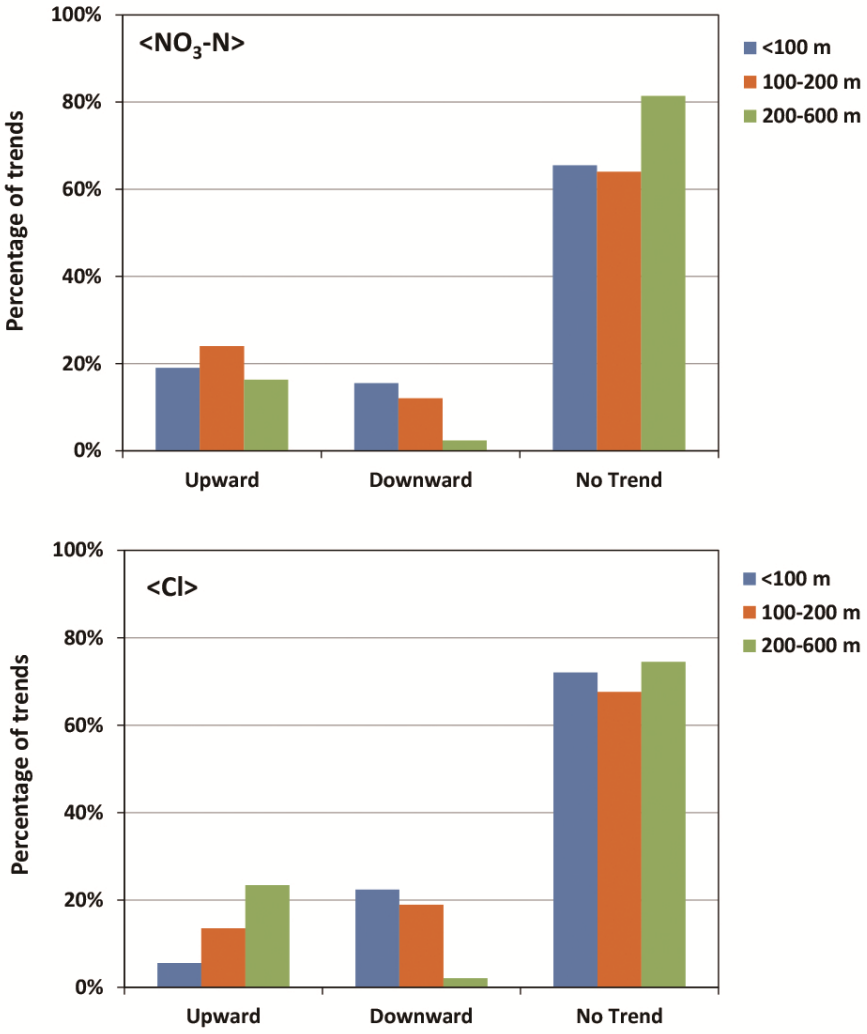

Fig.2.7. Variations of trends according to elevation.

Table 2.4. Information related to changes in agricultural land use according to elevation.

Elevation (m)	1995 (km^2)	2009 (km^2)	Change ratio
<100	398.4 (62.9%)[†]	431.4 (67.4%)	1.10
100–200	166.0 (46.0%)	200.0 (55.7%)	1.24
200–600	52.1 (8.8%)	113.2 (17.5%)	2.53

[†]Numbers in parentheses refer the percentage area of agricultural land in relation to the total land area at a particular elevation.

Relations between NO_3-N and Cl trends

In areas in which groundwater is contaminated by NO_3-N, the NO_3-N and Cl concentrations are usually found to have positive correlations because these species originate from the same contaminant sources (Babiker et al., 2004; Koh et al., 2007; Kaown et al., 2009). Trends in NO_3-N and Cl parameters were computed in this study using Sen's slope estimators from two factors classified in the four principal sectors of the island (Fig. 2.8). The results showed no clear concurrent upward trend for both NO_3-N and Cl. However, the negative slope estimators for both parameters (NO_3-N and Cl) in all areas except the eastern area generated a high correlation of 0.88. The decrease of the both NO_3-N and Cl concentration could be caused by a reduction of contaminant loadings on the water at the wells. Visser et al. (2007) and Hansen et al. (2011) showed that increasing trends of NO_3-N were reversed to downward trends after specific time periods when water quality managements (reduction of fertilizer usages, rearrangement of wastewater storage and treatment facilities in the rural areas and livestock houses) had been initiated. In the study area, an abnormal growth of citrus was occurred in 1995, which was resulted from over-accumulation of fertilizer components in soils from the excessive usages of chemical fertilizers for a long time. In order to solve the problem, an extensive management action to reduce the chemical fertilizer usages has been in place since 1996 (MAFRA, 2001). As part of the action, the application rate of chemical fertilizers of the island has been reduced dramatically since 1997 as shown in Fig. 2.9. More than half of the wells having the decreasing

trends of the NO_3-N and Cl concentrations are in areas of citrus orchards, and such reduction of the fertilizer usages was likely to cause lowering the NO_3-N and Cl concentrations at those wells.

In the eastern area, the NO_3-N concentrations tended to increase over time, accompanied by decreasing trends in Cl concentrations (Fig. 2.8). Koh et al. (2007) identified a relationship between NO_3-N and Cl concentrations in the groundwater of Jeju that were affected by anthropogenic contamination, and showed the concentration ratio of Cl/NO_3-N as 1.50 (Fig. 2.3). At those wells showing increasing trends of NO_3-N and decreasing trends of Cl, agricultural activities were expected to cause the increase of the NO_3-N concentration (Sen's slope estimators of NO_3-N: 0.04–0.25 mg/L per year). Therefore, the rate of increase in the Cl concentration could be estimated as increasing with the rate of 0.06–0.38 mg/L per year based on the ratio of 1.50 from Koh et al. (2007). However, the actual analyzed slopes of the long-term Cl concentration data using the Sen's method in this study had a range of −4.83 to −0.29 mg/L per year, showing a significantly larger decrease in magnitude. This result implies the involvement of a process that caused the Cl concentrations of groundwater to decrease predominantly over time against the effects of expansion of agricultural lands, which caused the upward trends of NO_3-N in the eastern part.

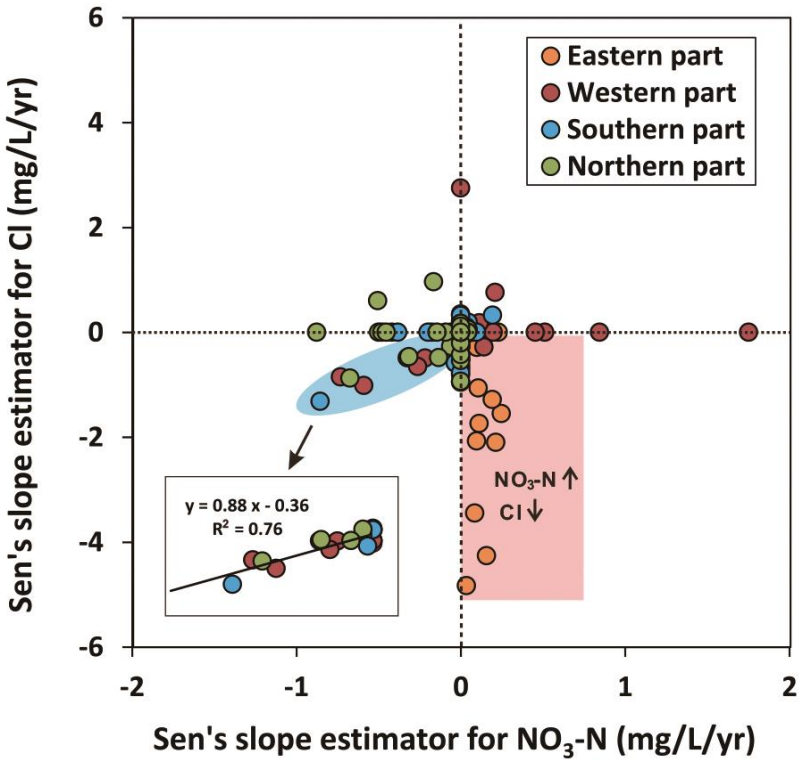

Fig.2.8. Sen's slope estimators of NO_3-N versus that of Cl.

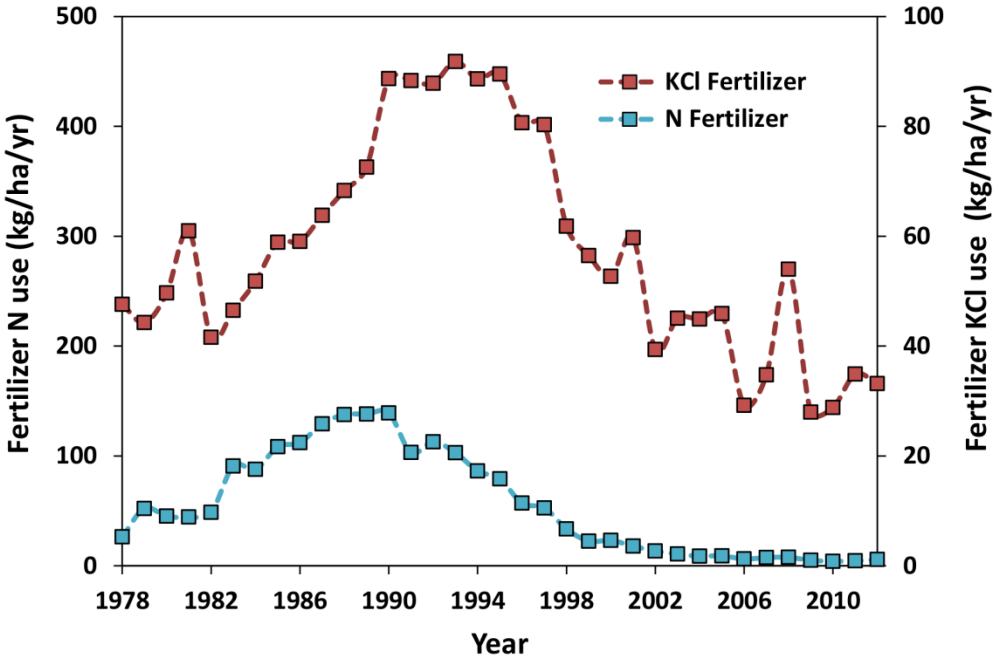

Fig.2.9. Annual usages of N and KCl fertilizers in Jeju Island from 1978 to 2012 (Jeju statistical yearbooks, 1984~2013).

Cl trends and groundwater management

Groundwater pumping near the coastal area has been shown to have caused lowering the groundwater levels, leading to seawater intrusion into fresh aquifers (Calvache and Pulido-Bosch, 1997; Bear et al., 1999; Mtoni et al., 2013). In the coastal fractured aquifer of Korea, intensive pumping has induced a decrease in the groundwater level and an increase in the electrical conductivity (EC), as shown by time series analysis (Park et al., 2012). Therefore, a commonly suggested management plan for preventing seawater intrusion is to control the pumping amount from coastal wells (FAO, 1997; Barlow, 2003). Barlow (2003) reported that a mandatory reduction in groundwater withdrawal in the New Jersey coastal plain, where large groundwater level declines were created by excessive groundwater pumping, resulted in groundwater level increases that in turn lessened the impacts of seawater intrusion into the fresh aquifer in the area. Such effective regulation for preventing seawater intrusion was also needed in the coastal aquifer of eastern Jeju Island.

Highly saline groundwater was reported in the eastern area when groundwater was first developed in that area (Han and Shin, 2000; Jeju Special Self-Government and JDI, 2012). Uncontrolled well installations and excessive withdrawals of groundwater intensified the deterioration in groundwater quality in relation to the high Cl content in the area. To prevent the depletion of groundwater and the intrusion of seawater due to the lack of regulations on groundwater use on Jeju Island, a groundwater permit system

was enacted into a special law on the island in 1991. Since 1991, installation and use of groundwater wells have been permitted by the Jeju Municipal Government based on an environmental impact assessment. Groundwater extraction from 24 wells in the eastern area (Figs. 2.10a and 2.10b) showing enriched Cl concentrations of 262–2,018 mg/L was suspended in 1991–2003; the total approved pumping rate was 40,444 m^3/day with 1,616 m^3/day per well (Jeju Special Self-Government and JDI, 2012). The approved pumping rate from the wells, which were newly installed since 1991, was decreased to 370 m^3/day per well after the groundwater regulations were enacted to control well installations and pumping rates in this area (Fig. 2.10b). The monthly averaged water levels in 1994 ~ 1999 were recorded (Koh, 1997), and the daily averaged water levels in 2004 ~ 2012 were monitored by the Institute of Water Resources of the Jeju Special Self-Governing Province (Institute of Water Resources, 2013). By using these data, the long-term changes in groundwater levels at five monitoring wells such as PD, SD, JD2, GS, and SS1 of the eastern area (Fig. 2.10a) were plotted in Fig. 2.10c. The changes in the average groundwater Cl concentrations at the wells showing upward trends in NO_3-N and downward trends in Cl in the eastern area (Fig. 2.8) are also presented in Fig. 2.10c. The annual groundwater levels increased slightly since 1994 with an abrupt decrease in the mean Cl concentration. Essentially, the strict restriction of groundwater development in the eastern area since 1991 has reduced the effect of seawater intrusion on groundwater quality, as supported by the less frequent occurrence of high Cl concentrations in the groundwater in this area.

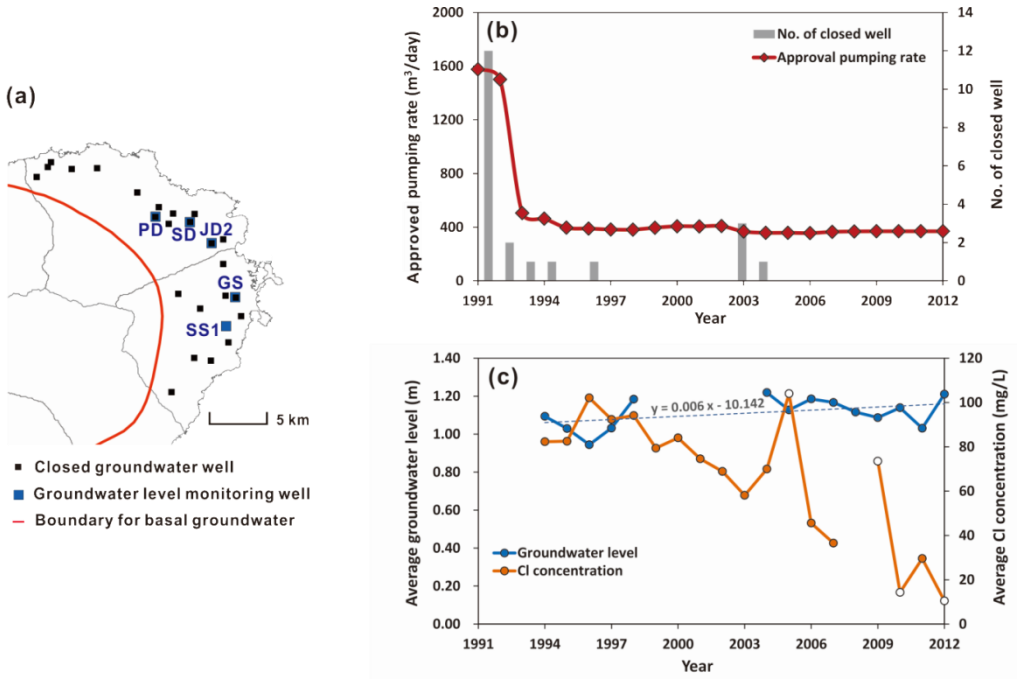

Fig. 2.10. (a) Location map of groundwater level monitoring wells (PD, SD, JD2, GS, and SS1) and closed wells in the eastern area; (b) approved pumping rate per well located at elevations lower than 100 m in the eastern area and the number of closed wells in 1991–2012; (c) average groundwater levels above sea level at the monitoring wells in 1994–2012 and average groundwater Cl concentrations at the wells which have downward (upward) trends in NO_3-N (Cl) of the eastern area. Open circles represent datasets less than 10.

The Jeju Municipal Government has imposed several management regulations to prevent NO_3-N contamination of groundwater on the island. For example, installation of groundwater wells within 20–200 m from septic tanks, waste treatment facilities, and animal farms is prohibited. Moreover, the requirement of annular space grouting was introduced as a well construction standard by the Jeju Special-Self Governing Province in 2004 to prevent the inflow of poor-quality surface water or contaminants into aquifer systems through the annulus between the drilled hole and the casing. Despite the regulations, upward trends in NO_3-N concentrations are expected to occur in the island through this study due to the increase of the agricultural lands with excessive application of synthetic fertilizers. In Jeju Island, there have been no specific regulations that limit the fertilizer use in agricultural lands for preventing the NO_3-N contamination in groundwater. Assessment of the N-mass balance or N-leaching rates from various agricultural systems is a prior step to determine the optimal application rates of fertilizers for protecting the water quality in the aquifer (Stites and Kraft, 2001; Gheysari et al., 2009; Constantin et al., 2010; Mishima et al., 2011; Bouraoui and Grizzetti, 2014). However, the N-mass balance has not been discussed in consideration of various agro-ecosystems of the island, although a wide range of N-leaching percentages (9.6%–50.8%) to the N-input mass by fertilizing (4.0-22.5 kg-N/ha) has been revealed by limited numbers of lab-scaled studies (Kang and Song, 2001; Lee et al., 2003). Therefore, based on the comprehensive understanding of N dynamics on the island, limitations on the application of fertilizers in agricultural areas are needed to

establish effective management plans for mitigating groundwater contamination by NO_3-N in the study area.

2.5 Conclusions

The results of the trend analysis in this study indicated that groundwater contamination by NO_3-N occurred across the island and in some places was increasing, whereas the concentration of Cl did not increase. The upward trend in the NO_3-N concentration was related to the expansion of agricultural land where the contaminants were discharged into the subsurface whereas the transition from agricultural to urban land use had a positive effect on the groundwater quality. In the eastern part of the island, opposite trends in NO_3-N and Cl concentrations were observed. The upward trend in NO_3-N concentration was caused by the increase in agricultural land use, whereas the downward trends in Cl concentrations were closely related to the groundwater management regulations enforced in the Jeju Province since 1991 to control with the seawater intrusion on the eastern side of the island. Comprehensive interpretation of trends in Cl along with NO_3-N and land use changes provided useful information associated with identifying regions of the island in which land development control is needed to protect groundwater resources. Along with the successful regulations on the saline groundwater in the eastern part of the island, effective management plans to reduce the NO_3-N contamination should be established for a sustainable use of the groundwater resource in the island.

Chapter 3. Leaky well impacts on the nitrate contamination in a layered aquifer system

Abstract

From this chapter, a focused study related to the continuous deteriorating contaminants of NO_3-N in Jeju Island was conducted in the Gosan agricultural area, western part of the island. The Gosan study site is characterized by severe nitrate pollution since 1970s. The hydrogeological features of the area are composed of complex hydrogeologic settings as a layered aquifer system and groundwater wells penetrating the aquifers. From the previous study, poorly constructed wells were resulted in deterioration of groundwater quality by carrying surface contaminants into a deep subsurface aquifer system. In this study, the impact of leaky wells on groundwater contamination was quantitatively evaluated in a layered aquifer system of the Gosan agricultural fields, Jeju Island, Korea. I introduced a leaky-well module and a double-domain integration method to compute nitrate cross-contamination through a layered

aquifer system. The simulation results clearly revealed that the leaky wells rapidly degraded the water quality of the underlying aquifer by acting as a direct pathway for nitrate-rich shallow groundwater. The model results predicted that in order to decrease the NO_3-N concentration at the regional groundwater wells below the maximum contamination level (MCL), the maximum allowable fertilizer amount of Gosan would be 45%–65% of the currently applied fertilizer level, whereas sealing of the regional groundwater wells would rapidly decrease the NO_3-N concentration below the MCL without reducing fertilizer usage. Our study demonstrated that the well conditions and hydrogeological system play major roles in the occurrence of nitrate in the underlying aquifer in Gosan; therefore, a proper groundwater management plan against nitrate contamination should be established on the basis of a comprehensive understanding of the hydrogeologic system of the area.

3.1. Introduction

Nitrate contamination has been a global issue in terms of groundwater quality for a long time, because extensive fertilizer usage on agricultural land may induce excessive N-leaching into subsurface aquifer systems (Postma et al., 1991; Widory et al., 2004; Koh et al., 2006b; Stadler et al., 2008). Nitrate components are easily exported into the aquatic system because of their high solubility into water and low sorption capacity on soil particles. When humans drink water that contains high levels of nitrate, health problems such as methemoglobinemia in infants and stomach cancer can result (Wolfe and Patz, 2002). Therefore, many countries regulate the maximum content of nitrate to less than 50 mg/L as NO_3^- or less than 10 mg/L as NO_3-N in drinking water (Goodchild, 1998; EPA, 2010; WHO, 2011; ME, 2014).

The occurrence of nitrate in groundwater is highly influenced by the hydrogeologic setting of the area. In general, shallow groundwater is more susceptible to nitrate contamination than deep groundwater because shallow aquifers are readily affected by leaching of surface contaminants (Spalding and Exner, 1993; Nolan and Stoner, 2000; Böhlke, 2002). In a layered aquifer system consisting of an upper shallow and a lower deep aquifer interbedded with an aquitard, nitrate barely reaches the underlying aquifer because the intervening aquitard acts as a barrier to prevent downward migration of surface contaminants. However, when the middle aquitard is penetrated, or when the shallow groundwater travels vertically through improperly constructed wells,

additional contamination of nitrate can occur in the underlying aquifer (Spalding and Exner, 1993; Santi et al., 2006).

Improperly constructed wells can rapidly degrade the water quality of an underlying aquifer by acting as a conduit for surface contaminants (Fig.3.1; Spalding and Exner, 1993; Church and Granato, 1996; Jiménez-Martínez et al., 2011; Koh et al., 2012). Several studies have discussed the influence of leaky wells on contaminant transport in multi-layered aquifer systems based on numerical interpretation (Reilly et al., 1989; Avci, 1992; Elci et al., 2001; Konikow and Hornberger, 2006; Landon et al., 2010). These studies noted that the amounts of water and solutes passing through a leaky well was significant and could result in cross-contamination of aquifers. However, there has been less effort on quantitative assessment of the effects of leaky wells on the groundwater contamination at the field scale. A complex hydrological setting of the layered aquifer system and leaky well hydraulics has restricted field-scale applications of numerical approach. Dragon et al. (2009) applied a numerical approach to explain aquifer cross-contamination via a leaky well at the field scale; however, in their model, the water leakage rate through the leaky well was simply inferred on the basis of the amount of groundwater usage, and the hydraulic connection between upper and lower aquifers via the leaky well was not considered in detail.

The Gosan area of Jeju Island, South Korea, is characterized by a layered aquifer system consisting of upper perched and lower regional aquifers separated by an

impermeable clay layer. Intensive cultivation activities in this area have led to severe nitrate contamination of both the perched and the regional aquifer (Koh et al., 2012). Elevated nitrate concentration in groundwater is a major issue, especially in the regional aquifer because it is the main source of potable and agricultural water for Jeju Island. A previous study (Koh et al., 2012) in the Gosan area observed great improvement of water quality in the regional aquifer after re-grouting a leaky well, and it concluded that aquifer cross-contamination through improperly constructed wells is the main cause of highly elevated nitrate concentrations.

To suggest an efficient management plan to protect the aquifer environment against nitrate contamination in the Gosan area, it is necessary to quantify the process of nitrate migration through the leaky wells. However, it was impossible to measure the leakage rate directly because all the groundwater wells in the study site are in use for supplying water to agricultural activities. In this case, an integrated investigation combining field measurements and a numerical approach can provide an alternative method to identify the sources of nitrate and to suggest an adequate groundwater management plan.

The objectives of this study are 1) to develop a new numerical model (double-domain approach) to simulate nitrate transport considering well leakage in the layered aquifer system; 2) to evaluate the impacts of the leaky wells on contamination of the underlying aquifer; and 3) to suggest a reasonable management direction to lower the

nitrate concentrations of the Gosan area. This study initially adopted a double-domain integration approach to represent leaky well dynamics in a layered aquifer system. The developed model was calibrated using field measurements and applied to assess the pathway of nitrate movement in the study site. Finally, the model was applied to predict the distribution of nitrate contamination under different remediation scenarios. This study will provide a useful tool for sustainable management of groundwater resources against cross-contamination by nitrate in multi-layered aquifer systems.

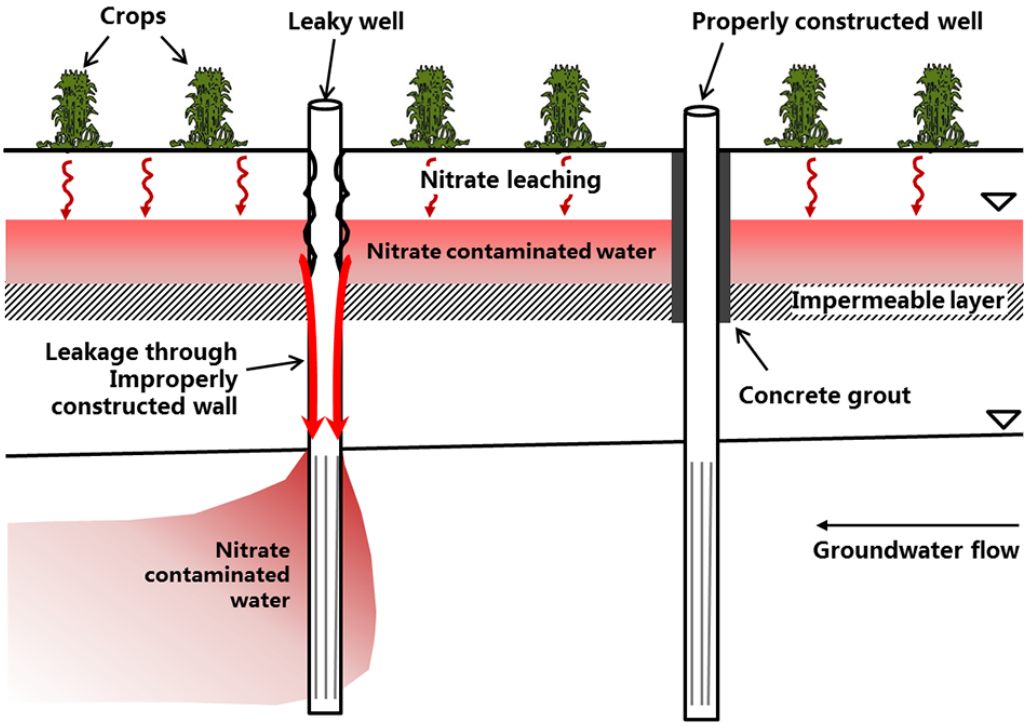

Fig.3.1. Schematic diagram of nitrate transport pathways in leaky and properly constructed wells in the layered aquifer system.

3.2 Study area description

The Gosan area is located in the Hankyung watershed in the western part of Jeju Island (Figs.3.2a and 3.2b). The study area is located on a flat lowland with an altitude of 0–114 m above mean sea level. The average precipitation rate at the Gosan weather station during 1992–2012 was 1151 mm/yr. Significant variation in the seasonal precipitation was observed in Fig.3.3: on average, 73% of annual precipitation was concentrated during the wet season between April and September (Korea Meteorological Administration, 2014). Significant variation in annual precipitation was observed in the study area and also, most precipitation was concentrated at the summer season because a climate of Korea is controlled by the seasonal wind. Previous studies in the Hankyung watershed reported that 39%–46% of total precipitation infiltrated into the subsurface to recharge the groundwater (Hahn et al., 1994; Won et al., 2006; KIGAM, 2011).

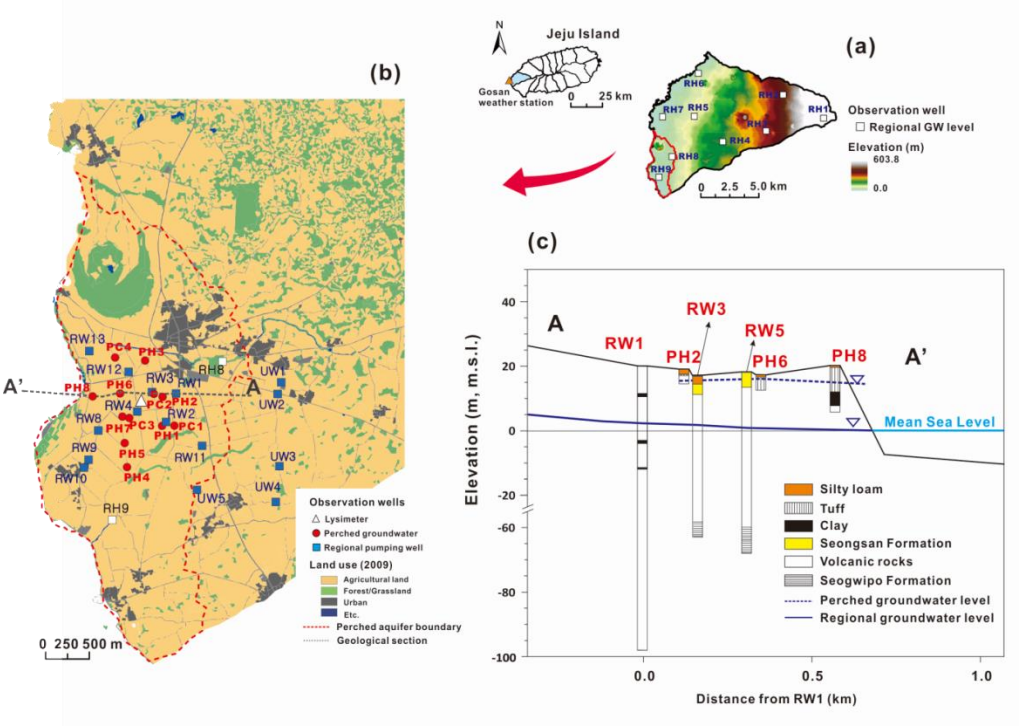

Fig.3.2 Location map of the Hankyung watershed showing the locations of the Gosan weather station and monitoring wells for regional groundwater levels (a), map of the Gosan area with observation wells, pumping wells, and land use information (b), and geological section A–A' (c).

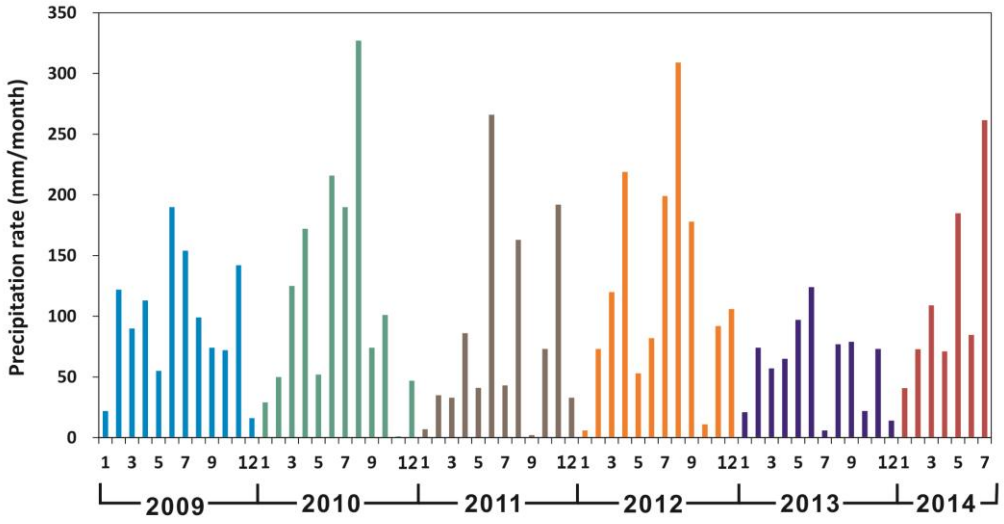

Fig.3.3 Monthly precipitation rate at the Gosan weather station during 2009~2014.

Hydrogelogical settings

As shown in the geological cross-sectional map of Fig.3.2c, the subsurface geology of the study area mainly comprises silty loam, tuff, clay beds, volcanic rocks, and the Seogwipo Formation. The top soils at 22 groundwater wells in the study area are mainly composed of silty loam with a thickness in the range of 0.5–9.0 m (average: 2.2 m). The tuff, which underlies the silty loam layer, is made up of substances from the Suwolbong tuff ring deposit and has a maximum thickness of 10.2 m (well RW13). Outcrop studies revealed that the Suwolbong tuff ring deposit layer is composed of lapillis, volcanic sand, and blocks that lie on top of a clay bed. This underlying impermeable clay bed, which is found at outcrops at the Jagunae port and Suwolbong coast and is typical for the Gosan area, is an important aquitard on top of which the perched groundwater accumulates. The impermeable clay beds were observed at the perched aquifer wells with a thickness of 0.4–1.2 m. Also, the clay was observed in the regional groundwater wells with a thickness of 2.3–11.7 m and was identified as the Seongsan Formation, which was defined as a mixture of tuff and clay in the well log data. A thick package of porous volcanic rock underlies the tuff and clay beds; the volcanic rock, which is composed of several lava flow sequences, is distributed between 1.5 and 11.0 m below surface and continues to ~40–60 m below sea level. This layer has a high permeability due to its numerous joints, vesicle, clinkers, and fractures (Won et al., 2006). The thick sedimentary Seogwipo Formation underlies the highly permeable volcanic rocks with top depths ranging from 37 to 100 m below sea

level. The Seogwipo Formation consists of gravelly sandstone, sandstone, sandy mudstone, mudstone, hyaloclastite, and shell fossils (Koh, 1997). The subsurface distribution of the Seogwipo Formation plays an important role in the distribution and occurrence of groundwater reservoirs in Jeju Island (Koh, 1997).

It was reported that the two layered aquifer system (i.e., perched and regional aquifers) is locally occurred in the study area due to the distribution of impermeable clay layers. UNDP and FAO (1972) found existence of the perched groundwater above the clay layer in the study area and the perched groundwater infiltrates downward and then it flows westward to the seepages along the sea cliffs. There is possibility for the perched groundwater to flow through gaps and weaknesses in the clay layer. Below the clay layer, the regional groundwater, which is the main aquifer system for water use in the island, is mainly located at the volcanic rocks layer. A perched aquifer occurs between the silty loam and a tuff/clay layer with the water table from 0.44 to 4.13 m below the surface. A regional aquifer is present underneath the perched aquifer and has a water table ranging from 11.80 to 24.35 m below the surface. Mean hydraulic conductivity of top silt loam and tuff layers was measured as 6.43E-6 m/sec (Koh, 2011) and that of volcanic rocks was 3.14E-4 m/sec (Won et al., 2006). To fully understand the hydrogeological process in the Gosan site, the presence of the perched aquifer should be considered.

Land uses

In this area, agricultural fields are distributed broadly resulting from readjustment of arable land in 1970s. Therefore, agricultural lands (cropfield, orchard, and greenhouse) are abundantly located as 74.3% of the total study area (34.39 km^2) in 2009 (Fig.3.2b). Other major categories of land uses like urban (3.2%), forest (5.8%), and grassland (10.3%) take minor proportions compared to the agricultural lands. Among the types of agricultural lands, crop field is extensively located as having 67.9% percentage of total area. Major crops are rice, bean, and sesame in summer season (April ~ October) and garlic, anion, radish, and cabbage in winter time (November ~ March) by using two crops per a year cultivation method. Regional groundwater pumping wells (Fig.3.2b) lined with PVC pipes were constructed between 1970 and 1980 in the Gosan area, and most of these wells are currently used for agricultural purpose (Jeju Water Resources Management Office, 2001). With the increase in agricultural fields, more chemical fertilizers have been used as well. A survey of annual fertilizer usage in the cultivated area showed the nitrogen loading of the study area to be very high with a value of 628 kg-N/ha (Koh et al., 2012), which is 3.7 times higher than the average usage of Jeju Island (171 kg-N/ha; Jeju Special Self-Governing Province, 2009).

General hydrogeochemical characteristics

Statistical information of water chemistry for perched and regional groundwater samples which were collected in 2009~2011 is generated at Tables 3.1 and 3.2. High average values of the electrical conductivity (EC) in the perched groundwater samples represent that dissolved ions are significantly distributed in the perched groundwater. Higher concentrations of HCO_3^-, Cl^-, NO_3-N, SO_4^{2-}, Na^+, Mg^{2+} and Ca^{2+} ions in perched groundwater samples, which related to the water quality affected by chemical fertilizers and manure (Frapporti and Vriend, 1993; Puckett and Cowdery, 2002; Kaown et al., 2009), are observed. The perched groundwater is severely contaminated by nitrate, average NO_3-N concentrations in all the 12 perched groundwater samples exceed the standard of drinking water as 10 mg/L of NO_3-N and 10 samples show higher average values of NO_3-N greater than 20 mg/L of NO_3-N as standard for agricultural use.

The average NO_3-N of total regional groundwater samples for the monitoring period in this study is observed as 11.8 mg/L (standard deviation: 8.1 mg/L), which is higher than standard of drinking water. Twelve wells of total 15 regional groundwater wells are deteriorated its water quality by nitrate showing higher average NO_3-N concentrations as >10 mg/L and the average NO_3-N concentrations in two wells are detected greater than 20 mg/L. Major dissolved constituents in the regional groundwater samples represent different chemical properties among wells (Table 3.2).

To delineate water types and similarities or differences in composition between the perched and regional groundwater samples, a Piper diagram is generated by using average values of each ion in the Tables 3.1 and 3.2 (Fig.3.4) and the size of circles is proportional to the average NO_3-N concentrations. Water samples in the regional groundwater are divided into three groups as 1) (Na, Mg)-HCO_3, 2) (Mg, Ca)-(HCO_3, Cl) and 3) Na, (K-Cl) water types. The group 1 of regional groundwater samples is characterized by low averaged concentration of NO_3-N below 3 mg/L as the upper limit of naturally occurring nitrate (Burkart and Kolpin, 1993; Babiker et al., 2004). The group 2 shows higher NO_3-N values and the samples in the Piper diagram are plotted similar to that in the perched groundwater samples. In the group 3, salinization of regional groundwater is observed along with the elevated NO_3-N concentrations.

The spatial distribution of the NO_3-N and Cl^- concentrations in the respective aquifers is shown in Fig.3.5. There are distinct differences in the spatial distribution of the NO_3-N concentrations of the perched and regional groundwater. The NO_3-N concentrations were higher in all perched groundwater samples, whereas the NO_3-N concentrations in the regional groundwater samples were lower at several wells (RW13, RW12, RW2) below 3 mg/L. Chloride ion did not show much spatial variations compared to NO_3-N composition but, at several regional wells, located in the westsouthern part of the study area, the enriched Cl cocentration of groundwater was observed.

Table 3.1 Statistical information of hydrogeochemical parameters of the perched groundwater (2009~2011).

Well ID	Elevation (m)	Well Depth (m)	Depth to water (m)	Temp. (°C)	EC (μS/cm)	DO (mg/L)	pH	ORP (mV)	HCO_3^- (mg/L)	Cl^- (mg/L)	NO_3-N (mg/L)	SO_4^{2-} (mg/L)	Na^+ (mg/L)	K^+ (mg/L)	Mg^{2+} (mg/L)	Ca^{2+} (mg/L)
PC1	17.2	2.6	0.8† (±0.7) ‡	17.4 (±4.2)	1239 (±177)	2.8 (±1.6)	6.7 (±0.3)	171.8 (±66.7)	371.2 (±101.9)	159.9 (±27.1)	13.8 (±17.5)	58.2 (±11.8)	62.7 (±9.2)	1.1 (±0.9)	72.5 (±12.1)	75.4 (±14.0)
PC2	19.0	1.3	0.7 (±0.4)	17.8 (±5.7)	872 (±208)	5.8 (±0.8)	7.3 (±0.2)	175.6 (±33.0)	113.1 (±31.9)	81.8 (±19.3)	46.6 (±19.7)	45.5 (±6.0)	33.6 (±7.8)	1.4 (±0.8)	42.1 (±19.3)	67.3 (±15.0)
PC3	17.6	2.7	1.5 (±0.6)	17.5 (±3.4)	632 (±83)	6.4 (±1.1)	6.8 (±0.2)	169.7 (±75.3)	70.5 (±11.1)	59.9 (±8.3)	27.8 (±4.3)	49.9 (±3.2)	28.8 (±5.0)	1.3 (±0.7)	32.0 (±5.4)	31.6 (±6.1)
PC4	16.9	3.1	1.9 (±0.7)	17.8 (±3.5)	848 (±81)	5.6 (±0.7)	6.9 (±0.3)	153.4 (±63.1)	88.4 (±9.3)	72.6 (±11.6)	46.2 (±8.2)	50.4 (±12.6)	31.3 (±7.4)	1.8 (±1.1)	45.4 (±9.1)	45.5 (±10.5)
PH1	13.8	4.7	1.1 (±1.7)	18.0 (±4.4)	784 (±190)	0.7 (±0.5)	7.0 (±0.2)	153.5 (±76.9)	185.2 (±66.7)	110.2 (±70.2)	23.2 (±19.5)	101.8 (±39.8)	49.4 (±26.6)	10.2 (±4.5)	71.9 (±39.1)	73.0 (±32.7)
PH2	18.2	4.5	2.0 (±1.5)	18.7 (±4.4)	869 (±158)	5.1 (±3.0)	6.7 (±0.3)	164.0 (±78.4)	141.9 (±71.8)	119.9 (±24.1)	41.3 (±14.9)	93.9 (±15.7)	49.7 (±9.7)	1.4 (±0.6)	74.4 (±17.9)	72.9 (±8.1)
PH3	14.4	4.6	1.6 (±1.3)	16.9 (±3.6)	832 (±460)	1.1 (±1.7)	7.0 (±0.2)	104.1 (±80.5)	234.8 (±148.2)	114.4 (±50.9)	13.0 (±9.0)	148.2 (±102.8)	88.7 (±50.9)	8.8 (±5.5)	58.6 (±26.6)	62.5 (±29.5)
PH4	10.8	4.6	1.6 (±2.0)	21.1 (±3.5)	678 (±306)	1.0 (±0.7)	7.0 (±0.2)	114.3 (±84.7)	168.1 (±94.9)	114.1 (±36.2)	27.5 (±14.0)	60.5 (±13.8)	41.6 (±7.8)	1.7 (±0.7)	59.5 (±18.0)	57.7 (±14.4)
PH5	14.9	5.0	1.3 (±0.4)	18.0 (±3.2)	593 (±217)	2.0 (±1.9)	6.8 (±0.1)	155.5 (±86.3)	89.0 (±24.2)	62.2 (±16.9)	21.7 (±9.8)	65.7 (±18.2)	32.6 (±6.7)	2.8 (±1.2)	40.1 (±10.9)	40.2 (±12.6)
PH6	17.3	5.1	1.9 (±1.7)	18.5 (±3.8)	516 (±171)	4.8 (±1.6)	6.6 (±0.3)	161.2 (±76.4)	51.1 (±29.7)	57.2 (±11.8)	29.4 (±18.0)	48.1 (±2.8)	24.2 (±3.2)	1.1 (±0.3)	36.5 (±9.6)	35.2 (±9.8)
PH7	17.2	4.9	1.7 (±0.6)	18.3 (±3.1)	621 (±104)	3.9 (±1.9)	6.7 (±0.4)	163.0 (±35.8)	119.1 (±60.0)	62.4 (±10.8)	29.7 (±8.6)	64.6 (±5.8)	28.0 (±1.5)	1.4 (±0.6)	46.7 (±8.0)	45.8 (±8.0)
PH8	13.6	5.1	2.7 (±1.9)	17.5 (±1.5)	967 (±276)	5.2 (±1.2)	7.2 (±0.3)	119.9 (±57.2)	53.4 (±25.8)	101.6 (±18.4)	75.2 (±27.9)	77.3 (±10.7)	42.9 (±4.8)	5.9 (±1.2)	69.3 (±17.0)	74.5 (±22.6)
Perched groundwater			1.4 (±1.2)	17.7 (±3.8)	872 (±329)	3.6 (±2.5)	6.9 (±0.3)	154.6 (±63.7)	170.3 (±129.7)	95.9 (±53.2)	29.5 (±20.2)	55.5 (±29.8)	41.3 (±17.4)	2.3 (±5.1)	48.9 (±22.7)	55.4 (±24.1)

† Average value, ‡ Numbers in parenthesis represent standard deviation value.

Table 3.2 Statistical information of hydrogeochemical parameters of the regional groundwater (2009~2011).

Well ID	Elevation (m)	Well Depth (m)	Depth to water (m)	Temp. (°C)	EC (μS/cm)	DO (mg/L)	pH	ORP (mV)	HCO_3^- (mg/L)	Cl^- (mg/L)	NO_3-N (mg/L)	SO_4^{2-} (mg/L)	Na^+ (mg/L)	K^+ (mg/L)	Mg^{2+} (mg/L)	Ca^{2+} (mg/L)
RW1	20.0	118.0	17.2 (±1.6)	17.5 (±0.5)	268 (±61)	5.7 (±1.1)	7.4 (±0.5)	166.1 (±62.1)	62.8 (±13.4)	26.4 (±4.9)	9.4 (±5.1)	23.9 (±23.7)	19.4 (±1.2)	4.8 (±0.6)	14.8 (±5.0)	15.8 (±3.0)
RW2	16.0	80.0	12.7† (±1.5)‡	17.7 (±0.8)	169 (±24)	3.1 (±0.9)	8.4 (±0.1)	129.7 (±75.5)	44.1 (±30.6)	15.9 (±3.0)	1.6 (±0.2)	5.5 (±0.4)	22.8 (±2.8)	5.3 (±0.4)	6.8 (±2.7)	7.6 (±2.2)
RW3	19.0	82.0	16.2 (±1.7)	17.7 (±0.3)	296 (±68)	6.0 (±1.4)	7.5 (±0.5)	148.5 (±65.3)	58.9 (±14.3)	29.9 (±6.8)	11.6 (±5.3)	19.6 (±6.1)	20.5 (±1.3)	4.4 (±0.4)	16.5 (±5.3)	17.8 (±2.6)
RW4	17.0	70.0	-	16.7 (±0.9)	384 (±65)	7.2 (±1.3)	6.9 (±0.3)	180.1 (±67.9)	48.6 (±10.6)	35.6 (±5.5)	20.0 (±4.1)	27.2 (±7.9)	19.7 (±2.0)	4.4 (±0.7)	20.0 (±3.8)	21.1 (±4.6)
RW8	20.0	70.0	-	17.3 (±0.5)	836 (±503)	7.6 (±1.5)	7.2 (±0.2)	150.4 (±71.6)	62.1 (±15.2)	183.0 (±184.7)	18.0 (±8.0)	48.8 (±32.9)	84.5 (±78.2)	7.6 (±4.8)	35.7 (±17.2)	31.7 (±11.2)
RW9	16.0	80.0	-	17.4 (±1.1)	1839 (±967)	5.9 (±1.6)	6.9 (±0.1)	129.9 (±40.9)	48.2 (±13.1)	468.1 (±370.7)	14.5 (±4.6)	87.2 (±53.8)	174.4 (±128.5)	13.4 (±8.1)	60.9 (±34.1)	54.8 (±27.8)
RW10	16.0	80.0	13.2 (±4.4)	16.3 (±3.3)	1170 (±722)	6.1 (±0.9)	7.1 (±0.2)	147.1 (±80.0)	64.3 (±33.1)	264.9 (±258.7)	17.5 (±3.8)	64.0 (±43.2)	133.4 (±117.6)	7.9 (±4.2)	45.3 (±24.4)	47.9 (±32.3)
RW11	20.0	85.0	16.3 (±1.5)	17.4 (±0.2)	289 (±45)	5.7 (±0.6)	7.3 (±0.4)	147.5 (±124.1)	50.4 (±19.3)	25.9 (±4.2)	12.2 (±3.6)	16.6 (±2.1)	18.4 (±1.2)	4.3 (±0.7)	14.9 (±0.6)	15.5 (±0.9)
RW12	17.0	90.0	14.8 (±0.6)	18.2 (±0.6)	201 (±22)	4.2 (±1.5)	8.3 (±0.3)	127.1 (±62.9)	68.4 (±16.3)	20.2 (±1.7)	2.2 (±1.2)	6.6 (±2.4)	21.1 (±1.7)	4.8 (±0.5)	7.5 (±3.2)	9.7 (±2.0)
RW13	17.0	85.0	13.3 (±4.8)	17.4 (±1.2)	182 (±36)	3.4 (±0.8)	8.5 (±0.3)	139.3 (±65.2)	69.8 (±18.4)	19.1 (±1.9)	1.8 (±1.0)	5.7 (±1.1)	21.2 (±1.3)	4.7 (±0.3)	7.0 (±3.3)	9.5 (±2.9)
UW1	30.0	90.0	24.5 (±5.4)	16.5 (±0.7)	321 (±57)	7.2 (±1.3)	7.0 (±0.2)	164.1 (±61.7)	40.3 (±9.7)	31.0 (±3.6)	17.1 (±3.6)	21.6 (±2.9)	17.9 (±1.3)	4.2 (±0.5)	17.9 (±3.3)	17.0 (±3.4)
UW2	29.0	80.0	21.8 (±9.2)	17.0 (±0.7)	298 (±49)	6.9 (±1.0)	7.0 (±0.3)	124.7 (±61.0)	37.1 (±11.6)	28.9 (±4.1)	15.1 (±2.3)	20.0 (±2.6)	17.9 (±2.9)	4.0 (±0.6)	16.2 (±3.0)	15.6 (±3.2)
UW3	31.0	90.0	-	16.7 (±0.8)	306 (±48)	6.5 (±0.0)	7.2 (±0.4)	80.2 (±0.0)	44.5 (±14.1)	27.6 (±3.3)	14.9 (±2.9)	18.2 (±5.2)	16.2 (±1.8)	3.6 (±0.2)	15.1 (±3.1)	16.8 (±1.5)
UW4	33.0	100.0	31.7 (±1.1)	16.9 (±1.0)	415 (±60)	6.3 (±0.0)	6.9 (±0.3)	153.2 (±131.1)	39.4 (±10.0)	38.5 (±3.9)	25.3 (±6.5)	29.0 (±4.2)	20.7 (±2.0)	4.2 (±0.2)	26.7 (±4.6)	28.0 (±6.2)
UW5	18.0	100.0	-	17.5 (±0.8)	301 (±61)	6.4 (±1.9)	7.3 (±0.3)	125.3 (±67.9)	56.6 (±19.5)	26.5 (±5.1)	13.5 (±6.0)	18.7 (±5.9)	19.0 (±3.6)	3.8 (±0.5)	16.1 (±3.9)	16.2 (±3.9)
Regional groundwater			15.8 (±5.6)	17.3 (±1.2)	416 (±436)	5.7 (±1.9)	7.5 (±0.7)	145.6 (±66.3)	56.1 (±20.1)	68.0 (±140.3)	11.8 (±8.1)	25.2 (±28.2)	39.9 (±61.8)	5.3 (±3.1)	19.6 (±17.4)	20.2 (±16.6)

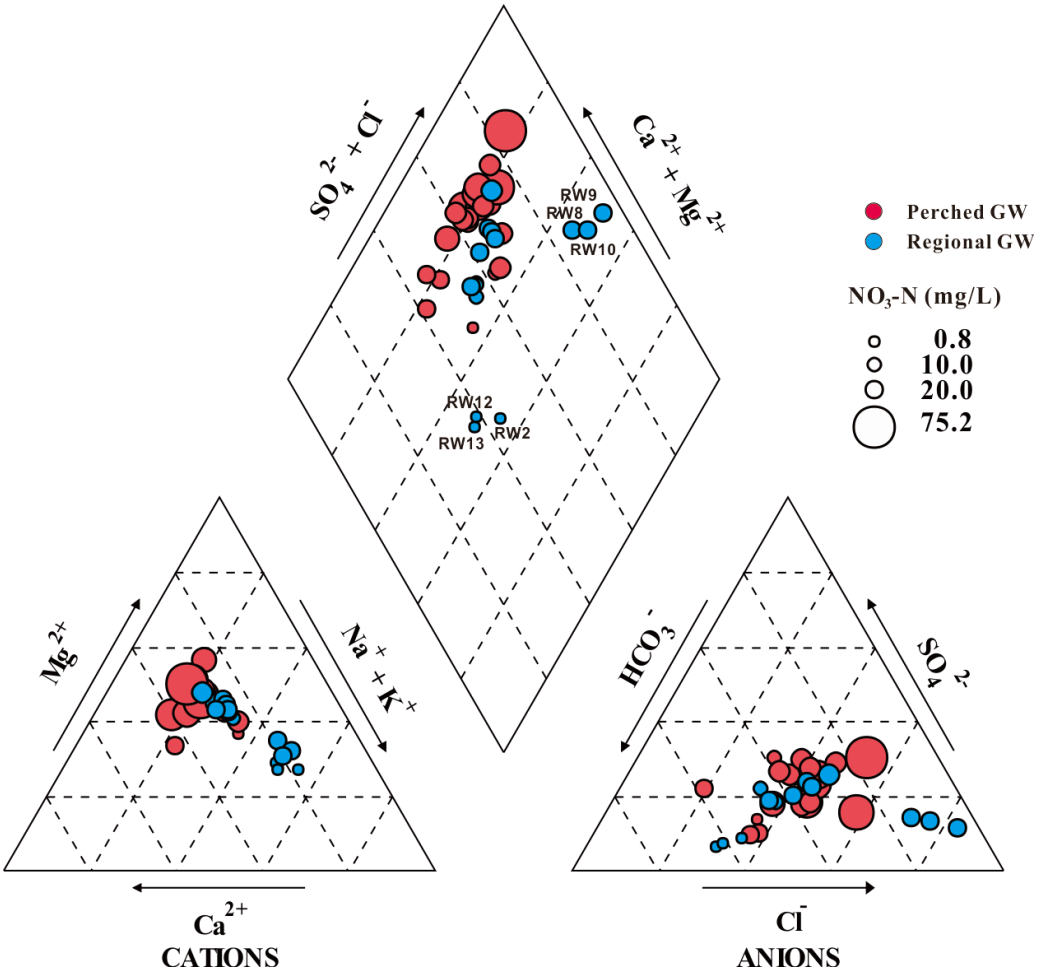

Fig.3.4. Piper diagram of the perched and regional groundwater.

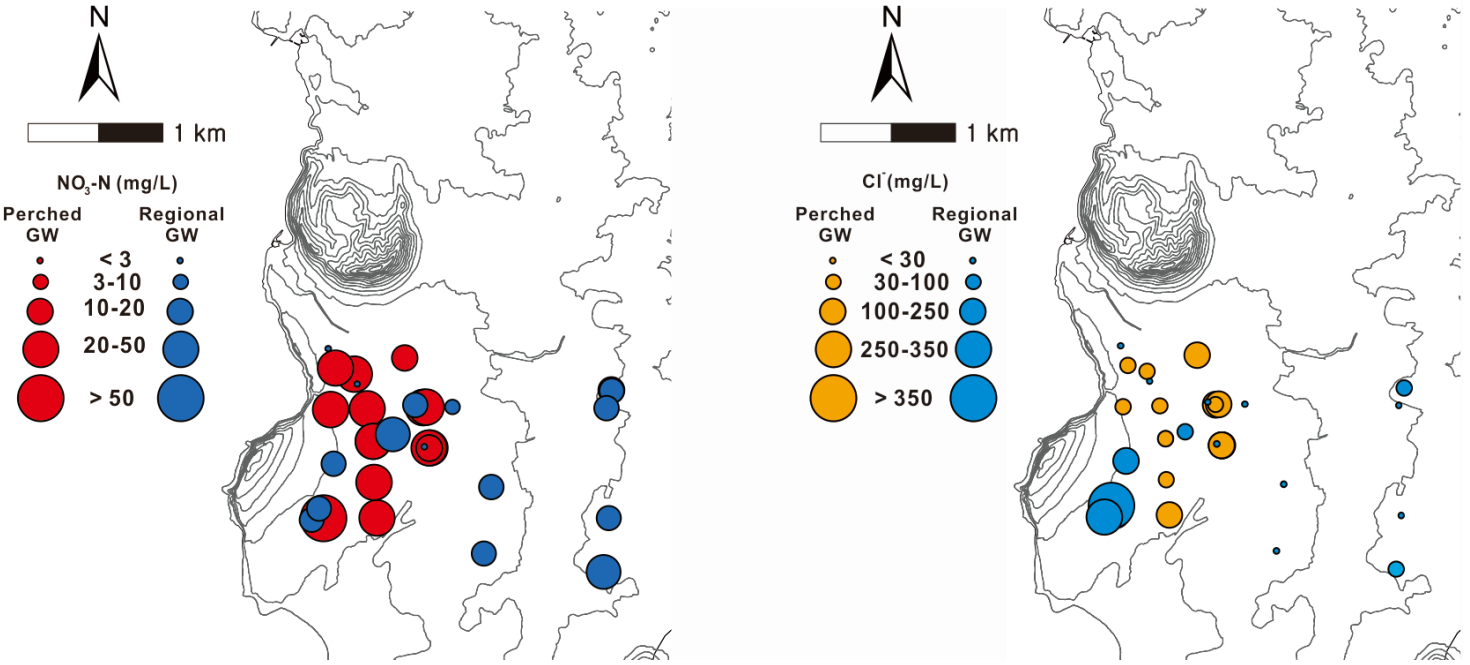

Fig.3.5. Spatial distribution of the average NO_3-N (left) and Cl^- (right) concentrations in the perched and regional groundwater.

Temporal variations of the NO_3-N concentrations

To assess the temporal variability of the NO_3-N concentrations, graphs of the NO_3-N concentration versus time are presented in Fig.3.6. In the perched groundwater, the NO_3-N concentration fluctuated significantly during the monitoring period (PC1: 15.1±6.3 (average±standard deviation) mg/L, PC2: 40.7±18.0 mg/L, PC4: 46.3±8.2 mg/L, and PH8: 16.8±4.6 mg/L). In the regional groundwater, the NO_3-N concentrations also fluctuated with time but the variations were relatively small compared to those of perched groundwater (RW1: 9.7±4.8 mg/L, RW2: 1.5±0.2 mg/L, RW3: 12.3±5.6 mg/L, RW10: 18.5±3.6 mg/L, RW12: 2.6±1.3 mg/L, RW13: 2.0±1.0 mg/L and UW1: 15.9±1.6 mg/L). The three wells RW2, RW12 and RW13 had NO_3-N concentrations <3 mg/L and little variability in the NO_3-N concentration throughout the monitoring period. Other regional groundwater wells (RW1, RW2 and RW10) which had higher NO_3-N concentrations showed marked changes of NO_3-N concentrations due to precipitation events. This seems to indicate that in some areas fertilizer-derived contaminants such as nitrate rapidly affect the regional aquifer depending on precipitation events. The fact that not all regional groundwater wells are equally affected demonstrates that the infiltration pathways of nitrate contaminants into the regional groundwater differ in the various areas of the study resulting in different levels of nitrate contamination of the regional groundwater.

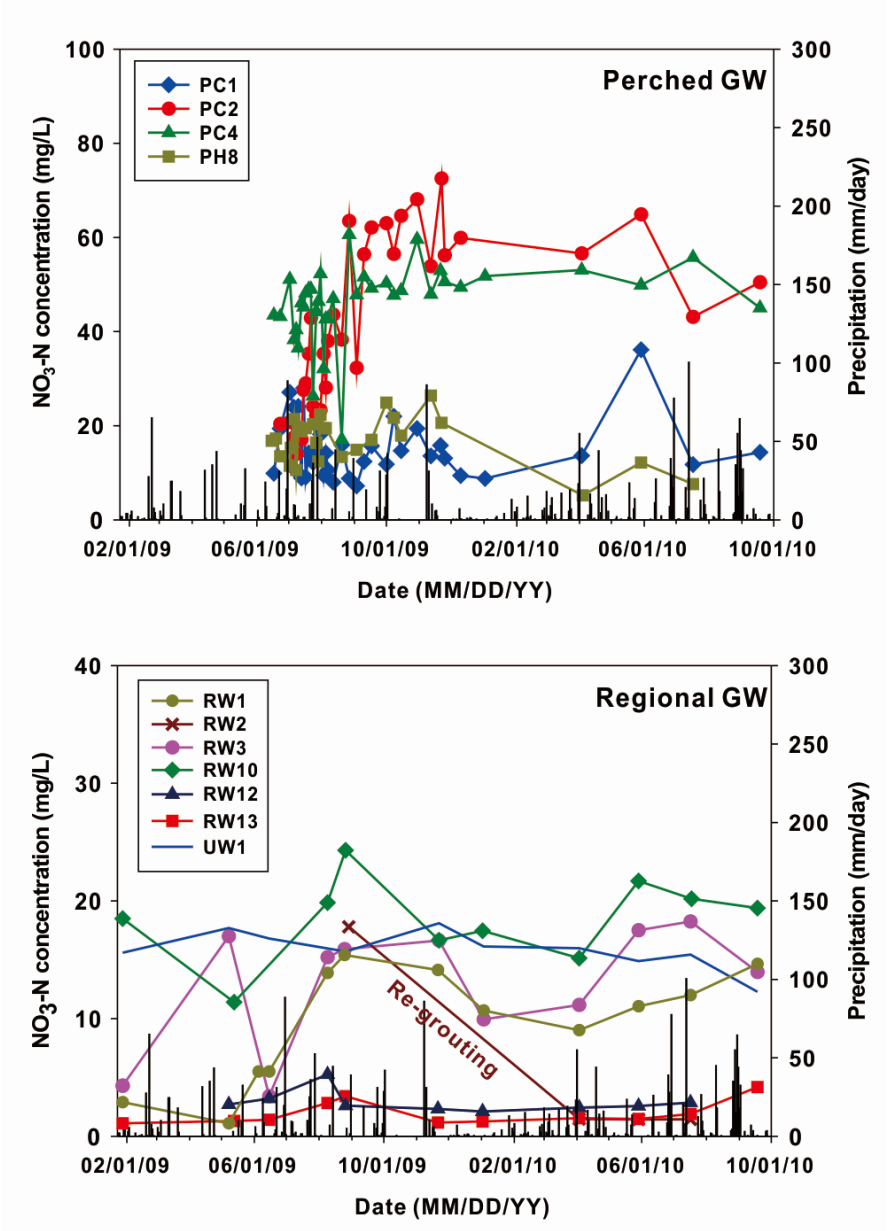

Fig.3.6. Temporal variations of the NO_3-N concentrations in perched and regional groundwater wells. At the RW2 well of the regional groundwater, the effect of re-grouted well casing is observed.

Denitrification process

Denitrification causes decreased NO_3-N concentrations and increased $\delta^{15}N$ and $\delta^{18}O$ values in the aquifer because the remaining nitrate becomes progressively enriched in ^{15}N and ^{18}O (e.g., Böttcher et al., 1990). Fig. 3.7a shows that nitrate in several samples from the perched aquifer (May, 2010; Mar., 2014) was characterized by elevated $\delta^{15}N$ and $\delta^{18}O$ values, which suggest that denitrification occurred. For denitrification to occur, DO concentrations below 2 mg/L are typically required (e.g. Cey et al., 1999). Dissolved oxygen concentrations of less than 2 mg/L were observed at the several perched groundwater wells (Fig. 3.7b). In contrast, the DO concentrations in the regional groundwater were greater than 2 mg/L (Fig. 3.7b); correspondingly, the $\delta^{15}N$ and $\delta^{18}O$ values of the nitrate were not elevated suggesting no denitrification in this aquifer. Usually, the anoxic condition is expected for the deep regional aquifer system rather than the shallow perched aquifer. In the Gosan study area, the oxic condition was observed in the regional aquifer oppositely due to the major geologic condition of porous volcanic rocks in Jeju Island. Plummer et al. (2000) demonstrated that high DO condition could be distributed in fractured-rock systems by barometric pumping which induces appreciable movement of atmospheric air into the deep subsurface.

In the perched aquifer, high concentration of DOC was detected over 1 mg/L (Fig. 3.7b), in which lower DOC levels were shown in the regional groundwater (< 1 mg/L). At the several perched groundwater wells, depleted DO level was occurred to initiate

the denitrification redox process. High HCO_3^- concentrations can indicate denitrification (Trudell et al., 1986; Böhlke, 2002) because HCO_3^- is produced by denitrification fueled by organic carbon. The HCO_3^- concentrations in samples from the perched groundwater wells showing the denitrification reduction were elevated (151~395 mg/L) compared to those of the other perched or regional groundwater samples (8~122 mg/L). This confirms that organic matter facilitates the conversion of nitrate to N_2 in the perched aquifer when conditions are suitable for denitrification.

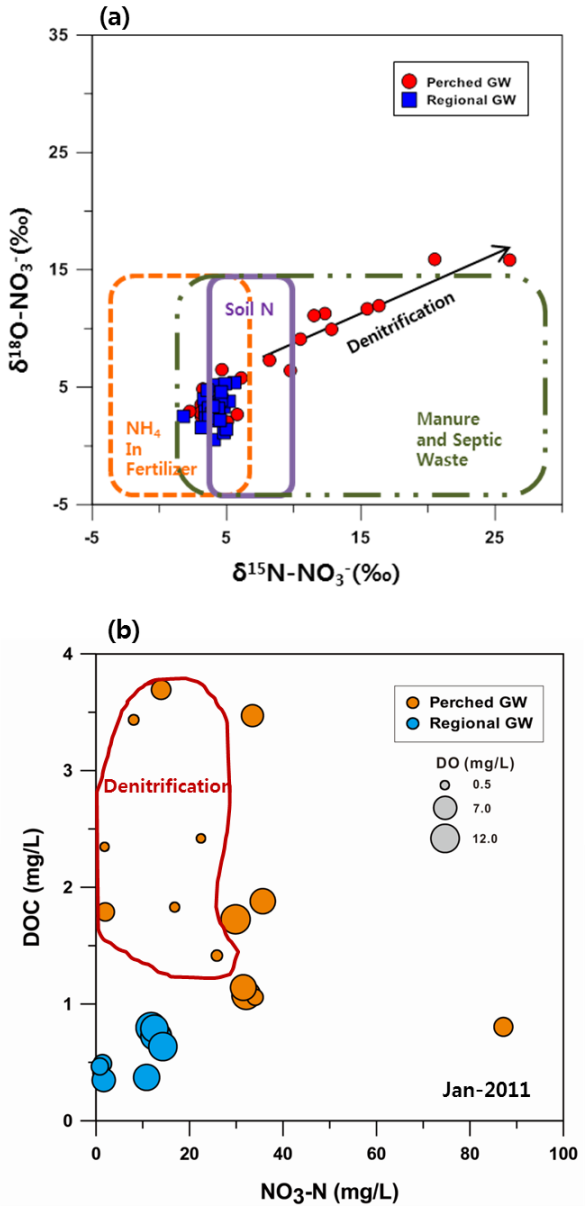

Fig.3.7. Estimation of (a) nitrate sources and fates and (b) relation of NO_3-N and DOC in the groundwater (GW) of the study area. In (a), ranges for possible nitrate sources and the arrow of the denitrification are from Kendall (1998).

Monitoring of the well leakage inflow at the regional groundwater well

Video-logging revealed inflows of the perched groundwater to the RW2 regional groundwater well from a depth of 2.33 m (Fig.3.8a). This leakage of groundwater from the perched aquifer into the regional aquifer resulted in elevated NO_3-N concentrations (14–18 mg/L) in the upper 50 m of well depth (Fig.3.8b). Although groundwater with different hydro-characteristics entered from ~37–39 m of well depth based on the vertical temperature and EC profiles, the impact of the leaked perched water remained detectable down to the depth of around 50 m. Below 50 m depth level, the NO_3-N concentrations continuously decreased towards 5 mg/L. This suggests that imperfect cementation results in the infiltration of nitrate-containing perched groundwater into the regional aquifer.

Due to the results of this study, the wall of the RW2 well was re-grouted in 2009 to prevent the inflow of perched groundwater into the regional aquifer. Monitoring of the variation of NO_3-N concentrations before and after re-grouting (Fig.3.6) revealed a remarkable decrease from 17.8 mg/L to 1.5 mg/L (average concentration for April to September 2010). This indicates that the nitrate contamination of the regional groundwater at the well RW2 was caused by the inflow of perched groundwater with high concentrations of NO_3-N and that this contamination can be prevented by proper well completions.

The annulus between the drilled hole and casing is grouted by regulation to prevent

inflows of poor quality surface water or contaminants towards aquifer systems in the subsurface. Improperly completed wells have generally been identified as causes of aquifer contamination from many researches (Gass et al., 1977; Hibberd, 1992; Lacombe et al., 1995; Yi et al., 2007). For this reason, grouting the annular space has been regulated in Jeju since 2004 in the well construction standards for groundwater of the Jeju Special-Self Governing Province (Fig. 3.9). The well RW2 was constructed in 1976 and almost all other regional groundwater wells were also constructed in the 1970s – 1980s (Jeju Water Resources Management Office, 2001) in Fig. 3.9, when the annular space grouting was not required. Therefore, it is likely that nitrate-contaminated regional groundwater at other areas of the study site was also a result of the inflow of perched groundwater with high concentration of NO_3-N either through improperly completed wells or discontinuity of the impermeable clay layer. In both cases nitrate from the perched groundwater causes contamination of deeper regional groundwater.

For the numerical simulation of the nitrate transport in this study, a conceptual model was estimated that the nitrate contamination of the regional groundwater in the Gosan study area may be affected by the inflow of nitrate rich perched groundwater. This can occur via badly completed wells constructed in the 1970s and 1980s as being demonstrated by video-logging data for the well RW2. Other regional groundwater wells (RW1, RW3, RW4, RW8, RW9 and RW10) distributed in the perched aquifer zone are considered as leaky wells based on the fact that the seasonal fluctuation of the

nitrate concentrations and constructed periods of the wells when the grouting regulation was not applied.

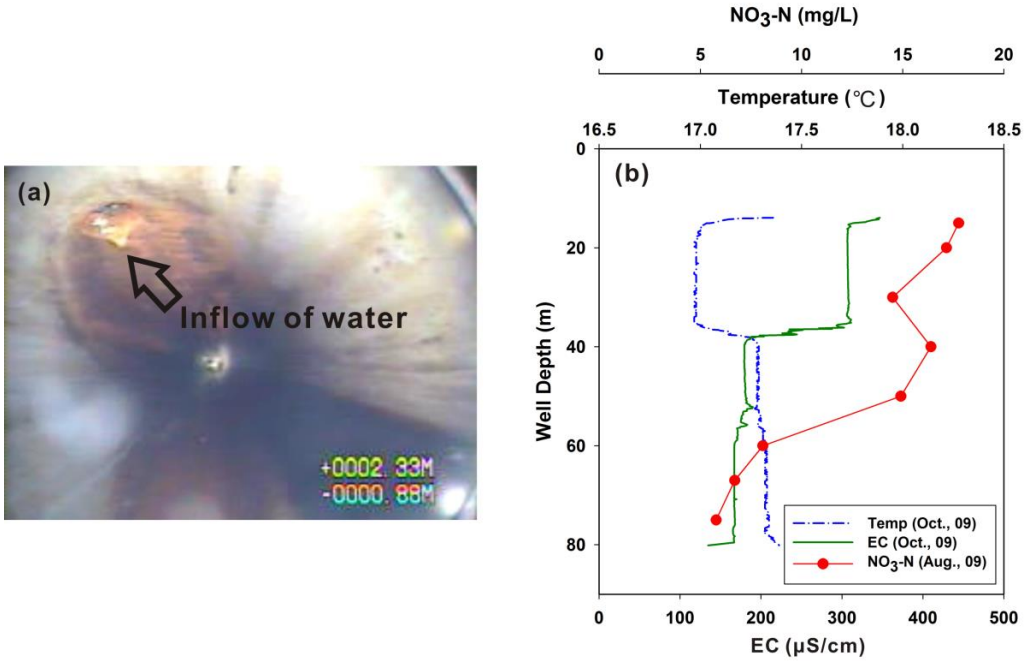

Fig.3.8. (a) Borehole camera image of perched water inflow toward regional groundwater and (b) vertical distributions of temperature (Temp), electrical conductivity (EC), and NO_3-N concentration in RW2 well.

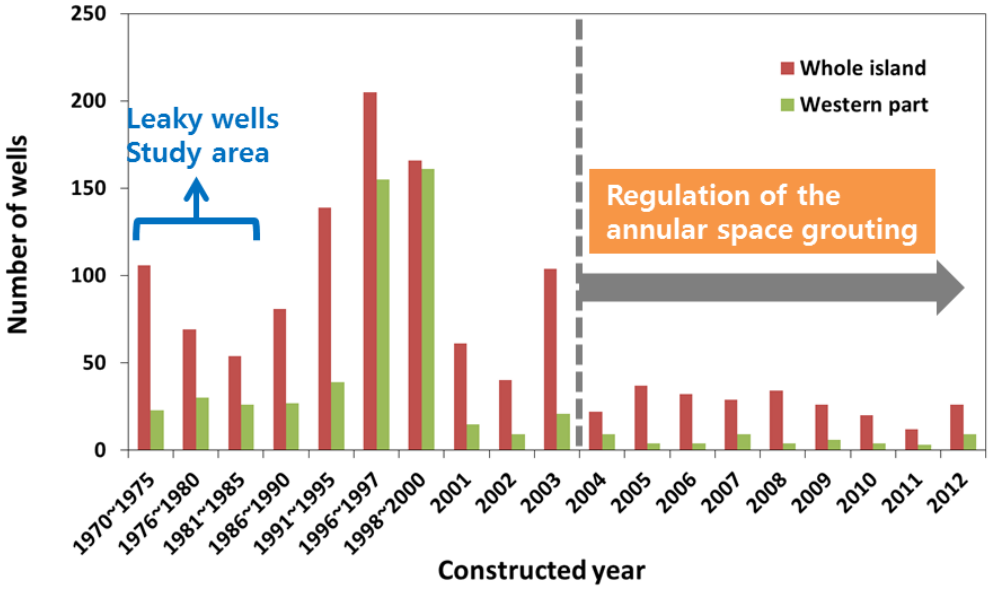

Fig. 3.9. The constructed periods of groundwater wells in whole Jeju Island and in the western part (Hankyung and Daejeong watersheds) of the island with showing the leaky wells in the Gosan study area (the regulation of the annular space grouting for the well construction has been initiated since 2004 in Jeju Island).

3.3 Numerical simulation methods

Double-domain integration approach

Although the process of groundwater leakage through damaged wells or badly installed wells can be simulated using one numerical domain consisting of multiple aquifer layers and boreholes penetrating the aquifers, the numerical stability and accuracy could be significantly decreased, especially when the model should consider variably saturated domains (such as a perched aquifer) or there are significant differences in hydraulic properties between adjacent model layers (such as boreholes and interbedded impermeable layers). In the case of the Gosan area, the complex hydrogeologic setting significantly affected the numerical stability of the simulation results. Numerical errors tended to increase, particularly along the elements where leaky boreholes, clay layers, and variably saturated volcanic rocks were in contact with each other. Therefore, an alternative modeling technique was required to represent the groundwater and nitrate transport of the study site.

This study adopted a double-domain integration approach to simulate groundwater and nitrate transport through leaky wells in a layered aquifer system. In the Gosan area, there are two major pathways that connect the perched and regional aquifer systems: (1) drainage of shallow groundwater through the clay unit; and (2) fast and direct groundwater flow via the leaky wells (Fig.3.10). I constructed two separate model domains for the perched and regional aquifers and coupled the two domains on the

basis of groundwater leakage rates through the clay layer and the leaky wells (Fig.3.11). The detailed coupling process of the double domains is described in the following sections. The double-domain integration approach used in this study was found to be numerically more stable than the single-domain approach fully combining the perched and regional aquifer system.

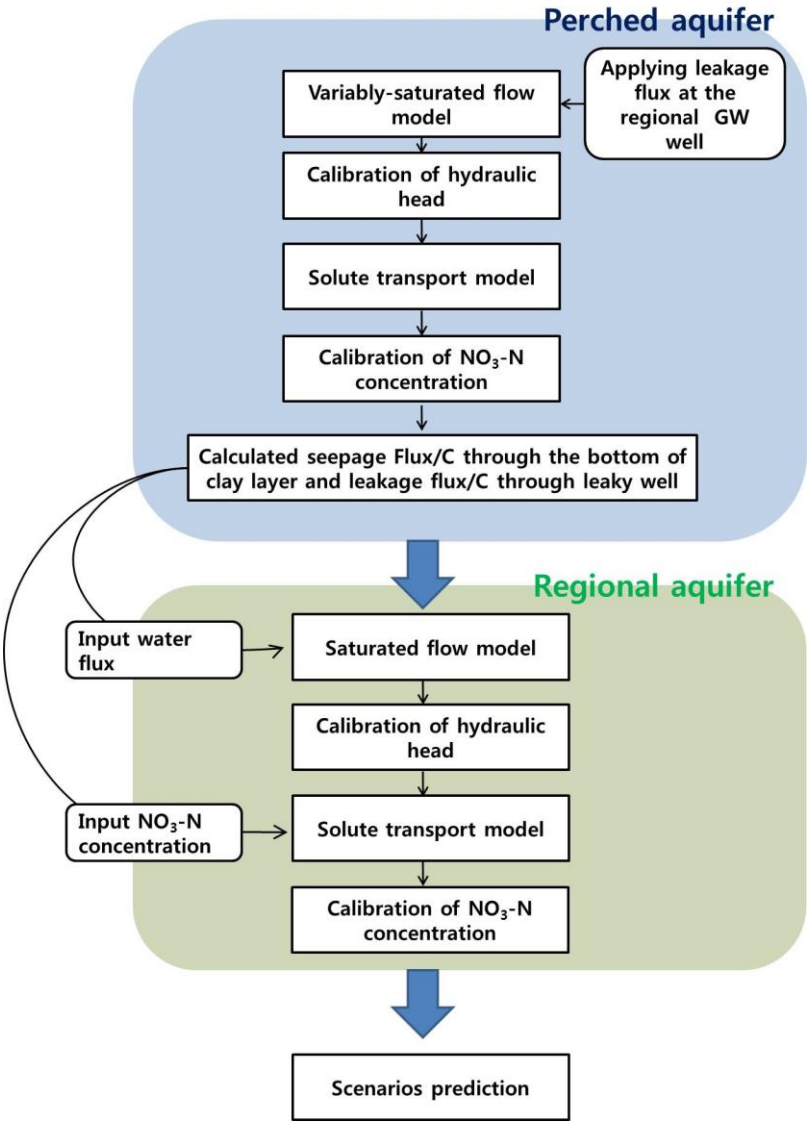

Fig.3.10. Flow chart for the simulation of two separated aquifer domains.

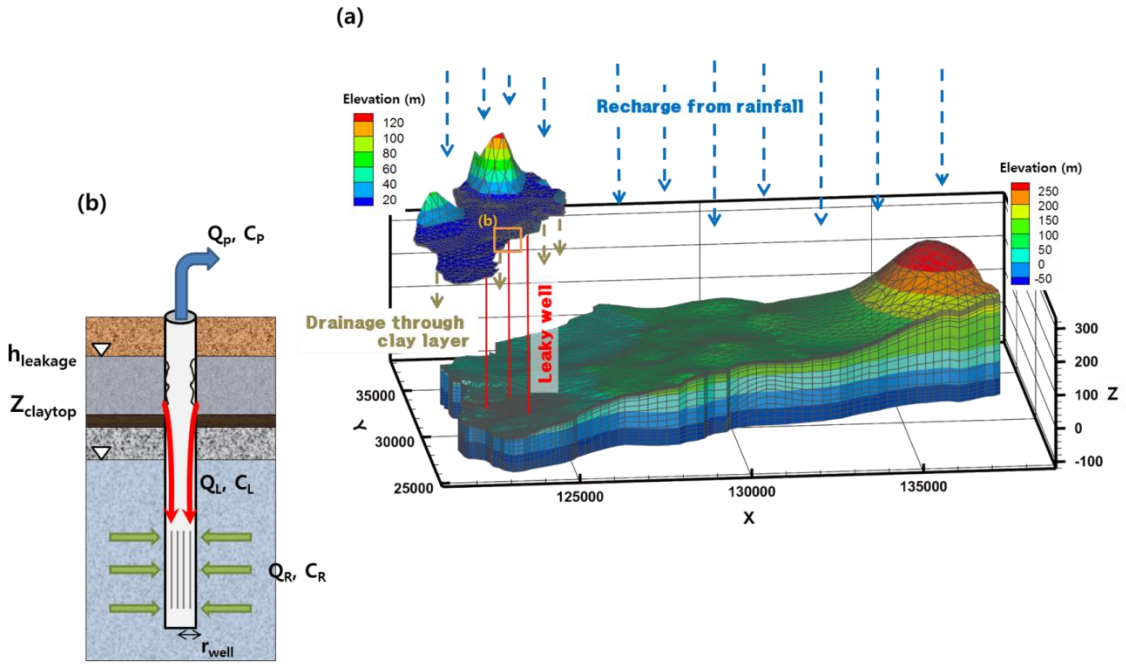

Fig.3.11. Double-domain integration approach for integrating groundwater flow between perched and regional aquifers (a), and conceptual diagram of the groundwater leakage process from a leaky well (b).

Domain construction

The numerical software HydroGeoSphere (Therrien et al., 2010) was used to simulate groundwater and nitrate transport. HydroGeoSphere is a numerical model which has been used for simulating variably-saturated groundwater flow and reactive solute transport (Li et al., 2008; Lee et al., 2010; Brunner and Simmons, 2012; Goderniaux et al., 2015). Fig.3.12 shows the numerical domains for the perched and regional aquifers. The domain area for the perched aquifer was delineated following the distribution of the clay layer of the Gosan site (Jeju Water Resources Management Office, 2001). The Hankyung watershed was used as the boundary of the regional aquifer domain (Fig.3.12b). The total area of the regional aquifer domain was 103.72 km^2, in which the perched aquifer system (8.13 km^2) was included.

The hydrogeologic layers of the model were assigned using the geologic logs from the boreholes (Jeju Water Resources Management Office, 2001). The perched aquifer domain consisted of three hydrogeologic layers: silty loam at the top, tuff in the middle, and clay at the bottom. The regional aquifer domain was composed of volcanic rocks underlain by impermeable marine sediment (the Seogwipo Formation; Koh, 1997). A finite-element triangular mesh was generated and the element size was refined at the perched aquifer area and at the leaky wells. The number of nodes and elements for the perched aquifer was 50,652 and 96,084 and those for the regional aquifer were 51,699 and 99,161, respectively.

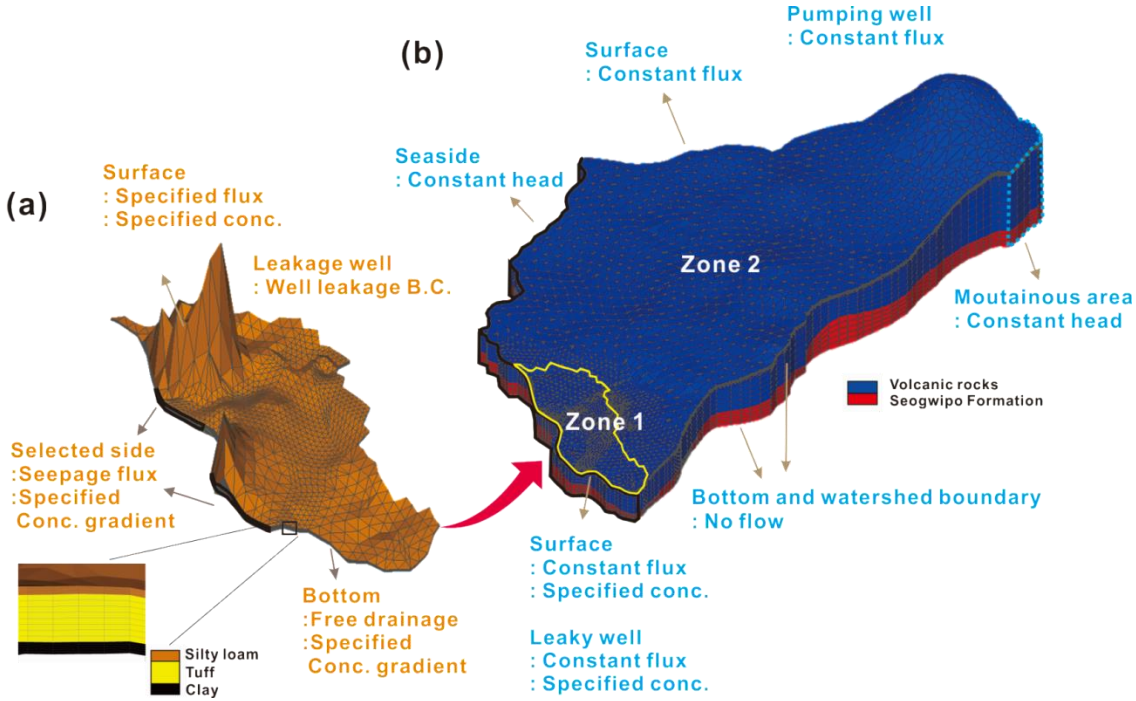

Fig.3.12. Numerical domains for the perched (a) and regional aquifer (b) and the boundary conditions (BC) used for simulations (orange text: BC for the perched aquifer, blue text: BC for the regional aquifer).

Model setup for the perched groundwater system

A variably saturated flow and transport simulation was conducted to represent the perched groundwater lens in the vadose zone. The unsaturated flow was described using the Richards equation and van Genuchten relationship (Richards, 1931; Van Genuchten, 1980).

The boundary conditions for the perched aquifer are illustrated in Fig.3.10a. A time-varying fluid flux was applied at the top surface by multiplying the groundwater recharge rate (40.7%) by the daily precipitation (KIGAM, 2011). Natural seepage from the perched groundwater was observed along the coastal cliff (UNDP and FAO, 1972). Thus, a seepage boundary was applied along the seaside. At the bottom of the domain, a free drainage boundary was assigned to account for leakage of shallow groundwater to the lower unsaturated zone.

A previous study of the Gosan area estimated that there were six leaky wells that showed elevated NO_3-N concentrations (RW1, RW3, RW4, RW8, RW9, and RW10 in Fig.3.2b; Koh et al., 2012). In our model, the leakage rate of perched groundwater at a damaged well (Q_L) is described by the following equation:

$$\mathbf{Q_L = 2\pi \cdot r_{well} \cdot \sigma_{leakage} \cdot (h_{leakage} - Z_{claytop})} \quad \mathbf{(h_{leakage} > Z_{claytop})} \quad \textbf{[Eq. 3.1a]}$$

$$\mathbf{Q_L = 0} \quad \mathbf{(h_{leakage} \leq Z_{claytop})} \quad \textbf{[Eq. 3.1b]}$$

where r_{well} is the radius of the leaky well, $\sigma_{leakage}$ is the well leakage coefficient

describing the ease with which groundwater can move through the damaged wall, $h_{leakage}$ is the perched groundwater level, and $Z_{claytop}$ is the elevation of the top clay layer. Eq. 3.1 explains that if the perched groundwater overlies a clay lens, the groundwater leakage rate is determined by the thickness of the perched groundwater ($h_{leakage} - Z_{claytop}$), the well radius ($r_{well}$), and the well leakage coefficient ($\boldsymbol{\sigma}_{leakage}$). Similar approach has been adopted by Mohamed and Rushton (2006) and Lee et al. (2010) to simulate groundwater inflow through a screened horizontal well of a collector well. Of these parameters, $\boldsymbol{\sigma}_{leakage}$ was estimated based on the mass balance estimation of groundwater and chemical species at the leaky well. The detailed process for obtaining $\boldsymbol{\sigma}_{leakage}$ is described in the following section. In every time step, the model calculated the groundwater leakage rate (Q_L) using the simulated groundwater level ($h_{leakage}$) and reassigned the water leakage rate at each leaky well. By adopting this approach, reasonable estimation of the groundwater leakage rate becomes possible without requiring a complex coupling process between the perched and the regional domain.

Numerical representation of the groundwater leakage process via improperly constructed wells

To represent the groundwater leakage process in a quantitative manner, I first conceptualized the mixing characteristics of perched and regional groundwater in a damaged well (Fig.3.11b). The amount of pumped water (Q_P) from the leaky well is the

sum of the perched groundwater entering through the damaged wall (Q_L) and the uncontaminated regional groundwater (Q_R) passing through the well screen (Eq. 3.2).

$$Q_L + Q_R = Q_P \xrightarrow{1/Q_P} \delta_L + \delta_R = 1 \quad \textbf{[Eq. 3.2]}$$

In Eq. 3.2, δ_L and δ_R denote the mixing ratios of perched and regional groundwater in the leaky well, respectively. Estimation of these mixing ratios can be achieved by the mass balance calculation of dissolved chemical species at the leaky wells using Eq. 3.3.

$$\delta_L C_{L,i} + \delta_R C_{R,i} = C_{P,i} \quad \textbf{[Eq. 3.3]}$$

where $C_{L,i}$, $C_{R,i}$, and $C_{P,i}$ are the concentrations of the i^{th} chemical species in the perched groundwater, regional groundwater, and the pumped water at the leaky well, respectively. The chemical species Cl^-, Br^-, and SO_4^{2-} were chosen as input parameters because these species are conservative and have different concentrations (end-member values) depending on the sources of agricultural activities and seawater mixing (Fig.3.13 and Table 3.3). Measured Cl^-, Br^-, and SO_4^{2-} concentrations of the end-members showed significant standard deviation values due to spatial and seasonal variations as provided in Table 3.3. Especially, seawater mixing event was occurred irregularly near the coastal area, which greatly affected the end-member concentration. Large variations in the concentration of the end-members can cause uncertainty on the estimation of the leakage factors. Therefore, the Mix Program (Carrera et al., 2004) was used to calculate mixing ratio of leaky wells in this study, in which the program

can adjust concentrations of end-members and mixed samples within the measured variations to reduce uncertainty based on the maximum likelihood method. By using the average concentrations of species, representative mixing ratio of the perched groundwater (δ_L) can be obtained to describe the leaky well dynamics in the complex field condition of the study area.

The average groundwater pumping rates (Q_P) were obtained from a previous survey by the Korea Rural Community Corporation Jeju regional headquarters. $C_{L,i}$ and $C_{R,i}$ were assumed to be the average concentrations of chemical species from the perched groundwater wells and properly constructed regional groundwater wells (i.e., regional groundwater wells with low NO_3-N concentrations (<3 mg/L)), respectively (Koh et al., 2012). The mean concentration of the chemical species in each leaky well was used as $C_{P,i}$. Further information on $C_{L,i}$, $C_{R,i}$, and $C_{P,i}$ is provided in the supplementary materials (Tables 3.3 and 3.4). Table 3.5 shows that the amount of perched groundwater entering the leaky well (Q_L) ranged from 1.32E−04 to 9.06E−04 m^3/sec, contributing approximately 14%–33% of total pumped water.

The well leakage coefficient ($\boldsymbol{\sigma_{leakage}}$) was estimated using the following equation.

$$\boldsymbol{\sigma_{leakage} = Q_L/2\pi \cdot r_{well} \cdot (h_{leakage} - Z_{claytop})} \qquad \textbf{[Eq. 3.4]}$$

Table 3.5 shows the calculated well leakage coefficients ($\sigma_{leakage}$). In Eq. 3.4, Q_L was referred from Eqs. 3.2 and 3.3 (Table 3.5). The r_{well} and $Z_{claytop}$ were obtained from field

measurements and the groundwater levels from the steady-state simulation were used as the perched water level ($h_{leakage}$). The value of $\boldsymbol{\sigma}_{leakage}$ ranged from 1.95E−04 to 1.07E−03 m/sec (Table 3.5). Because the leakage coefficient derived from Eq. 3.4 was inferred based on the field measurement, it reflects integrated signal of possible well leakage processes of the study site without describing complex well leakage hydraulics separately in detail. Consequently, these values were used as the input parameters for simulating the perched groundwater leakage process through the damaged wells.

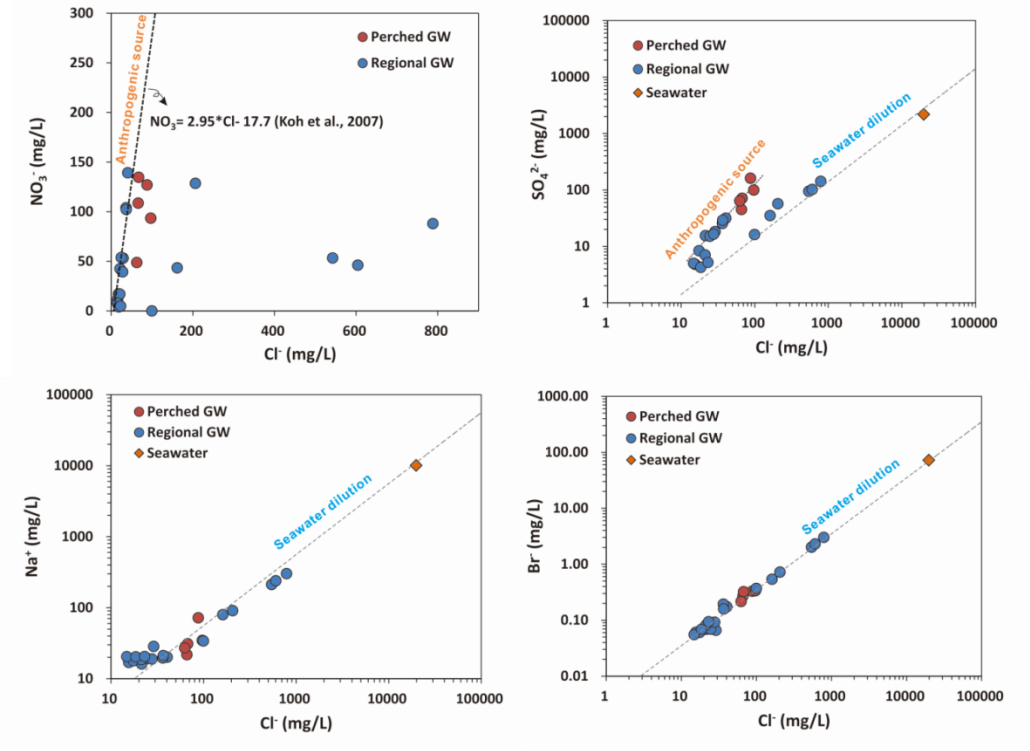

Fig.3.13. Bivariate diagrams of NO_3^-, SO_4^{2-}, Na^+, Br^- verses Cl^- in water samples of Apr. 2014. Dashed line represents the seawater dilution line.

Table 3.3. The average concentrations of chemical species from perched and properly grouted regional groundwater wells in Eq. 3.3.

Component	Statistic parameter	$C_{L,(Cl\ or\ SO42\ or\ Br)}$	$C_{R,(Cl\ or\ SO42\ or\ Br)}$
		mg/L	
Cl^-	Mean	79.49	18.82
	Standard deviation	47.55	2.63
	Number of data	98	32
SO_4^{2-}	Mean	60.48	5.57
	Standard deviation	28.15	1.65
	Number of data	98	25
Br^-	Mean	0.33	0.09
	Standard deviation	0.32	0.11
	Number of data	23	8

Table 3.4. The average concentration of the chemical species in each leaky well in Eq. 3.3.

Well ID	Statistic parameter	NO_3-N	Cl^-	SO_4^{2-}	Br^-
				mg/L	
RW1	Mean	10.69	27.17	18.59	0.18
	Standard deviation	5.18	4.95	23.16	0.19
	Number of data	16	16	11	4
RW3	Mean	12.47	28.06	19.45	0.19
	Standard deviation	5.10	6.74	6.25	0.14
	Number of data	16	16	12	4
RW4	Mean	20.46	36.08	25.97	0.16
	Standard deviation	4.02	5.28	7.49	0.21
	Number of data	15	15	11	3
RW8	Mean	16.03	101.13	35.07	0.63
	Standard deviation	7.82	180.00	31.83	0.18
	Number of data	16	16	11	3
RW9	Mean	12.87	428.73	75.47	2.30
	Standard deviation	4.38	342.99	50.64	0.12
	Number of data	6	6	6	2
RW10	Mean	18.10	132.00	44.97	1.33
	Standard deviation	3.78	258.69	43.16	0.93
	Number of data	13	13	10	4

Table 3.5. Estimated groundwater leakage rates and well leakage coefficients of the damaged wells in Gosan. Detailed information about the parameters is provided in the explanation of Eqs. 3.3 and 3.4

Well ID	Average pumping rate (m^3/sec)	δ_L	Q_L (m^3/sec)	delta h (m)	r_{well} (m)	$\sigma_{leakage}$ (m/sec)
RW1	1.16E−03	0.19	2.17E−04	1.48	0.05	4.67E−04
RW3	6.33E−04	0.21	1.32E−04	2.16	0.05	1.95E−04
RW8	1.37E−03	0.28	3.88E−04	5.58	0.05	2.21E−04
RW4	2.78E−03	0.33	9.06E−04	2.70	0.05	1.07E−03
RW9	2.33E−03	0.14	3.19E−04	1.66	0.05	6.12E−04
RW10	2.42E−03	0.32	7.63E−04	2.32	0.05	1.05E−03

Model setup for the regional groundwater system

The model domain of the regional aquifer was divided into two regions: (1) the area located below the perched aquifer domain (zone 1), and (2) the remainder of the area (zone 2) (Fig. 3.12b). The groundwater and nitrate influx into zone 1 was controlled by the water and solute leakage from the perched aquifer, whereas that of zone 2 was not. Different types of boundary conditions were assigned to zones 1 and 2 to account for the impact of the perched aquifer on the regional groundwater system.

At the surface of zone 1, the simulated drainage rates of the perched groundwater and NO_3-N concentration through the clay layer were assigned as the groundwater recharge and solute flux boundaries, respectively. The leaky wells in the regional domain were treated as specified flux nodes to represent the inflow of shallow groundwater. The inflow rates of groundwater and NO_3-N were determined from the computation results of the perched aquifer (i.e., the leakage rates of perched groundwater through the damaged wells, Eq. 3.1). In zone 2, the top surface was treated as the recharge boundary condition considering the groundwater recharge rate of the watershed (KIGAM, 2011). Inflow of NO_3-N to zone 2 was not included in our model because the major source of nitrate in the regional aquifer of Gosan is likely to originate from the perched groundwater (Koh et al., 2012). At the eastern upstream side of the domain, a constant head boundary (75.0 m) was applied considering the hydraulic gradient of the regional groundwater in the Hankyung watershed (Jeju Water Resources Management

Office, 2013). The western part of the domain was bordered by the sea and a constant head boundary (0 m) was assigned. Pumping wells were set as well boundaries with time variant pumping rates (monthly averaged values for 2000–2012). No reactive transport was considered in the regional groundwater model because the dissolved oxygen concentrations (average: 5.7 mg/L) were high enough to prevent denitrification, which is also supported by isotopic data (Koh et al., 2012).

The total simulation period was the same as that of the perched aquifer. The aquifer properties were referred from previous measurements (Jejudo, 2003) and were calibrated by comparing groundwater levels between the measured and simulation data.

NO_3-N transport model

The NO_3-N concentrations observed using the lysimeter (Fig.3.2b) were averaged on a monthly basis and a time-varying concentration boundary was applied on the top surface. A previous study confirmed the occurrence of a local denitrification process at several perched groundwater wells on the basis of $\delta^{15}N$ and $\delta^{18}O$ isotope data (Koh et al., 2012). Therefore, the model considered the denitrification process using the first-order decay of nitrate with a calibrated reaction ratio of 5.16E−8 s^{-1}.

The total simulation period was years 2000–2012, which included the target study period (2009–2010). To obtain the initial conditions, a pseudo steady-state simulation was conducted for 1,000 years. The maximum time step size was limited to 0.5 day to maintain the numerical stability of the variably saturated system. Table 3.6 summarizes the model parameters used for simulation. The model parameters were obtained from a previous field survey (Jejudo, 2003) and calibrated by comparing simulated groundwater levels with the field measurements. Longitudinal and transverse dispersivities were obtained from Gelhar (1986).

Table 3.6. Calibrated parameter values used for the simulation

Hydrostrati-graphic units	Calibrated hydraulic conductivity (m/sec)		Porosity[a]	S_s[b]	Van Genuchten function parameter[c]			Dispersivity[d] (m)	
	$K_{xx} = K_{yy}$	K_{zz}		(m^{-1})	S_{wr}	A (m^{-1})	β	a_L	a_T
Silt loam	7.0E−7	7.0E−8	0.45	1.0E−5	0.22	1.87	1.64	30.0	3.0
Tuff	6.6E−7	6.6E−8	0.44	1.0E−5	0.22	1.87	1.64	30.0	3.0
Clay	1.0E−9	1.0E−10	0.42	1.0E−3	0.27	4.54	1.51	0.1	0.01
Volcanic rocks	2.5E−4	7.0E−5	0.35	1.5E−4	-	-	-	50.0	5.0
Seogwipo Formation	1.0E−7	1.0E−8	0.40	1.0E−4	-	-	-	0.1	0.01

[a]Jejudo (unpublished results); [b] Batu, 1998; [c] Hodnett and Tomasella, 2002; [d]Gelhar, 1986

3.4. Results and discussion

3.4.1 Flow dynamics and NO_3-N transport of the perched aquifer

To obtain initial steady-state hydrological conditions for a transient simulation, a calibration between observed and simulated hydraulic heads at the perched groundwater wells was completed by changing hydraulic conductivities of three geological layers (Fig.3.14). In the steady-state simulation, hydraulic conductivity was assumed as isotropic. The correlation coefficient between the measured and simulated groundwater levels was 0.82 (Fig.3.14), which means that the simulated steady-state water levels were well matched with the field data. As well as calibration of the steady-state model, formation of the perched groundwater was importantly considered in this step. Calibrated groundwater levels and water content were shown in Fig.3.15. High groundwater levels in the perched aquifer were computed at the high altitude area and water was saturated mainly in the low land. The formation of the perched groundwater was able to be simulated in this modeling approach.

Figure 3.16 shows the groundwater level fluctuations of perched aquifer wells (PH1, PH3, and PH4 in Fig.3.2b) during the monitoring period (June, 2010 to Sept., 2011; Fig.3.16a). I observed that the perched aquifer is directly affected by rainfall events. The monitored water levels rose rapidly in response to precipitation with a short time lag (<1 day).

The model calibration was performed by changing hydraulic conductivities of model layers using a trial-and-error method. In Fig.3.16, the calibrated groundwater level generally matched well with the observed data. The average values of the simulated water level were 13.2 m (PH1), 13.4 m (PH3), and 10.2 m (PH4), which were close to the observed values (PH1, 13.3 m; PH3, 13.3 m; and PH4, 10.2 m). The response of the groundwater level to rainfall was also reproduced well by the model although a small discrepancy exists between observed and simulated data, especially after the heavy rainfall (Fig.3.16b). This is partly due to the heterogeneity in the silt loam and tuff layer of the study site. In addition, some preferential flow through macropores of surficial soil and secondary features of the sedimentary rock (tuff layer) could accelerate movement of water and nitrate into underlying groundwater (Šimůnek et al., 2003).

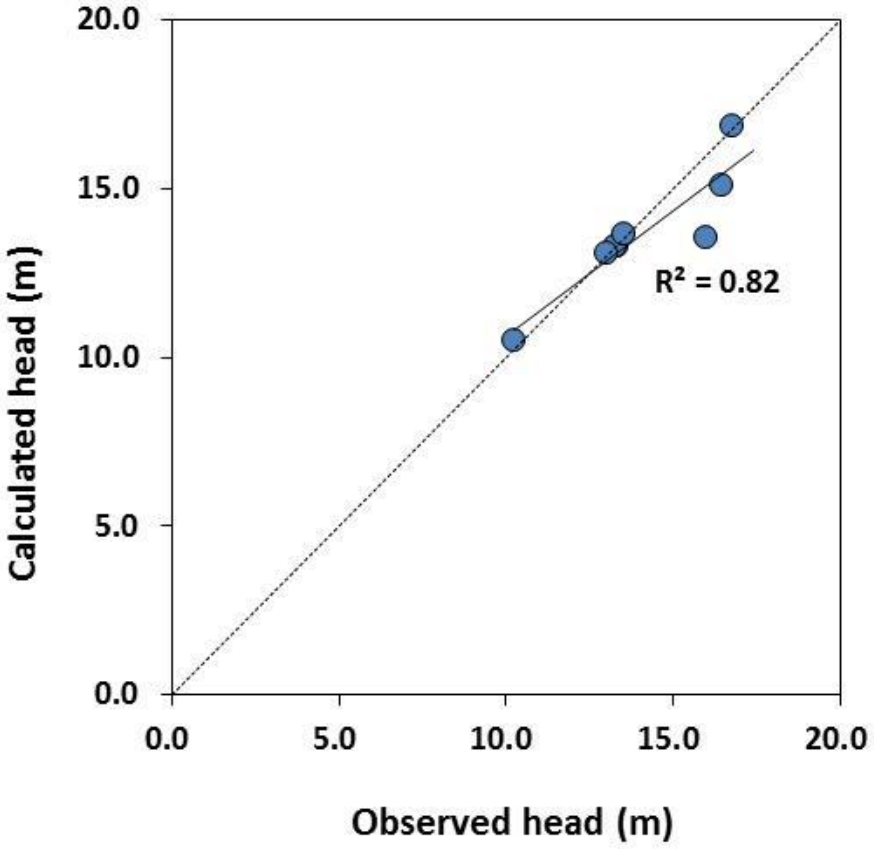

Fig.3.14. The steady-state calibration of the observed and calculated perched groundwater level.

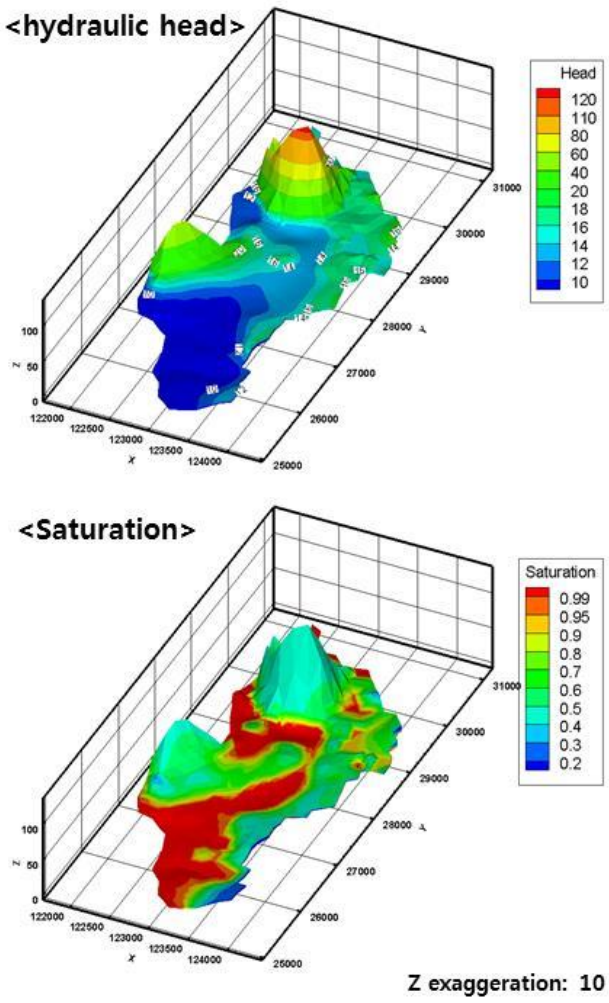

Fig.3.15. Simulated hydraulic head and saturation distribution.

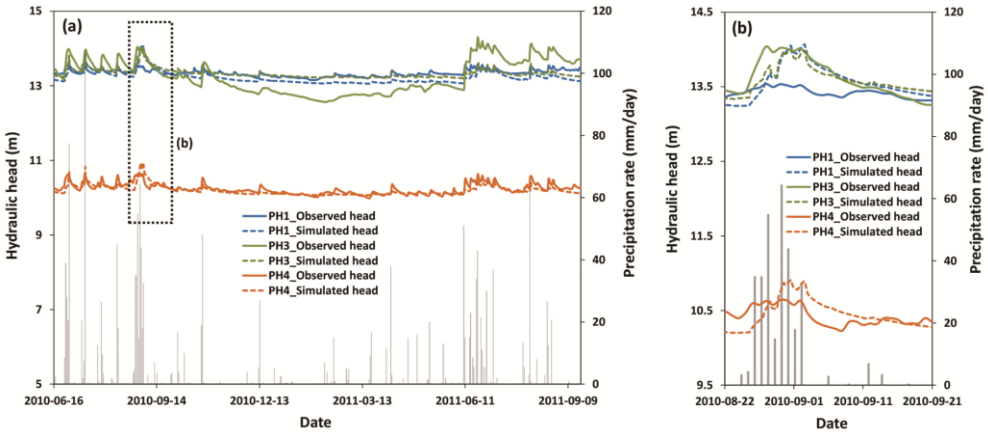

Fig.3.16. Comparison of the observed and computed hydraulic heads of the perched aquifer for monitoring periods between June, 16, 2010 and Sept., 9, 2011 (a) and for one month between Aug., 22, 2010 and Sept., 21, 2010 (b).

After calibrating the model parameters of the perched domain, a transport simulation was carried out and the model results were compared with field measurements (Fig.3.17). The observed NO_3-N concentration of all perched wells exceeded the maximum contamination level (MCL, 10 mg/L), reflecting that the perched groundwater was prone to contamination from surface loading. Large fluctuations in the NO_3-N concentration were observed in field measurements, especially in PC2, indicating that temporal and spatial variations in fertilizer usage in each agricultural field could significantly affect NO_3-N concentration. Comparison of the observed and simulated data showed that the temporal variations of NO_3-N concentration were not well reproduced by the model because of the lack of data to explain the spatio-temporal variations in the NO_3-N concentration of surface soil caused by the individual agricultural practices in small-scale crop fields. Notwithstanding, the model successfully calculated the average NO_3-N concentrations of the perched aquifer (observed NO_3-N—PC1: 15.5 mg/L; PC2: 55.9 mg/L; PC3: 28.8 mg/L; PC4: 48.3 mg/L; simulated NO_3-N—PC1: 17.6 mg/L; PC2: 55.7 mg/L; PC3: 28.0 mg/L; PC4: 47.6 mg/L).

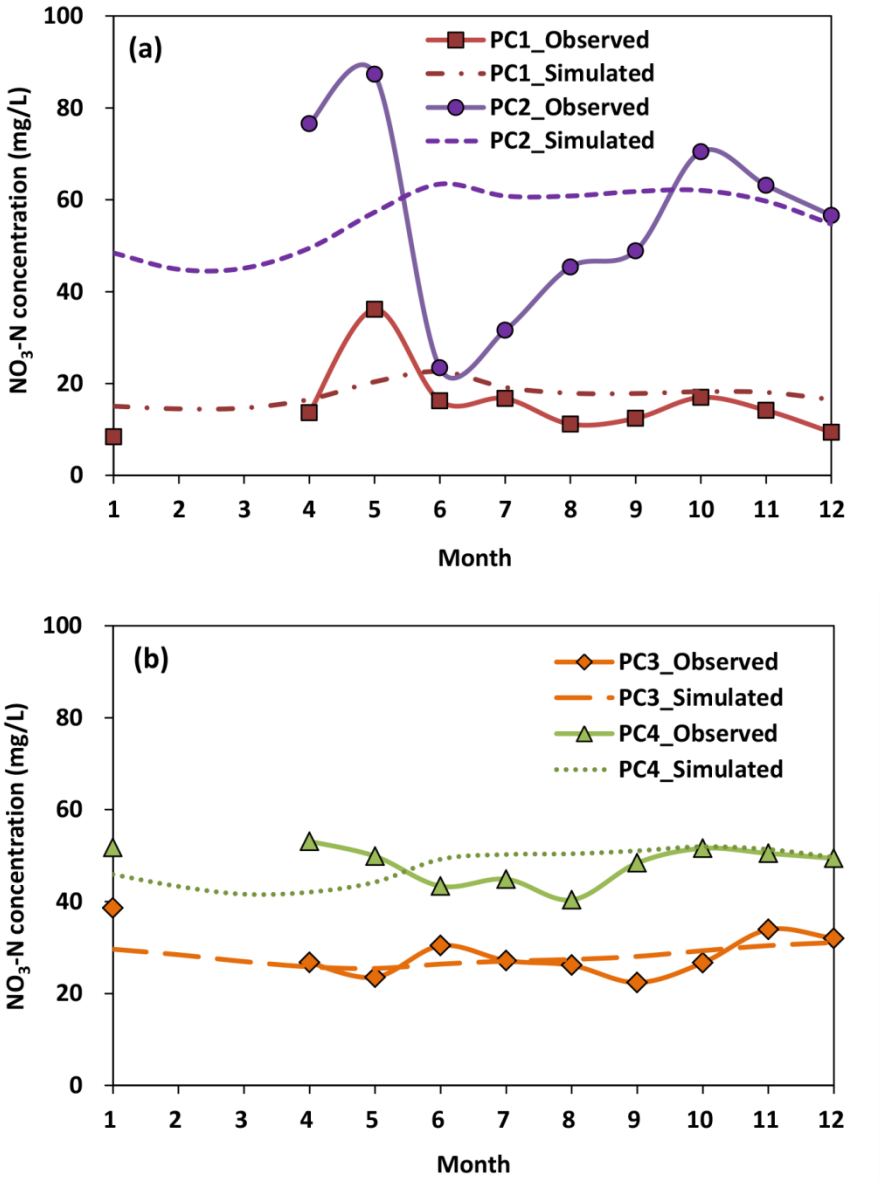

Fig.3.17. Comparison of observed and calculated NO_3-N concentrations (monthly averaged for 2009 and 2010) of the perched aquifer.

3.4.2 Evaluation of NO_3-N leakage flux through damaged wells and the fate of NO_3-N in the perched aquifer

Quantitative estimation of the contaminated groundwater leakage rate through the damaged wells becomes possible by utilizing the simulation results. Fig.3.18 shows the calculated groundwater and NO_3-N leakage flux through the leaky wells. The water leakage flux is directly affected by the perched groundwater level, and shows a clear response to rainfall events. The mean groundwater leakage rates via these wells during the target period (2009–2010) were 17.9±1.4 m^3/day (RW1), 11.4±0.6 m^3/day (RW3), 73.7±3.1 m^3/day (RW4), 33.7±2.0 m^3/day (RW8), 27.6±1.7 m^3/day (RW9), and 65.5±2.8 m^3/day (RW10). The differences in the leakage rates between these wells are attributed to the differences in the amount of well damage degrees (represented as $\sigma_{leakage}$) and the perched groundwater levels. The modeled leakage rates are similar to the estimated ones based on the field data (Table 3.5) with minor differences (0.04~5.85%). This finding indicates that the numerical performance of the well leakage boundary using Eq.3.1 acted properly in the model.

From the simulation results, perched groundwater traveling through the leaky wells was estimated to contain high levels of NO_3-N (average value for 2009–2010: RW1, 16.0±1.4 mg/L; RW3, 21.2±3.4 mg/L; RW4, 20.0±1.5 mg/L; RW8, 19.9±1.4 mg/L; RW9, 20.8±2.9 mg/L; and RW10, 17.7±2.5 mg/L). The simulated NO_3-N concentration even exceeded 20 mg/L, particularly after strong rainfall events (maximum value: RW3,

29.3 mg/L; RW4, 22.3 mg/L; RW8, 22.0 mg/L; RW9, 27.5 mg/L; and RW10, 23.6 mg/L). Such high levels of NO_3-N at the leaky wells would directly act as a point source of contamination, resulting in an increase in the NO_3-N levels of the regional aquifer.

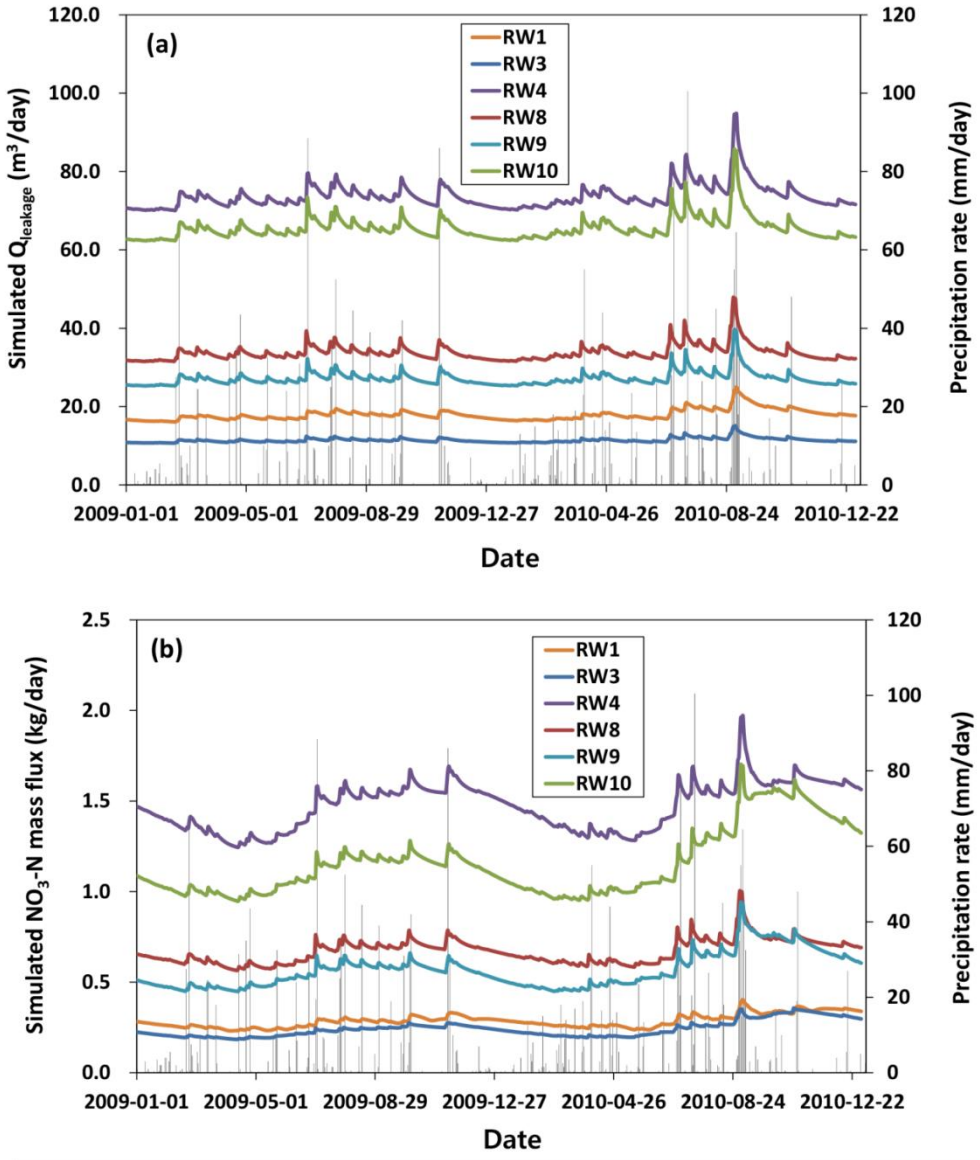

Fig.3.18. Simulated (a) $Q_{leakage}$ and (b) NO_3-N concentration at the leaky wells.

The NO_3-N mass flux moving along the leaky well is illustrated in Fig.3.18b. The average NO_3-N fluxes entering the regional aquifer through the leaky wells were 0.3±0.04 kg/day (RW1), 0.2±0.04 kg/day (RW3), 1.5±0.13 kg/day (RW4), 0.7±0.07 kg/day (RW8), 0.6±0.10 kg/day (RW9), and 1.2±0.18 kg/day (RW10). In Fig.3.16b, an increase in NO_3-N leakage flux after rainfall events is apparent, along with an increase in the groundwater leakage rate. For example, significant increases in the NO_3-N leakage flux (2.1–3.8 times higher than the mean leakage flux) occurred at all leaky wells after heavy rainfall (256.5 mm in 8 days) during late August 2010. This observation is consistent with previous work by Koh et al. (2012), who reported an increase in the NO_3-N concentration of the regional aquifer after heavy rainfall events.

Based on the simulation, the amount of NO_3-N entering the perched aquifer is approximately 83,400 kg-N/yr. A previous survey in the Gosan area reported that the total chemical fertilizer usage was 158,000 kg-N/yr (Koh et al., 2012). From these data, approximately 53% of applied fertilizer was estimated to move to the perched aquifer and 47% (75,000 kg-N/yr or 296 kg-N/ha/yr) to be removed by plant uptake and surface runoff. The calculation results showed a range similar to that of Song et al. (2002), who reported NO_3-N uptake by crops from Jeju Island of 181–187 kg-N/ha. Lee et al. (1996) also reported that the uptake amount ranges from 78 to 212 kg-N/ha depending on the vegetable type in Korea, which is a similar range to our simulation results.

3.4.3 Impact of leaky well hydraulics on nitrate contamination of the regional aquifer

Transient groundwater flows and NO_3-N concentrations in the regional aquifer were simulated on the basis of the initial values calibrated from the previous steady-state model (not illustrated). Comparison between the observed and the simulated values of hydraulic head was performed at the monitoring wells located within the main study area (automatic groundwater level monitoring wells: RH8 and RH9 in Fig.3.2a, and leaky wells: RW1, RW3, and RW10 in Fig.3.2b). The results of the comparison are presented in Figs. 3.19a and b. In general, the groundwater hydrographs showed reasonable agreement between the monitored and simulated data, although small discrepancies were observed in some parts of the monitoring periods. In well RH8, sudden decreases in the groundwater level occurred several times during the monitoring period regardless of the precipitation rate and the groundwater level at well RH 9 dropped below sea level. These exceptional values of observed water levels were likely to have been affected by additional factors (e.g., changes in the groundwater pumping rate or heterogeneous hydrogeologic properties), which were not considered in our model.

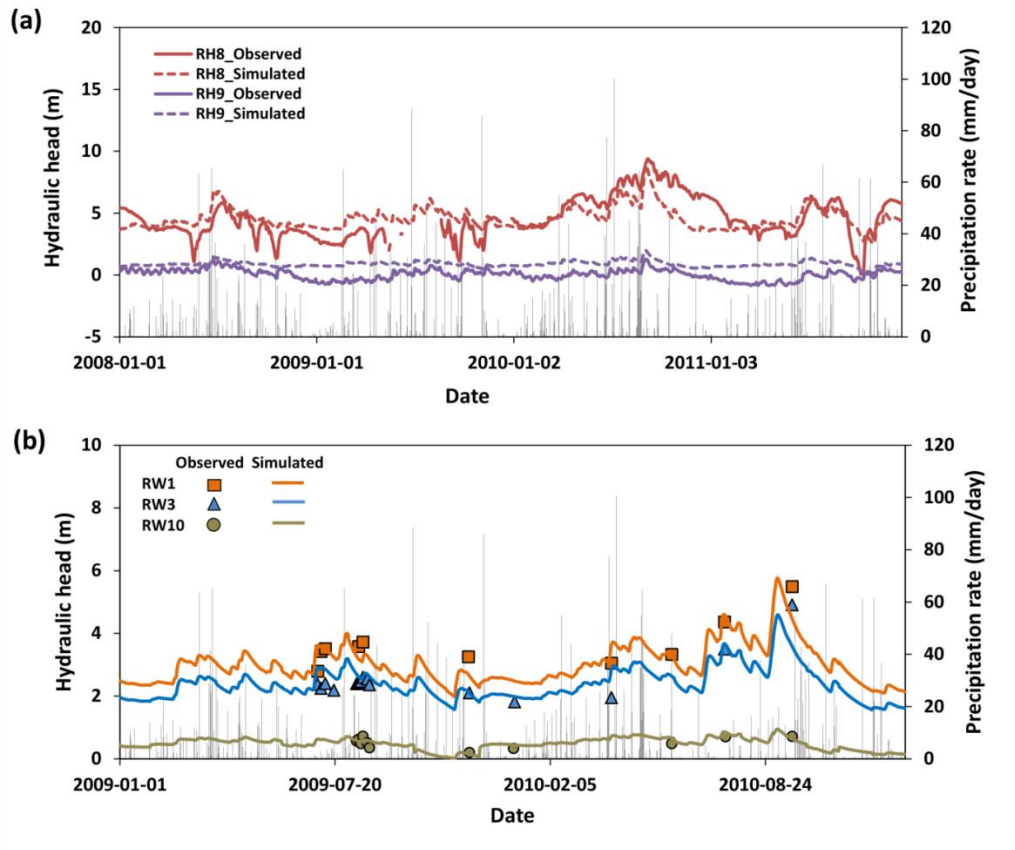

Fig.3.19. Observed and computed hydraulic heads of the regional aquifer at automatic monitoring wells (RH8 and RH9) (a) and at leaky wells (RW1, RW3, and RW10) (b).

From Fig.3.20, the NO_3-N concentrations at all leaky wells exceeded or were close to the MCL. The average and standard deviations of the observed concentrations were 9.6±4.8 mg/L (RW1), 13.7±4.2 mg/L (RW3), 19.7±4.3 mg/L (RW4), 19.6±8.1 mg/L (RW8), 18.2±2.5 mg/L (RW9), and 18.0±3.7 mg/L (RW10). The simulated concentrations showed a reasonable match with the observed ones (RW1: 14.1±1.9 mg/L; RW3: 16.1±4.0 mg/L; RW4: 19.8±1.5 mg/L; RW8: 19.2±1.5 mg/L; RW9: 20.4±2.9 mg/L; and RW10: 17.6±2.5 mg/L). Fig.3.20 also revealed that the observed NO_3-N concentrations of the leaky wells showed strong temporal fluctuations, similar to that for the perched aquifer. The abrupt changes in NO_3-N concentrations could not be replicated in our model due to a lack of measured data.

The migration process of the nitrate-rich groundwater in the regional aquifer is illustrated in Fig.3.21. In the plan view image, it can be observed that all the NO_3-N plumes in the regional aquifer originate from the leaky wells. The plumes move from these wells toward the seaside following the groundwater flow directions. The cross-sectional image clearly shows that the leaky wells act as conduits between the perched and regional aquifer, facilitating downward migration of nitrate-rich groundwater (Fig.3.21b).

The model also indicates that if the leaky wells in the regional domain were not considered, the NO_3-N concentrations from these wells would have significantly decreased up to 2.2 mg/L. This finding implies that groundwater leakage through the

clay layer was insignificant in the Gosan area. Based on these observations, I identified the leakage of nitrate-rich groundwater from the damaged wells as the major source dominating the nitrate contamination of the regional aquifer in the Gosan area.

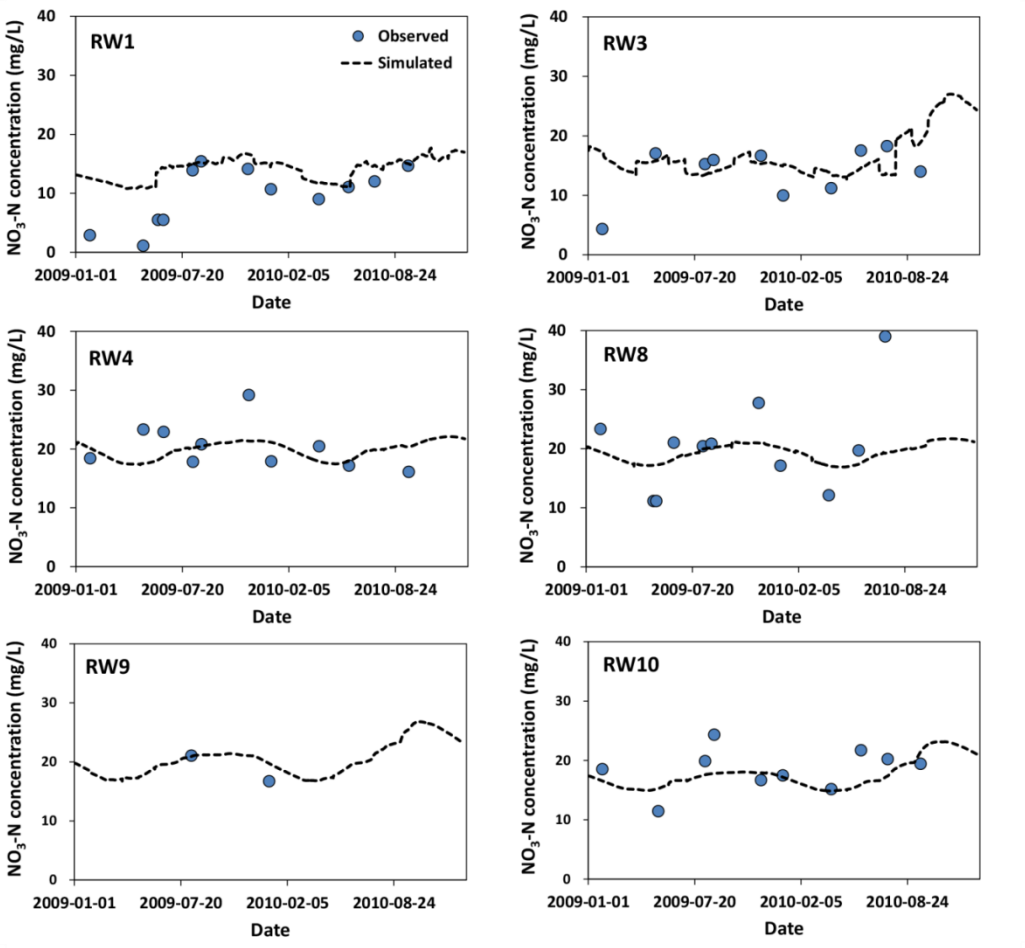

Fig.3.20. Observed and computed NO_3-N (2009–2010) concentrations at the leaky wells (RW1, RW3, RW4, RW8, RW9, and RW10) of the regional aquifer.

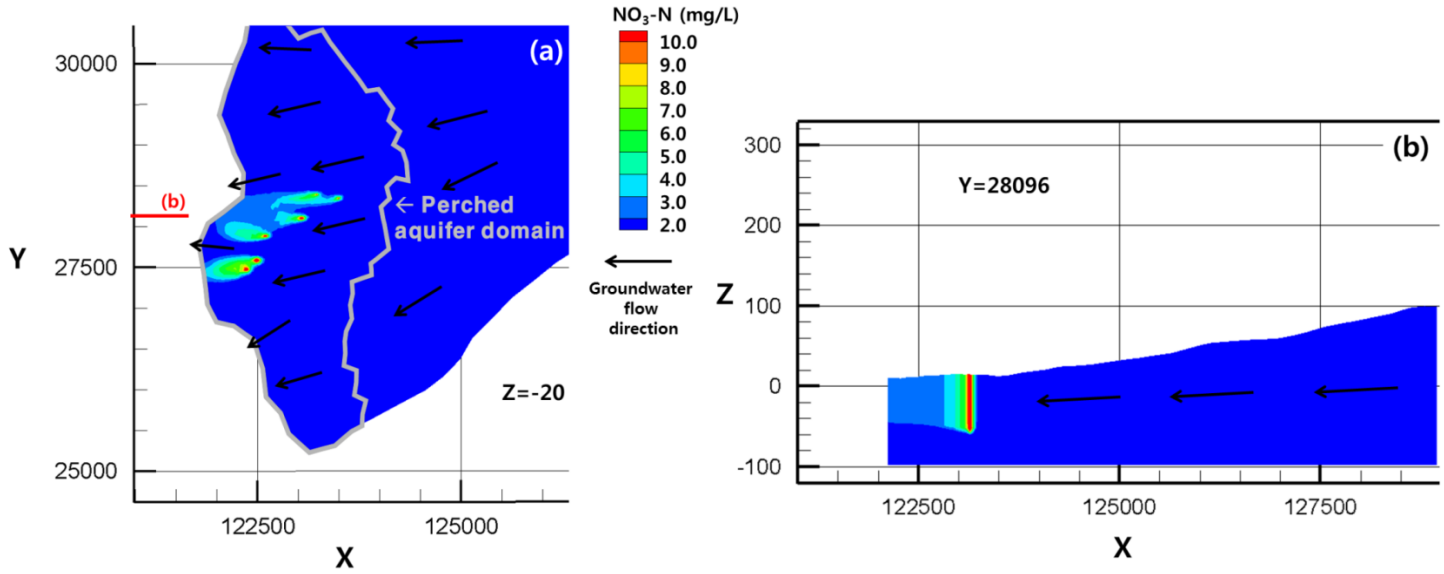

Fig.3.21. Simulated NO_3-N distribution of the regional aquifer in 2010 (a: plan view at a depth of −20 m, b: cross-sectional view across a leaky well)

3.4.5 Long-term predictions of regional aquifer sustainability in terms of NO_3-N contamination

To suggest a management plan to protect the regional aquifer system against cross-contamination, I predicted the long-term occurrence of NO_3-N under different remediation scenarios. For the prediction, I extended the simulation period for 30 years (2013–2042) using the monthly averaged precipitation data (1992–2012) and NO_3-N concentration as boundary conditions. Similar approach has been adopted by Zhang and Hiscock (2010) and Bonton et al. (2011) to predict the impact of land use change and agricultural practices on nitrate contamination. I considered three cases: case 1, the base case considering the same conditions as the current state (same fertilizer usage and leaky wells); case 2, reducing fertilizer usage to lower the NO_3-N concentrations without re-grouting the leaky wells; and case 3, sealing the leaky wells without reducing fertilizer usage.

From Fig.3.22a, which shows the prediction result for case 1, the NO_3-N concentrations are expected to exceed the MCL at all regional groundwater wells. Based on Fig.3.22a, natural attenuation or removal of nitrate would barely occur; therefore, new actions are needed for sustainable management of the regional groundwater system.

Numerical experiments of the case 2 scenarios with different amounts of fertilizer usage suggested that at least 55% of the NO_3-N entering the subsurface system should

be removed to reduce the concentration below the MCL at all leaky wells (Fig.3.22b). The recovery time to lower the NO_3-N concentration below 10 mg/L will be less than 1 year. Based on the predicted result, I estimated the maximum allowable loading of fertilizer use in the Gosan area by considering the minimum and maximum range of NO_3-N removal by plant uptake and surface runoff. If I assume that NO_3-N removal by plants and runoff would be reduced in the same ratio as total fertilizer usage, the maximum allowable loading of NO_3-N would be 282 kg-N/ha/yr (45% of current fertilizer usage). If the plant uptake and surface runoff of NO_3-N would be constantly maintained regardless of the reduction in fertilizer usage, 408 kg-N/ha/yr of NO_3-N would be the maximum allowable loading in the Gosan area (65% of current fertilizer usage).

For the results of the sealing case (case 3, Fig.3.22c), the NO_3-N levels rapidly decreased below the MCL for all leaky wells within 15–20 days. In addition, the concentration would be reduced to less than 3 mg/L within approximately 250 days. Of the three suggested scenarios, case 3 was the most efficient in terms of decreasing the NO_3-N concentration of the regional aquifer. From the previous reports (Powers, 1992; Harter, 2003), properly constructed wells with grout seal would have a long lifetime over half a century or more except for wells having corrosion problems. Therefore, improvement in the groundwater quality resulted by the re-grouting construction of the case 3 may be maintained for a long-term periods more than 50 years.

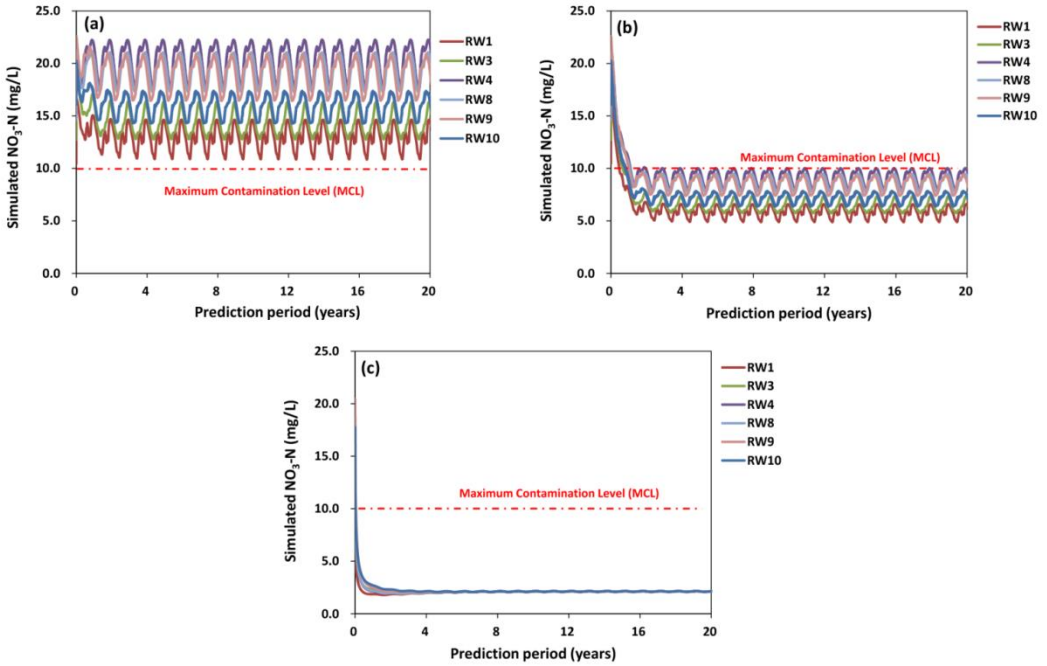

Fig.3.22. Long-term predicted NO_3-N concentrations in the leaky wells of the regional aquifer under different remediation scenarios (a: case 1, b: case 2, and c: case 3; detailed explanation of the model cases is provided in the manuscript).

In many countries where nitrate contamination in groundwater is an important issue, restriction of fertilizer usage is the most effective approach to protect water quality (Almasri and Kaluarachchi, 2005; Peñe-Haro, 2010; Bonton et al., 2011; Cerro et al., 2011; Kay et al., 2012). However, such restrictions may be confronted with objections from farmers because the harvest of agricultural products is directly linked to their means of living. In Korea, since agricultural activities are mostly performed in small-scale crop fields, it is difficult to control the agricultural practices of the individual farmland. Although reduction of fertilizer usage is inevitable to reduce the nitrate mass leaching into the aquifer system, for a specific field situation such as the Gosan area, where improperly constructed well casings are the main factor in groundwater quality deterioration, re-organization of the well facilities should be considered as the initial action in advance of reduction of fertilizer usage on agricultural lands.

3.5. Conclusions

In this study, I investigated the impacts of leaky wells on nitrate dynamics in the two-layered aquifer system in the agricultural area of Gosan, Jeju Island, by applying numerical simulation and field measurements. I first introduced the double-domain integration approach as an alternative method to represent the nitrate migration process in the multi-layered aquifer system. The suggested model successfully provided a reasonable estimation of the nitrate concentration in both the upper perched and underlying regional aquifers, without requiring numerically complex calculation processes. In addition, the model significantly increased the numerical stability and efficiency, especially compared with the one-domain approach that has been widely used for multi-layered aquifer simulation.

The simulation results clearly demonstrated that the leaky wells facilitated downward migration of nitrate-rich groundwater, resulting in contamination of the underlying regional aquifer. The input of shallow groundwater via the leaky wells acted as the dominant source for the nitrate contamination in the regional aquifer. This observation implies that when developing an adequate groundwater management plan for the Gosan agricultural area, the leaky wells should be regarded as the major factor controlling groundwater quality. The predicted NO_3-N concentrations in the leaky wells also suggested that sealing the damaged groundwater wells would efficiently lower the NO_3-N concentration below the MCL.

To protect both perched and regional aquifer systems against nitrate contamination, it is necessary to reduce the amount of fertilizer usage. Based on the computation results, the maximum allowable fertilizer amount for Gosan was estimated to be 45%–65% of the currently applied fertilizer level to reduce the NO_3-N concentration at the leaky wells below the MCL. However, such restrictions regulating fertilizer amounts could hardly be achieved in a short time, given that agricultural activities in Korea are mostly performed in small-scale crop fields by individual farmers. In this case, re-organization of the poorly constructed well facilities can be considered as the first action to be adopted in advance of reduction of the fertilizer usage to protect the aquifer environment of the agricultural area.

Chapter 4. Groundwater age mixing in a complex aquifer system

Abstract

In this chapter, interpretation of the groundwater age was applied to evaluate the nitrate contaminant dynamics in the Gosan area in consideration of complex aquifer settings. In an aquifer system with complex hydrogeologic features, mixing of groundwater ages would be expected due to migration through various flow pathways. Interpretation of the groundwater age occurrence in the complex aquifer system can be derived differently by three groundwater age estimation methods (environmental tracer age dating, lumped parameter model and numerical model). In this chapter, I assessed differences in the groundwater age estimation in a layered aquifer system (shallow perched and deep regional aquifers) with well leakage dynamics by applying the three age computation methods. Furthermore, the obtained groundwater ages was utilized to compare evaluations of the regional aquifer vulnerability to nitrate contamination for

long-term periods. As the tracer age dating method, the apparent ^{3}H-^{3}He ages were relatively older than the lumped parameter model due to inconsideration of the age mixing process. Delayed response in the regional groundwater to the surface fertilizer use was expected by the tracer age approach. Although the lumped parameter model could derive the simple mixing process between the young and old groundwater, the numerical simulation could generate the entire age distribution of water particles with various groundwater flow components. Based on separation of the water flow components by the numerical models, the major deteriorating pathway related to the nitrate contamination was evaluated as direct inflow of the highly contaminated perched groundwater via well leakage process. In the complex aquifer systems, the numerical modeling approach is needed to proper evaluation and prediction of the aquifer vulnerability to contaminants.

4.1 Introduction

Groundwater age generally refers to the time elapsed since water particles entered into the subsurface aquifer system (Bethke and Johnson, 2008; Suckow, 2014). Groundwater age can provide invaluable information for characterization of subsurface flow systems such as history of groundwater recharge (Solomon and Sudicky, 1991; Ekwurzel et al., 1994; Cook and Böhlke, 2000), pathways of water movement in the subsurface system (Kolbe et al., 2016), and the reaction rates of contaminants (Katz et al., 2004; Koh et al., 2006b; Visser et al., 2007; Green et al., 2010, 2016). Constraining the time scale of groundwater can be particularly useful to assess aquifer vulnerability to contamination (Böhlke, 2002; Koh et al., 2005; Kaown et al., 2009; Han et al., 2015). For example, in agricultural areas where surface fertilizers infiltrate into a subsurface system along with precipitation and cause aquifer deterioration, groundwater age can offer valuable information to identify periods of surface fertilizer loads and pathways within the subsurface systems (Böhlke and Denver, 1995; Manning et al., 2005; Alikhani et al., 2016; Jurgens et al., 2016).

Despite the usefulness and wide applications of groundwater age for water resource management, the concepts behind age estimation approaches require careful interpretation (Suckow, 2014). The word “age” can be interpreted as a unique scalar value corresponding to specific entity (such as human age), but in many cases, groundwater samples are composed of a mixture of groundwater parcels with different

flow paths. In such cases, it is more reasonable to consider that groundwater age represents an integrated estimate of groundwater parcels with different ages. This is particularly useful in assessing groundwater age in heterogeneous geologic media in complex hydrogeologic settings where groundwater at the discharge or sampling point can be composed of various ages of water particles. Therefore, for proper understanding and assessment of the groundwater age, its mixing mechanisms need to be considered (Weissmann et al., 2002; Bethke and Johnson, 2008). Recent studies related to interpretation of the groundwater ages have mainly focused on the age mixing phenomenon (Maloszewski and Zuber, 1982; Zuber et al., 2005; Cornaton and Perrochet, 2006; Visser et al., 2013; Green et al., 2014; McCallum et al., 2014).

There are three major methods used to assess groundwater ages; 1) Apparent ages (also known as “piston age”); 2) lumped parameter models (LPM); and 3) numerical modeling approaches. For apparent age, radioactive isotopes (^{3}H-^{3}He, ^{14}C and ^{36}Cl) and synthetic chemical compounds (CFCs, SF_6 and ^{85}Kr) are used to determine the groundwater age (Smethie et al., 1988; Aeschbach-Hertig et al., 1998; Busenberg and Plummer, 2000; Castro et al., 2000). The apparent age assumes a closed flow system since water entered into an aquifer, which means that mixing of different water particles from various flow paths does not occur. The use of the apparent age can bring uncertainties especially when groundwater is pumped from a long or multiple screened well or it originates from a heterogeneous aquifer system. To reflect groundwater mixing dynamics, analytical models, or “lumped parameter” models have been

suggested that account for the effects of dispersion and mixing within an aquifer or a wellbore. Various LPMs have been developed based on different types of distribution functions such as exponential and inverse Gaussian (Maloszewski and Zuber, 1982; Maloszewski et al., 2004) or heavy-tailed functions (Green et al., 2016). The simplicity of the age distribution functions makes LPMs computationally efficient, but occasionally, the models can be difficult to apply to regional scale aquifer systems with varying hydrogeological complexity (Turnadge and Smerdon, 2014). Recent studies have suggested a numerical approach for groundwater age assessment which is based on hydraulic simulation of groundwater and solute transport. In a numerical age assessment model, groundwater age can be treated as a solute in the advection-dispersion transport equation. The numerical models represent groundwater age as a probabilistic function rather than as a single age considering groundwater sample as a mixture of various water particles with different ages. The model can be readily applied to regional scale estimation (Goode, 1996; Varni and Carrera, 1998; Cornaton and Perrochet, 2006) in consideration of a heterogeneous geological domain with varying complexity (Lemieux and Sudicky, 2010; Molson and Frind, 2012; Kolbe et al., 2016). The numerical model can also provide transient characteristics of the groundwater age by incorporating different types of time-series data, such as precipitation, groundwater pumping history, and surface contaminants loading history (Park et al., 2008; Zuber et al., 2011; Engdahl and Maxwell, 2015).

The Gosan area, Jeju Island has suffered from severe nitrate contamination in

groundwater as a result of intensive agricultural activities since the 1960's. The study site is characterized by a multi-layer aquifer system composed of shallow perched and deep regional groundwater (UNDP and FAO, 1972; Koh et al., 2012) and groundwater wells penetrating the aquifers (Koh et al., 2016). Elevated nitrate concentration in the regional aquifer has been a major issue because it is the main source of potable and agricultural water for Jeju Island. In a complex hydrogeological system such as Gosan, delineation of the groundwater mixing mechanisms and pathways of nitrate are necessary for establishment of long-term groundwater resources management plans (Böhlke, 2002; Starn et al., 2014).

The objectives of this study are 1) to apply different age estimation models for characterizing the age of groundwater in Gosan 2) to compare the results between the models and evaluate the groundwater age distribution in consideration of the complexity of hydrogeologic setting and 3) to identify the nitrate input history and its major pathways influencing groundwater quality in the regional aquifer. Previous studies of the study area (Koh et al., 2012; 2016; 2017) characterized groundwater flow and the nitrate transport pathways based on isotope analysis, numerical models and statistical analysis, but none of these studies compared age-estimation methods to describe the history of nitrate contamination. In this study, I applied three different age estimation approaches (apparent age, LPM, and numerical model) with ^{3}H-^{3}He and CFC measurements. Then I compared estimated groundwater age distributions between the models and identified the hydrogeologic factors causing the discrepancy in the

estimated groundwater ages. Based on the obtained age distributions, I reconstructed the long-term nitrogen-loading history to the regional aquifer and evaluated major pathways that affect the regional aquifer quality. The study results are useful in identifying existing and historical sources of nitrate that are responsible for groundwater quality deterioration, and hence provide key information for long-term groundwater quality management plans in a regional setting with consideration of local aquifer geometry.

4.2. Study area description

The Gosan study area is situated in the lowland of the Hankyung watershed in the western part of Jeju Island, Republic of Korea (Fig.4.1a and b). The measured precipitation rate at the Gosan weather station (Fig.4.1a) from 1992-2014 was an average value of 1137.4 ± 259.7 mm/year, which is below the whole island average of 1639.4±509.1 mm/year (Korea Meteorological Administration, 2015). Jeju Island was formed from multiple volcanic eruptions, and volcanic rocks are the major hydrogeologic unit (major aquifer) of the island (Fig.4.1c). Geologically, the study area is composed of unconsolidated marine sediments (Seogwipo Formation; SGF), volcanic rocks, interbedded clay, tuff, and alluvial silty loam. Due to the existence of a locally distributed clay unit above the volcanic rock, the study area is characterized

by two aquifer systems consisting of an upper perched zone and lower regional groundwater separated by the impermeable clay layer (UNDP and FAO, 1972; Koh et al., 2012). The perched groundwater occurs at the top silt loam layer or tuff layer (depth to water: 0.6~3.1 m) and the regional groundwater is distributed in the volcanic rocks (depth to water: 12.5~27.5 m). Below the volcanic rocks, the SGF, which has a low permeability, inhibits downward groundwater flow.

As shown in Fig.4.1b, most of the land surface in Gosan is covered with agricultural land uses (76 % of the total area) as a result of an increase in crop lands since the 1960s (Koh et al., 2017). Consequently, intensive agricultural activities have been carried out for more than 50 years in the study area, leading to excessive usage of synthetic fertilizer (Koh et al., 2012). With an increase in fertilizer usage, degradation of groundwater quality by nitrate has been frequently observed (Oh et al., 2010; Koh et al., 2012; Jung et al., 2014). The perched aquifer contains consistently high levels of nitrate (observed average NO_3-N in 2009-2010: 39.4 ± 24.9 mg/L) due to its relatively high exposure to the surface nitrate loading (Koh et al., 2012). The regional aquifer, on the other hand, shows greater spatial variations of nitrate concentration. According to the previous survey by Koh et al. (2012), eight out of total 12 regional wells located in the lowland area contained a level of NO_3-N exceeding the drinking water standard (10 mg/L of NO_3-N) between 2009 and 2010 while the remaining wells showed low NO_3-N concentrations. Previous studies demonstrated that nitrate-rich groundwater from the perched aquifer leaked through the improperly constructed

wells and facilitated contamination of the underlying regional aquifer (Koh et al., 2012; 2016).

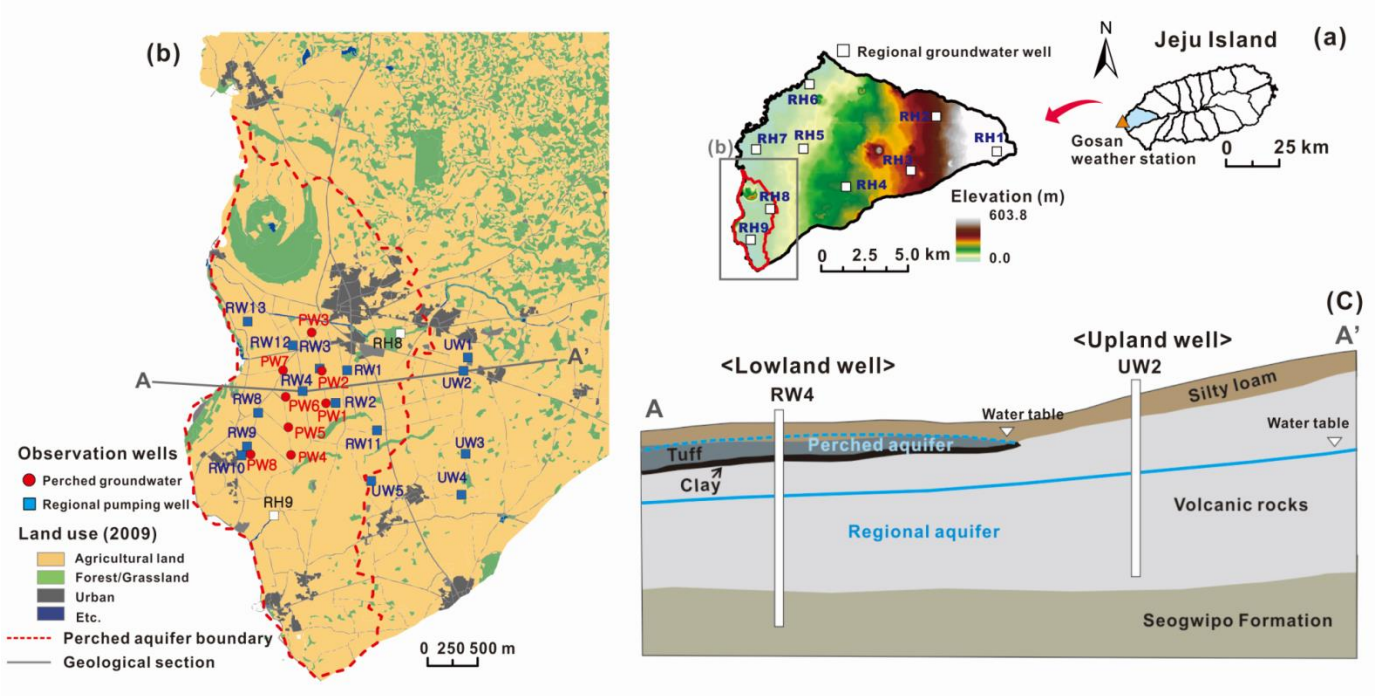

Fig.4.1. Site map showing (a) location of the Hankyung watershed (regional aquifer), (b) the Gosan study area (perched aquifer) with land use in 2009 and observation wells, and (c) cross-sectional hydrogeologic diagram.

4.3 Materials and methods

4.3.1 Hydrogeochemical and isotopic investigation

To analyze the dissolved concentration of environmental tracers (^{3}H and CFCs) and noble gases (He, Ne, Xe, Ar, Kr) in groundwater, three rounds of water sampling were conducted (June, 2012; Dec., 2013; Mar., 2014) for both the perched and regional aquifers. The locations of the wells used for data collection are shown in Fig.4.1b. Sampling wells in the regional aquifer were divided into the regional lowland (RW in Fig.4.1b) and upland wells (UW) based on the presence of the clay layer and perched aquifer above it. CFC samples taken in 2012 and 2013 were lost during the experiment due to an equipment malfunction; thus, these samples were excluded in this work. Instead, I included the previous study results from Koh and Kang (2011) for further analyses that measured ^{3}H and CFC (CFC-11, CFC-12, CFC-13) concentrations at the regional groundwater wells in Oct., 2009.

Groundwater was sampled following the procedure of Koh et al. (2012). Water samples for ^{3}H analysis were collected in 1 L HDPE bottles. ^{3}H analysis for the 2012 and 2013 water samples was conducted using the liquid-scintillation counting method at the Korea Institute of Geosciences and Mineral Resources, with a detection limit of 0.6 TU (Yoon et al., 2007). For the 2014 water samples, enriched analysis was applied to measure the ^{3}H content (detection limit: 0.6 TU) at Isotope Tracer Technologies Inc., Waterloo, Canada. Duplicated copper tubes were used for sampling the dissolved noble

gases, with both ends sealed using clamps. To avoid collection of gas bubbles, a high pressure was maintained during sampling by closing a valve installed in the discharge line. For CFCs, triplicate samples were collected in 60 mL borosilicate glass bottles, with flame-sealing at the ampoule neck using apparatus similar to that of Busenberg and Plummer (1992). The sampled noble gases in the copper tubes and CFCs were analyzed at the Dissolved and Noble Gas Lab., University of Utah, USA. Measurement errors for noble gases were less than 1% for the ^{3}He-^{4}He ratio and ^{4}He, 2 % for ^{20}Ne and ^{40}Ar, and 4 % for ^{83}Kr and ^{131}Xe. Aqueous concentrations for samples CFC-11, CFC-12, and CFC-113 were measured on a purge and trap gas chromatograph with an electron capture detector with precisions of 2 % for CFC-11 and CFC-12 and 3 % for CFC-113.

4.3.2 Computation of groundwater ages

1) Environmental tracer age estimation

Apparent ^{3}H-^{3}He age

Atmospheric ^{3}H concentration was dramatically increased over 1000 TU as a result of a thermonuclear test conducted in 1952–1962 (Weiss et al., 1979; Kim et al., 1988; Clark and Fritz, 1997). The highly elevated concentration of ^{3}H was infiltrate into the subsurface system with precipitated water. Because ^{3}H is a radioactive isotope, ^{3}H content decays with producing ^{3}He ($^{3}He_{trit}$) with a half-life ($T_{1/2}$) of 12.32 years.

Tolstikhin and Kamensky (1969) first suggested a ^{3}H-^{3}He age dating by applying the radioactive properties of ^{3}H decay into ^{3}He with time using reconstruction of initial ^{3}H concentration (Eq. 4.1). For using radioactive tracers to estimate groundwater age (apparent age), an assumption is applied that the tracer traveled from the recharge area to the observation point of the aquifer (e.g., discharge area, well) in a closed system.

$$\tau = \frac{T_{1/2}}{ln2} ln\left(1 + \frac{3He_{trit}}{3H}\right) \quad \textbf{[Eq. 4.1]}$$

The measured concentration of $^{3}He_{tot}$ in groundwater consists of several sources of ^{3}He, such as: 1) tritiogenic 3He ($^{3}He_{trit}$), which is produced by ^{3}H decay; 2) $^{3}He_{eq}$ equilibrated with the atmosphere; 3) $^{3}He_{exc}$ equilibrated with excess air; and 4) $^{3}He_{terr}$ from the crust and mantle. To calculate ^{3}H-^{3}He ages in a groundwater sample, it is necessary to extract the tritiogenic ^{3}He ($^{3}He_{trit}$) from the total concentration of ^{3}He ($^{3}He_{tot}$) as presented below,

$$4He_{tot} = 4He_{eq} + 4He_{exc} + 4He_{terr} \quad \textbf{[Eq. 4.2a]}$$

$$3He_{tot} = 3He_{eq} + 3He_{exc} + 3He_{terr} + 3He_{trit} \quad \textbf{[Eq. 4.2b]}$$

$$3He_{tit} = 4He_{tot}(R_{tot} - R_{terr}) - 4He_{eq}(R_{eq} - R_{terr}) - \left(\frac{4He}{20Ne}\right)_{exc} * (20Ne_{tot} - 20Ne_{eq}) * (R_{exc} - R_{terr}) \quad \textbf{[Eq. 4.2c]}$$

where R_{tot} is the measured $^{3}He/^{4}He$ in a water sample, R_{terr} is the $^{3}He/^{4}He$ from terrigenic sources, R_{eq} and R_{exc} are the $^{3}He/^{4}He$ for atmospheric air and excess air,

respectively, for which R_{exc} is 1.384 x 10^{-6} R_{eq}. $^{20}Ne_{tot}$ is the measured ^{20}Ne concentration in the sample and $^{20}Ne_{eq}$ is the equilibrium concentration of ^{20}Ne with the atmosphere. The ratio of ^{4}He /^{20}Ne in excess air is assumed as 0.288.

In this study, the amount of excess air in $^{3}He_{exc}$ was estimated by an excess air model in closed equilibrium using the NOBLE90 program (Aeschbach-Hertig et al., 1999) with measured levels of the noble gases (Ne, Ar, Kr, Xe) except He. Information about recharge elevation and temperature, required as input data for the program, was assumed to be the elevation of the sampled wells and measured temperature of the water sample. The best fit results were obtained by minimizing the uncertainty-weighted squared deviations between modeled and observed noble gas concentration.

Apparent Chlorofluorocarbons (CFCs) ages

Chlorofluorocarbons are stable and synthetic product developed since 1930 and its concentration in the atmosphere becomes continuously increasing from 1950s to 1990s, therefore CFCs have been utilized to groundwater age dating for relatively young groundwater less than 50 years (Thompson and Hayes, 1979; Plummer and Busenberg, 2000). To estimate apparent CFCs ages, dissolved CFCs concentration in groundwater samples should be converted to atmospheric mixing ratio based on the Henry's law solubility, in which gas solubility is determined by partial pressure (p_i) and temperature at the recharge time.

The partial pressure (p_i) can be defined as (Warner and Weiss, 1985),

$$p_i = x_i(P - p_{H2O}) \quad \textbf{[Eq. 4.3]}$$

where x_i is the dry air mole fraction of the CFC, P is the total atmospheric pressure and pH_2O is the water vapor pressure. For ideal gases, the dry air mole fraction is replaced with the air mixing ratio, volume per volume. Henry's law then gives the CFC solubility in water (C_i),

$$C_i = K_H p_i \quad \textbf{[Eq. 4.4]}$$

where K_H is the Henry's law constant for the CFC. K_H has been measured in pure water and seawater for CFC-11 and CFC-12 (Warner and Weiss, 1985), and for CFC-113 (Bu and Warner, 1995).

Then, the converted atmospheric mixing ratio compares with the atmospheric CFCs input history to estimate recharge year. Identical to the computation of He_{exc} for estimating the apparent ^3H-^3He ages above, I used well elevation and groundwater temperature in samples to determine the atmospheric mixing ratio of CFCs. The average measured temperature in the groundwater sample was 17.3±0.4˚C for Oct., 2009 and 17.6±0.6˚C for Mar., 2014, which presents a minor difference (within 2˚C) to the average annual air temperature of 15.6˚C (1981-2010) in the Gosan area. Only 1~3 years uncertainty for the CFCs ages would be caused by the uncertainty in the recharge temperature less than 2˚C (Busenberg and Plummer, 1992). I used the Northern

Hemisphere values of CFC-11, CFC-12 and CFC-113 for the CFCs age dating based on similarity to atmospheric CFCs in Jeju Island (Cunnold et al., 1994; Koh et al., 2006b).

2) Lumped parameter model

The lumped parameter model estimates tracer concentrations at an outlet position transported from an inlet position (recharge area) through various groundwater flow path in a subsurface aquifer system. To compute the tracer concentration at the outlet position (C_{out}), the tracer input history (C_{in}) is converted by a decay function and a transit time distribution (TTD) function (g(t-t')).

$$C_{out}(t) = \int_{-\infty}^{t} C_{in}(t')g(t-t')e^{-\lambda(t-t')}dt' \qquad \textbf{[Eq. 4.5]}$$

where C_{out}(t) is outlet tracer concentration, C_{in}(t') is tracer concentration at the inlet at time t', t is the sample date, t' is the date at which a water parcel entered the system, λ is the decay constant (fraction of loss per unit time), and t-t' is the age of the water parcel. To derive the TTD functions, several groundwater flow models, such as the piston flow model (PFM), exponential mixing model (EMM), exponential piston flow model (EPM), partial exponential model (PEM), and dispersion model (DM), have been developed and used in many studies (Maloszewski and Zuber, 1982; Jurgens et al., 2012). In this study, to delineate the age distribution and mean age accounting for the aquifer mixing of tracers, the TracerLPM program (Jurgens et al., 2012) was used and

a binary mixing model (PDF and DM) determined by previous work (Koh et al., 2006b) in Jeju was applied.

A binary mixing model (BMM) describes two mixing components which can be evaluated by other mixing models such as PFM, EMM, and DM. The general form of the BMM is similar to the two conservative components mixing equation as follow,

$$C_{out} = f_1 C_1 + (1 - f_1) C_2 \qquad \textbf{[Eq. 4.6]}$$

where C_1 and C_2 are first and second components concentration and f_1 is fraction of the first component. The BMM model is suitable for estimating the age tracer mixing occurred at wells with screens over multiple aquifers and in the aquifer system which characterized by short-circuit pathways (Jurgens et al., 2012).

The piston-flow model (PFM) has an assumption that an input tracer from a recharge area migrate along a groundwater flow channel the aquifer medium without any dispersion and mixing with other groundwater flow pathways. The PFM can be applied the aquifer system in which advective transport of solute is much larger than the dispersive transport. The convolution equation for the PFM as below,

$$C_{out}(t) = C_{in}(t - \tau_s) e^{(-\lambda - \tau_s)} \quad for\ t = \tau_s \qquad \textbf{[Eq. 4.7]}$$

where τ_s is mean age of the water sample and Cout would be 0 for $t \neq \tau_s$.

The dispersion model (DM) describes the 1-D solution of the dispersion equation for

a semi-infinite medium (Maloszewski and Zuber, 1982) according to dispersion parameter (*dp*) as shown below equation.

$$g(t-t') = \frac{1}{\tau_s}\frac{1}{\sqrt{4\pi DP\frac{t-t'}{\tau_s}}}e^{\left(\frac{\left(1-\frac{t-t'}{\tau_s}\right)^2}{4DP\frac{t-t'}{\tau_s}}\right)} \qquad \textbf{[Eq. 4.8]}$$

where τ_s is mean age of the water sample. The dispersion parameter can be calculated as D/vx (D is the dispersion coefficient, v the velocity, and x the outlet position) and represents the relative impact of dispersion to advection.

Koh et al. (2006) demonstrated that in the western part of Jeju Island, age tracers (^{3}H and CFC-12) showed a binary mixing pattern between relatively young groundwater which can be described by the DM and old water with low ^{3}H content (<0.5 TU). They suggest that the old water component was likely to originate from the SGF layer that underlies the permeable volcanic rocks of Jeju Island (Koh, 1997). Therefore, in this work, I described the young water component using the DM (Maloszewski and Zuber, 1982) with a dispersion parameter (dp) that accounts for the rate of dispersion during transport. I applied two dp values (0.01 and 0.5) following Koh et al. (2006b; 2011) who estimated the dp based on the matching observed and modeled age tracers in the regional groundwater of Jeju island. The old water component from SGF does not have a specific age because these age-tracer concentrations (^{3}H and CFCs) do not vary for water >60 years. For BMM, therefore, the age of the old groundwater was assumed to

be over 60 years (Koh et al., 2006b) and the age of the young groundwater was calibrated to minimize differences (less than 5%) between the tracers and the modeled equivalents.

Tritium and CFC-12 were chosen as input tracers for the LPM with each having a differently shaped input history (Fig.4.2). CFC-12 was selected as the target tracer among three CFCs (CFC-11, CFC-12 and CFC-113) due to its higher stability against degradation as compared to the others, lower solubility, and less contamination during sampling (Plummer et al., 1993; Burow et al., 1999; Plummer and Busenberg, 2000). Due to a lack of continuous long-term monitoring of ^{3}H in the study area, the input history of ^{3}H had to be reconstructed following previous work (Koh et al., 2005). The ^{3}H input history curve was constructed through correlation equations between measured ^{3}H at worldwide IAEA stations (Ottawa, Vienna, Washington) and those in Tokyo and Ryori, Japan (adopted as a proxy for Jeju Island based on the geographical proximity and the similar climatic condition; Koh et al., 2005). The pre-bomb ^{3}H value before 1961 was assumed as 5 TU, based on the measurements in Europe and North America (Solomon and Cook, 2000).

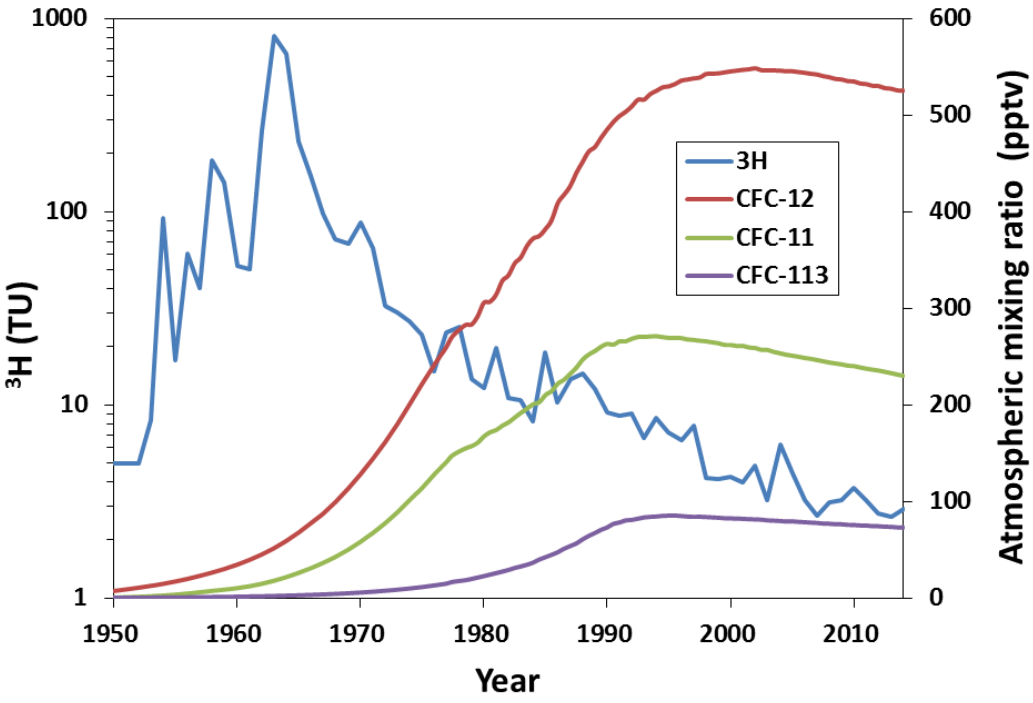

Fig. 4.2. Reconstructed historical curves of ^{3}H and CFCs in precipitation.

3) Numerical age simulation

Numerical simulations were carried out to obtain the mean age of groundwater and age CDF (cumulative distribution function)/PDF (probability density function) using HydroGeoSphere (HGS) numerical software (Therrien et al., 2010). I adopted the "double-domain integration approach" suggested by Koh et al. (2016) for simulating groundwater flow and well leakage hydraulics through the layered aquifer system. Koh et al. (2016) observed from their numerical experiments that the complex hydrogeologic setting of Gosan associated with leaky boreholes and layered aquifers significantly affected the numerical stability of the simulation results. To resolve such problems, they separated perched and regional aquifer domains and integrated the two domains on the basis of hydraulic connections between the two aquifers which include (1) drainage of shallow groundwater through the clay unit and (2) direct groundwater flow via the leaky wells (Fig.4.3). More details of the domain construction and integration processes are provided in Koh et al. (2016).

The HGS modeling program can solve variably-saturated flow and advective-dispersive transport of the age PDF (probability density function)/CDF (cumulative distribution function) or mean age itself, simultaneously. Transport of mean age with time and space can be directly solved by the advection-dispersion equation, in which solute concentration is replaced with the mean age, with an aging term related to the porosity of the model domain. The age probability describes the probability density for

the time (age PDF) required by water particles to travel from an inlet position to the outlet position. The age PDF at a position x in an aquifer can be evaluated by solving the ADE when a unit pulse of conservative tracer is uniformly applied on the recharge area. For a transient flow field, the PDF can be obtained from a solution for the CDF, which is estimated based on the following equations,

$$\frac{\partial \emptyset G}{\partial t} = -\nabla \cdot qG + \nabla \cdot \emptyset D \nabla G - q_O G \quad in\ \Omega \qquad \textbf{[Eq.4.9a]}$$

$$G(x,0) = 0 \quad in\ \Omega \qquad \textbf{[Eq.4.9b]}$$

$$[qG(x,t) - D\nabla G(x,t)] \cdot n = q \cdot n \quad on\ \Gamma\_ \qquad \textbf{[Eq.4.9c]}$$

$$[qG(x,t) - D\nabla G(x,t)] \cdot n = 0 \quad on\ \Gamma_0 \qquad \textbf{[Eq. 4.9d]}$$

where G(x, t) presents the forward travel time CDF, q is the water flux vector (L/T), q_O is fluid sink terms, respectively (1/T), D is the tensor of macro-dispersion (L^2/T), x = (x; y; z) is the vector of Cartesian coordinates (L), t is time (T), θ = θ (x) is porosity or mobile water content (-), n is a normal outward unit vector, and δ(t) is the time-Dirac delta function (1/T), which ensures a pure impulse on Γ_. The boundary condition applied at the inlet boundary (Eq.4.9c) is specified as the first-type condition G(x, t)=1. The age PDF (1/T) is estimated by differentiation of the computed travel time CDF with time as below:

$$g(x,t) = \frac{\partial G(x,t)}{\partial t} \qquad \textbf{[Eq. 4.10]}$$

Transient simulations from 1961 to 2014 were carried out to obtain the hydraulic head

and ^{3}H distributions for both perched and regional aquifers. Fig.4.3 and Fig.4.4 show the model boundary conditions used for simulation. For representing the hydraulic connection between the perched and regional aquifers, the computational results from the perched aquifer domain (drainage of the perched groundwater through the bottom clay and leakage of shallow groundwater via the leaky wells) were utilized as input data for the regional aquifer simulation. For ^{3}H simulation, time variant ^{3}H concentration (Fig.4.2) was applied at the top surface recharge boundary. Because there was no available data showing the history in ^{3}H concentrations at the mountainous boundary, the temporal change in ^{3}H at this area was reconstructed using a LPM and used as the model boundary. I applied the DM and fitted the simulated values with observed ^{3}H from the wells near the boundary (Fig.4.5). The best fit results estimated the mean groundwater age at this area as 17 years.

Initial model parameters were taken from a previous study (Koh et al., 2016), then calibrated using a trial and error method. For model calibration, the average hydraulic head and ^{3}H concentration measured at the perched and regional groundwater wells were used as target observations. ^{3}H concentration was chosen for the model calibrations rather than the apparent age because the latter approach can introduce bias in age estimation (Cornaton et al., 2011; McCallum et al., 2014). The model parameters used for simulations are shown in Table 4.1.

Based on the calibrated model set-up, the mean age/age CDF simulations were

implemented to generate the spatial mean age distribution and CDF of the study area. For age model boundaries, the first-type condition corresponding to the mean age of each boundary was specified. In the case of the regional aquifer, there are four inlet boundaries with different groundwater ages, including rainfall, upstream flow from mountainous area, drainage from the clay, and the leaky wells (Fig.4.4).

Transient simulation of nitrate (1961-2014) was carried out to reconstruct historical nitrate concentration in the study area. The historical variations in NO_3-N concentration were inferred based on the N-fertilizer use history of Jeju Island (Jeju Special Self-Governing Province, 2015) and the measured NO_3-N concentrations in groundwater of Gosan (2009-2011), and then utilized as the solute transport boundary. A previous study confirmed local denitrification at several perched wells (Koh et al., 2012). Therefore, the model included denitrification in the perched zone with a calibrated, first-order reaction rate of 5.16E-8 s^{-1} (Koh et al., 2016). In the regional aquifer, no nitrate reduction was introduced because the dissolved oxygen concentrations in the regional wells were high enough to inhibit denitrification (greater than 6.0 mg/L), which is also supported by isotopic data analysis (Koh et al., 2012; 2016).

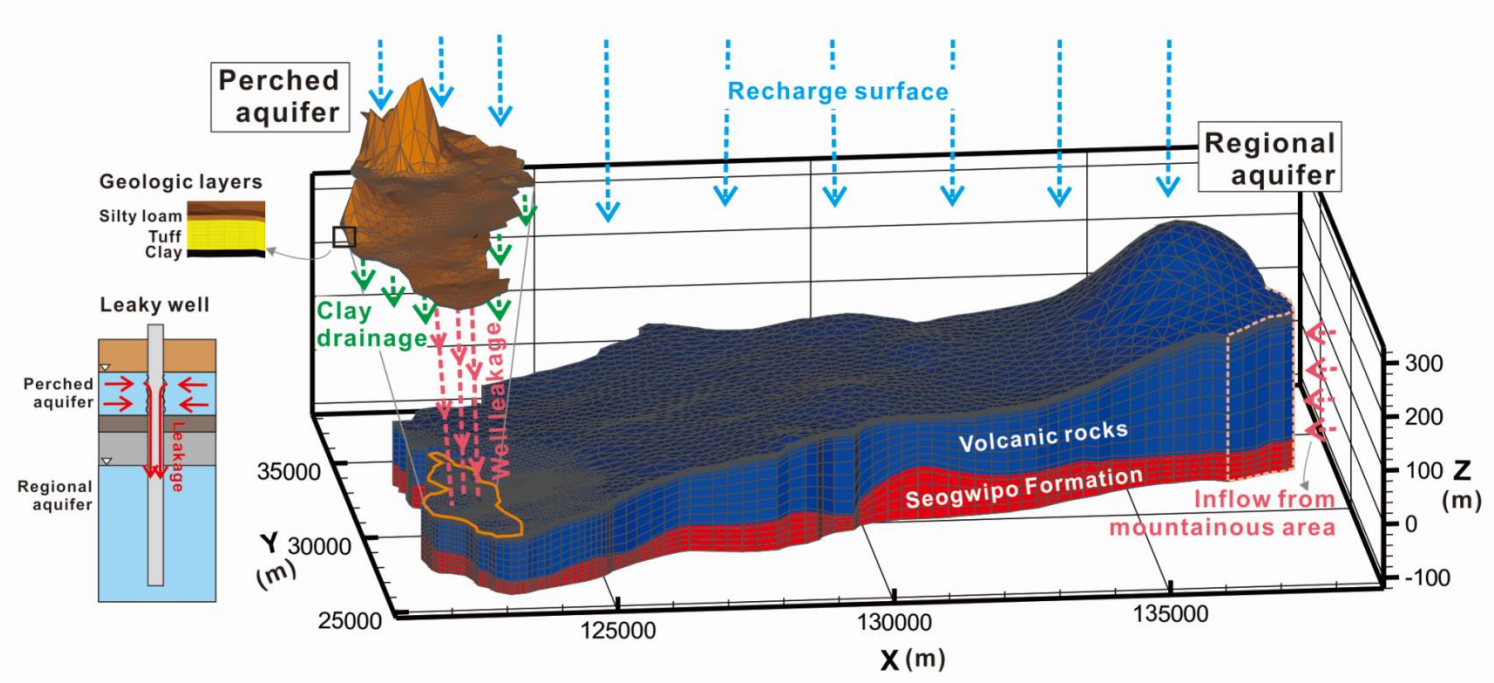

Fig.4.3. Numerical model domains and boundary conditions for the perched and regional aquifer systems.

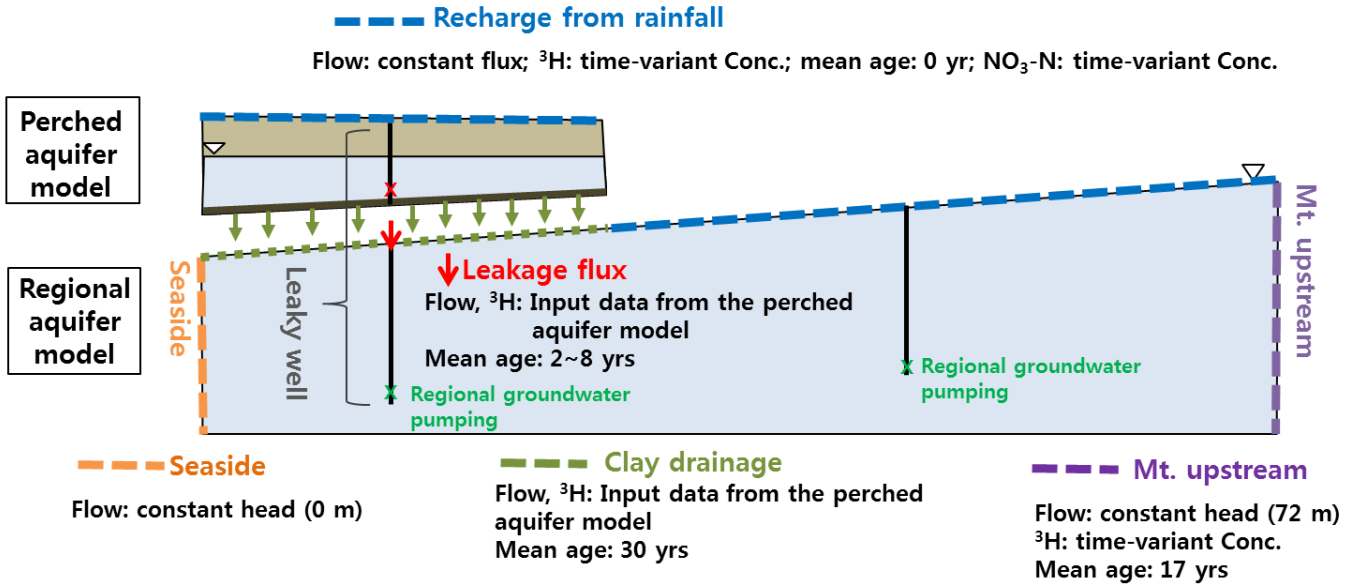

Fig.4.4. Boundary conditions used for the groundwater flow, ^{3}H, mean age (CDF), and NO_3-N simulations.

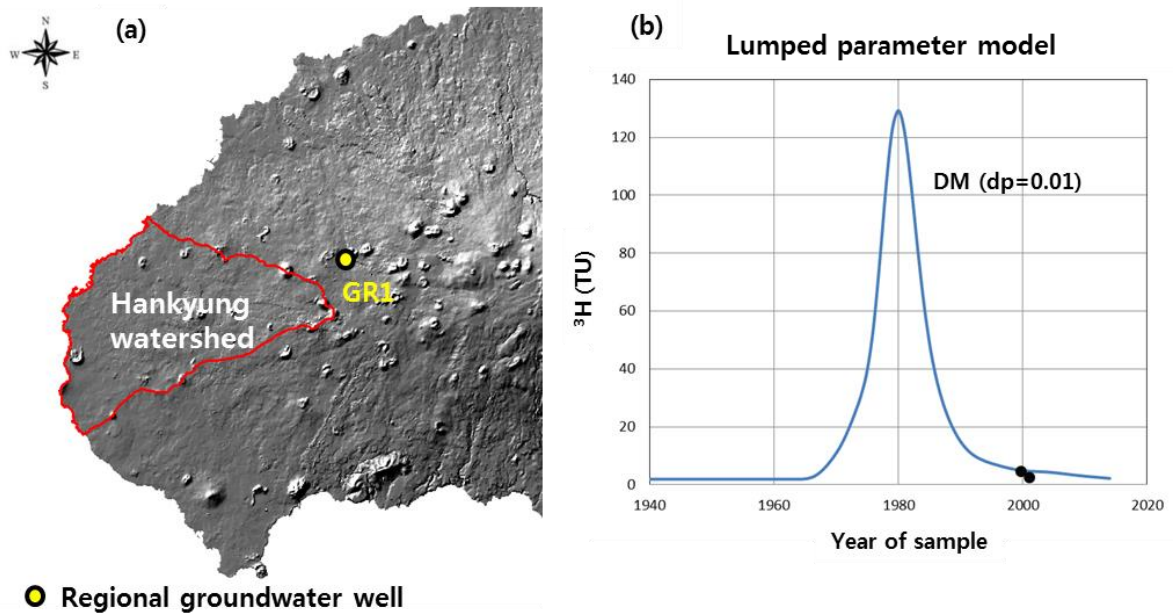

Fig.4.5. (a) Location map of a regional groundwater well (GR1) near the mountainous boundary for the regional model; (b) reconstructed ^{3}H-time graphs for the GR1 showing DM (dispersion model) with a mean age of 17 years.

Table 4.1. Calibrated parameter values used for the age simulation

Hydrostrati-graphic units	Calibrated hydraulic conductivity (m/sec)		Porosity[a]	S_s[b]	Van Genuchten function parameter[c]			Dispersivity[d] (m)	
	$K_{xx} = K_{yy}$	K_{zz}		(m^{-1})	S_{wr}	A (m^{-1})	β	a_L	a_T
Silt loam	8.5E−7	8.5E−8	0.45	1.0E−4	0.22	1.87	1.64	20.0	2.0
Tuff	6.6E−7	6.6E−8	0.44	1.0E−4	0.22	1.87	1.64	20.0	2.0
Clay	1.0E−9	1.0E−10	0.42	1.0E−3	0.27	4.54	1.51	0.1	0.01
Volcanic rocks	3.5E−4	8.5E−5	0.35	1.5E−4	-	-	-	30.0	3.0
Seogwipo Formation	1.0E−7	1.0E−8	0.40	1.0E−4	-	-	-	10.0	1.0

[a]Jejudo (unpublished results); [b] Batu, 1998; [c] Hodnett and Tomasella, 2002; [d]Gelhar, 1986

4.4. Results

4.4.1. Apparent ages: ^{3}H-^{3}He and CFCs

The relationship between ^{4}He and Ne concentrations of samples (Fig.4.6) can be used to identify components that comprise the total concentration of ^{4}He ($^{4}He_{tot}$). Because Ne originates only from equilibrium and excess air components while $^{4}He_{tot}$ in groundwater consists of several sources, including $^{4}He_{eq}$ equilibrated with the atmosphere, $^{4}He_{ex}$ equilibrated with excess air, and $^{4}He_{terr}$ from the crust and mantle. Consequently, elevated $^{4}He_{tot}$ concentrations relative to Ne can be used as the indicator of other ^{4}He sources besides $^{4}He_{eq}$ and $^{4}He_{exc}$. According to our analysis, most of the perched groundwater samples lay on the equilibrium and excess air lines, while samples from the regional groundwater tend to show enriched concentrations of ^{4}He compared to Ne (Fig.4.6). Such enrichment of ^{4}He in regional groundwater is likely to be from $^{4}He_{terr}$. Similar observations were found in a previous study by Koh et al. (2006).

For apparent age estimation, the extraction of $^{3}He_{eq}$ (equilibrated ^{3}He with the atmosphere) and $^{3}He_{exc}$ (equilibrated ^{3}He with excess air) from $^{3}He_{tot}$ (total concentration of ^{3}He) was performed using the NOBLE90 program (Aeschbach-Hertig et al., 1999). In addition, $^{3}He_{terr}$ (^{3}He from the crust and mantle) also needs to be removed from $^{3}He_{tot}$ to obtain the $^{3}He_{trit}$ (^{3}He decayed from ^{3}H) component which is required for groundwater tracer age estimation. Following Stute et al. (1992) and

Aeschbach-Hertig et al. (1998), the terrigenic $^{3}He/^{4}He$ ratio (R_{terr}) was defined from a plot of the excess air corrected ^{4}He with normalization to $^{4}He_{eq}$ versus the $^{3}He/^{4}He$ ratio corrected for excess air components (Fig 4.7). The R_{terr} values are determined from the y_0 intersect of the mixing line between the air-saturated water (ASW) and regional groundwater samples with low ^{3}H content ($^{3}H < 0.5$ TU). The range of estimated R_{terr} values is 8.8×10^{-6} to 1.0×10^{-5}, which is similar to previous estimates (8.2×10^{-6} to 9.2×10^{-6}) by Koh et al. (2006). Then, I corrected the $^{3}He_{terr}$ in the surplus ^{3}He using the estimated R_{terr} for regional samples and the typical value of R_{terr} (2.0×10^{-8}) for perched samples (Mamyrin and Tolstikhin, 1984), and derived the $^{3}He_{trit}$ and the ^{3}H-^{3}He apparent ages as provided in Table 4.2.

The apparent ^{3}H-^{3}He ages of perched groundwater were relatively young, from 3 to 10 years (Table 4.2), demonstrating that the perched aquifer is mainly affected by direct surface recharge events (Koh et al., 2012). The regional groundwater samples showed older ages (18–61 years) compared to perched groundwater. In order to evaluate whether the apparent ^{3}H-^{3}He ages were properly estimated, the reconstructed initial ^{3}H content and recharge year of the samples were compared to the ^{3}H input history of precipitation (Dunkle et al., 1993; Stute et al., 1997). If there was no mixing of water particles with different ages and ^{3}H loss, initial ^{3}H should plot on the ^{3}H input curve (Ekwurzel et al., 1994; Aeschbach-Hertig et al., 1998). In Fig.4.8., most of the samples showed a relatively good match with the ^{3}H input history curve, but some regional groundwater samples had lower initial ^{3}H values than the curve.

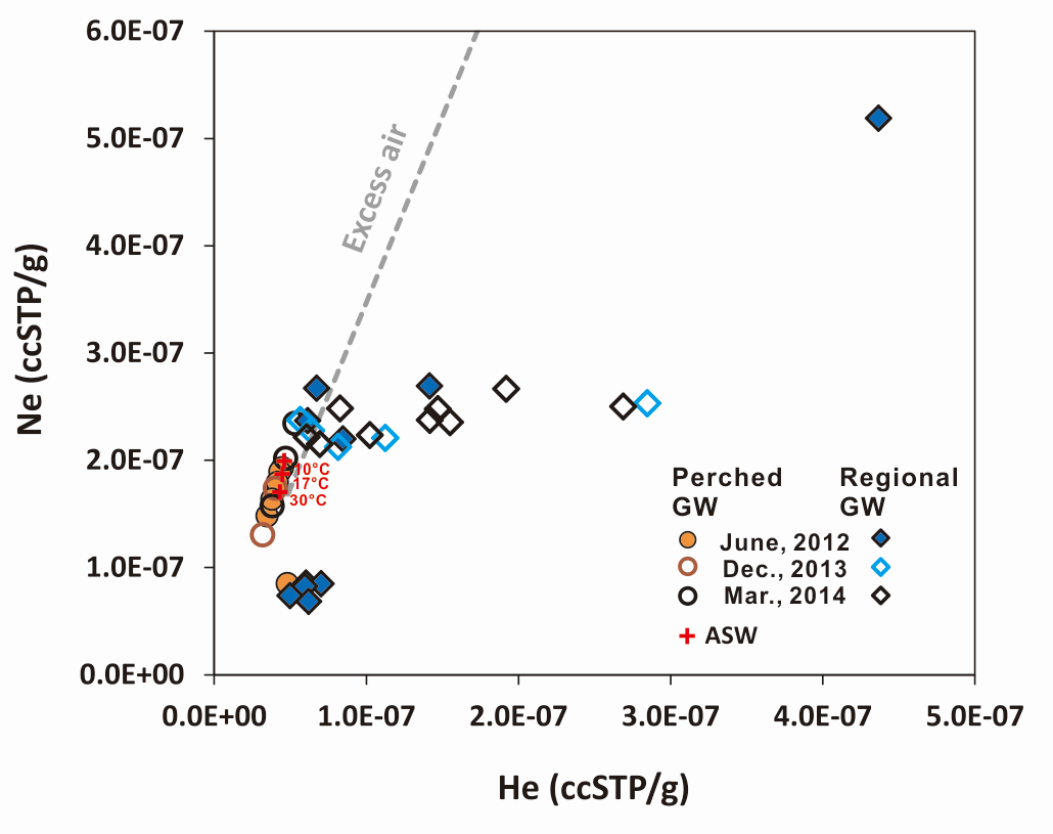

Fig.4.6. Relations between He and Ne for groundwater samples in 2012, 2013 and 2014. ASW indicates air-saturated water at 10˚C/17˚C/30˚C, 19 m altitude for the study area. Excess air presents unfractionated excess air ($[Ne_{ex}]/[He_{ex}] = [Ne_{air}]/[He_{air}] = 3.47$).

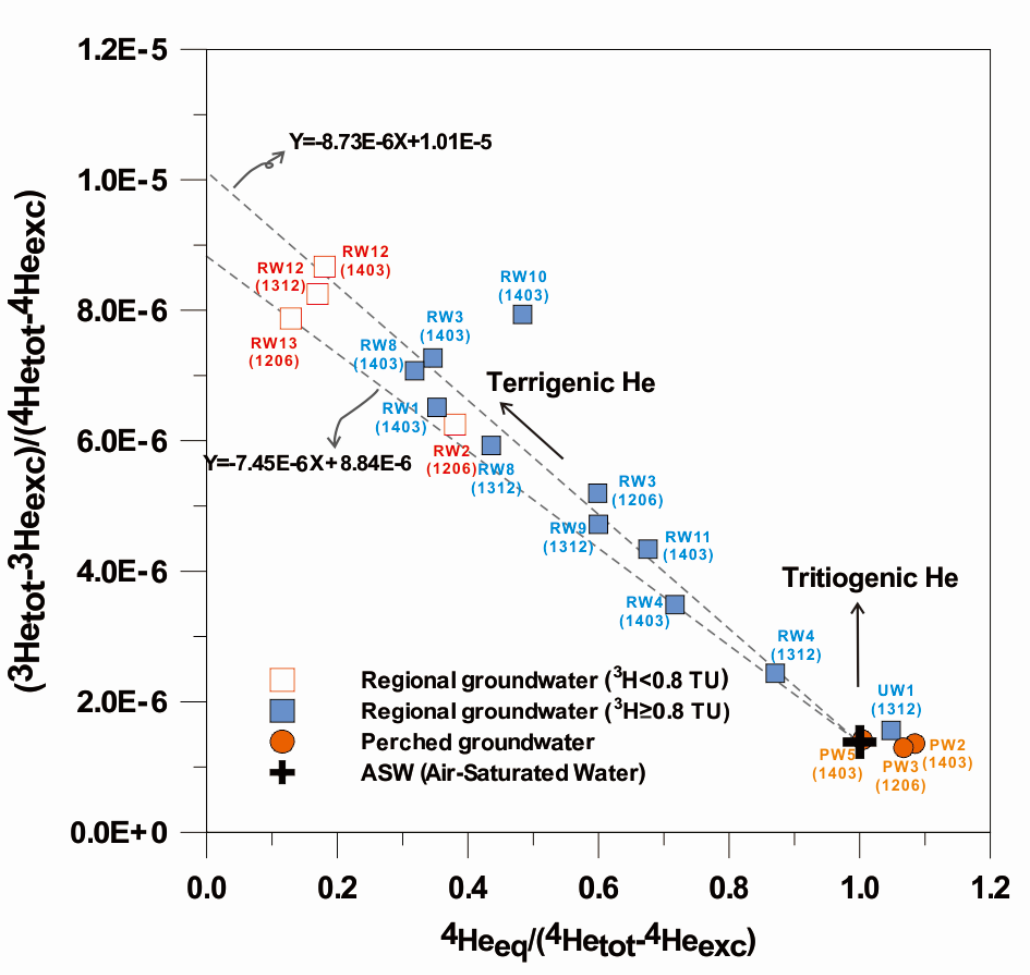

Fig.4.7. Excess air corrected $^{3}He/^{4}He$ ratio verses solubility equilibrium ^{4}He divided by excess air-corrected ^{4}He concentrations. The R_{terr} value was determined by the intercept y_0 values of the lower and upper trend lines of samples that had low ^{3}H concentration (<0.5 TU).

Table 4.2. Computed apparent ^{3}H-^{3}He age of the perched and regional groundwater samples.

Aquifer type	Well ID	Well Depth (m)	Date	Depth to water table (m)	^{3}H (TU)	Ne_{tot} (ccSTP/g x 10^{-8})	^{4}He (ccSTP/g x 10^{-8})	R_s/R_a †	$3He_{trit}$ (TU)	Apparent ^{3}H-^{3}He age (yr)	Initial ^{3}H (TU)
Perched GW	PW1	4.7	2012-06	0.2	1.5 ±0.8	14.8	3.45	1.04		No $^{3}He_{trit}$	
			2014-03	0.4	3.3 ±0.7	15.7	3.80	1.01		No $^{3}He_{trit}$	
	PW2	4.5	2012-06	0.6	2.4 ±0.6	19.3	4.47	0.99	1.8 ±0.7	10.0 ±2.0	4.3 ±1.4
			2014-03	0.8	4.3 ±1.0	23.4	5.29	0.99		No $^{3}He_{trit}$	
	PW3	4.6	2012-06	0.7	3.1 ±0.8	18.9	4.30	0.94	0.5 ±0.8	2.6 ±0.6	3.6 ±1.5
			2013-12	1.4	1.7 ±0.8	13.0	3.17	0.99		No $^{3}He_{trit}$	
	PW4	4.6	2012-06	0.6	3.7 ±0.7	17.9	4.15	0.96		No $^{3}He_{trit}$	
	PW5	5.0	2013-12	1.8	2.5 ±0.6	17.4	4.01	1.00		No $^{3}He_{trit}$	
			2014-03	1.8	2.2 ±0.8	20.2	4.70	1.02	1.0 ±1.6	6.6 ±2.0	3.2 ±2.4
	PW8	5.1	2012-06	3.0	2.8 ±0.8	16.4	3.77	1.02		No $^{3}He_{trit}$	
Regional GW	RW2	89.0	2012-06	16.0	< 0.5	26.9	1.41	3.98		No $^{3}He_{trit}$	
	RW3	82.0	2012-06	16.4	1.0 ±0.9	22.0	8.45	3.41	12.8 ±1.7	47.2 ±14.8	13.8 ±2.6
			2014-03	17.6	0.9 ±0.7	24.7	14.70	4.82	26.1 ±4.0	60.5 ±13.4	27.0 ±4.7
	RW4	70.0	2014-03	-	1.3 ±0.6	21.5	6.93	2.47		No $^{3}He_{trit}$	
	RW8	70.0	2014-03	-	1.3 ±0.5	23.5	15.50	4.81	5.9 ±4.2	30.5 ±5.6	7.2 ±4.7
	RW9	80.0	2013-12	17.6	1.4 ±0.9	21.2	8.14	3.25	2.4 ±1.8	17.9 ±6.9	3.8 ±2.6
	RW10	80.0	2014-03	14.5	2.5 ±0.7	22.3	10.2	5.37		No $^{3}He_{trit}$	
	RW11	85.0	2012-06	15.2	2.0 ±0.9	23.7	6.15	1.57		No $^{3}He_{trit}$	
			2014-03	17.4	1.3 ±0.5	24.8	8.27	2.75	6.5 ±1.7	31.7 ±5.7	7.8 ±2.2
	RW12	90.0	2013-12	-	<0.5	25.3	28.5	5.65	11.6 ±9.0	N/A‡	
			2014-03	14.9	<0.8	25.0	26.9	5.96	62.4 ±9.0	N/A	
	RW13	85.0	2012-06	-	<0.5	51.9	4.37	4.61		No $^{3}He_{trit}$	
	UW1	90.0	2013-12	-	1.2 ±0.9	23.7	5.66	1.10	9.3 ±1.6	38.3 ±11.6	10.5 ±2.2
			2014-03	17.4	1.5 ±0.7	23.7	14.2	4.41		No $^{3}He_{trit}$	
	UW4	90.0	2012-06	-	1.7 ±0.7	26.7	6.74	1.25	7.6 ±1.5	30.0 ±5.6	9.4 ±2.2
			2014-03	32.5	2.0 ±0.6	22.2	6.08	1.67		No $^{3}He_{trit}$	

†R_s: measured $^{3}He/^{4}He$ of the sample; R_a: atmospheric $^{3}He/^{4}He$ (1.384×10^{-6}).

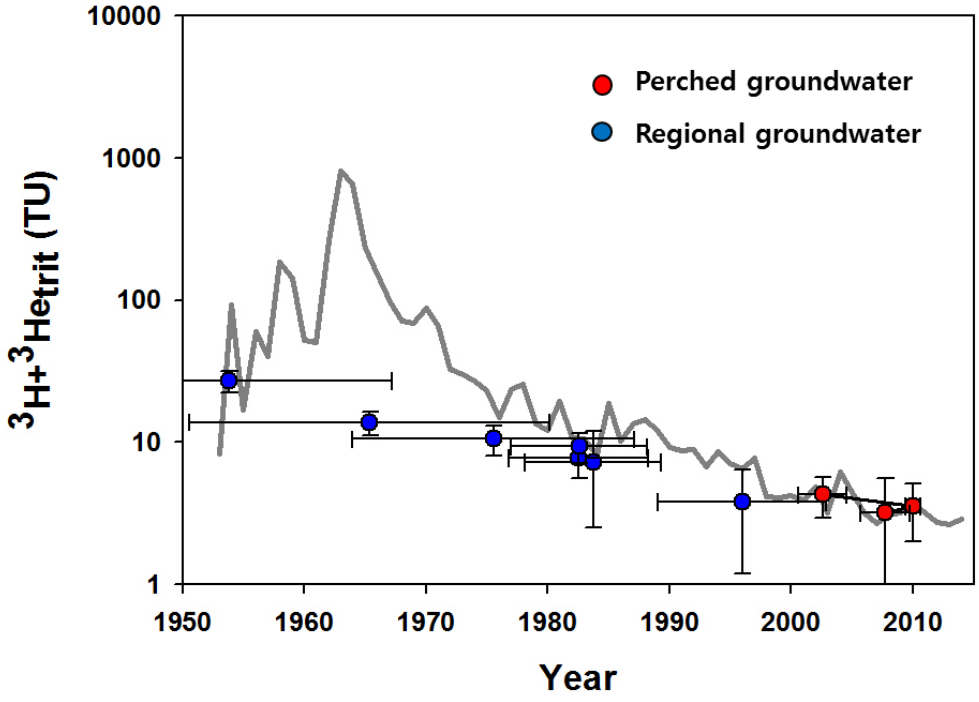

Fig.4.8. Comparison between the estimated initial ^3H ($^3H+^3He_{trit}$) values in the perched and regional groundwater and the reconstructed historical input curve of ^3H in precipitation.

The apparent ages estimated by CFCs (CFC-11, CFC-12 and CFC-113) in the perched and regional groundwater are listed in Table 4.3. For the perched groundwater, the CFC-12 apparent ages were determined as 24.7~33.5 years, which showed older ranges comparing to the apparent ^{3}H-^{3}He ages above. The difference between ^{3}H-^{3}He and CFC-12 ages could be related to local anaerobic conditions in the perched aquifer, which can affect CFC concentrations in groundwater (Plummer and Busenberg, 2000). Therefore, I excluded the CFCs from the perched groundwater samples for further analysis. The apparent CFC-12 ages of the regional groundwater have ranges of 18.0 to 55 years (average: 30.6 years, STDV: 12.8 years) in Oct., 2009 and 27.9 to 45.5 years (average: 34.5 years, STDV: 6.2 years) in Mar., 2014 (Table 4.3), which are similar to the age ranges estimated by the ^{3}H-^{3}He method.

Table 4.3. Computation of the apparent CFCs ages in the perched and regional groundwater

Sample ID	Sampling date	Measured concentration (pg/kg)			Atm. mixing ratio (pptv)			Apparent age (year)		
		CFC-12	CFC-11	CFC-113	CFC-12	CFC-11	CFC-113	CFC-12	CFC-11	CFC-113
RW1	Oct., 2009	210.4	292.7	37.0	457.7	151.7	47.3	21.8	31.8	24.3
RW4		315.8	353	31.1	Contam.	178.4	38.6	NA	28.8	25.8
RW8		178.7	360.3	28.7	385.5	184.9	36.2	25.3	28.3	26.3
RW11		71.5	396.9	36.8	151.5	199.7	45.5	38.3	26.3	24.8
RW12		25.6	53.6	14.2	56.9	28.4	18.6	46.3	44.8	31.8
RW13		7.2	17.2	13.0	15.8	9.0	16.7	55.3	50.8	32.3
UW1		237.5	372.3	33.4	517.2	193.1	42.7	<18.0	27.3	25.3
UW2		207.3	319.8	35.9	434.2	158.8	43.7	22.8	31.3	25.3
UW3		98.8	248.0	29.3	208.9	124.4	36.1	35.8	34.3	26.3
UW4		307.8	262.6	30.9	Contam.†	133.6	38.6	NA‡	33.8	25.8
UW6		249.8	293.4	34.2	531.8	148.4	42.5	<18.0	32.3	25.3
PW1	Mar., 2014	172.3	210.6	26.2	319.5	91.2	27.5	33.5	41.4	33.0
PW2		264.3	476.3	52.6	460.7	192.6	51.1	25.9	31.5	28.2
PW3		256.0	Contam.	59.8	480.5	Contam.	63.7	24.7	Contam.	26.2
PW5		201.5	476.5	41.9	389.1	216.0	46.2	29.5	29.2	28.9
RW1		79.2	205.7	15.0	178.0	110.4	19.9	41.5	40.0	35.5
RW2		50.2	97.0	10.3	111.6	51.5	13.5	45.5	45.5	38.5
RW3		100.3	292.4	18.1	224.8	156.6	24.0	39.2	36.0	34.0
RW4		190.3	459.6	34.7	409.9	235.5	43.8	28.4	27.4	29.4
RW8		121.5	322.0	20.7	267.0	168.7	26.8	37.0	34.4	33.4
RW9		134.7	366.6	23.4	298.5	193.8	30.6	34.9	31.5	32.0
RW10		163.6	391.1	28.9	369.9	211.4	38.7	30.7	30.0	30.2
RW11		157.5	321.1	29.9	337.5	163.6	37.6	32.4	35.2	30.5
UW1		197.6	458.0	37.0	419.3	230.7	45.8	27.9	27.9	29.0
UW4		198.6	518.1	35.7	418.9	259.1	43.9	28.0	25.5	29.2

† CFC contamination in samples

‡ Not analyzed

4.4.2. Lumped parameter model (LPM)

Using the tracer input history of CFC-12 and ^{3}H, the age PDF function (g(t) in Eq. 4.5) from the LPM was determined for the regional groundwater samples. The observed concentrations of the two tracers could be explained by the BMM combining recently recharged water described by the DM and ^{3}H-free old water (Fig.4.9). Until now, there has been no attempt to estimate the age of groundwater from the SGF although it has been generally accepted that the groundwater age in this unit is over 60 years (Koh et al., 2006b). Because of the difficulty of estimating the mean ages without the specific values for the age of the old groundwater components, I only estimated the ages and fraction of the young groundwater components (Table 4.4).

The mean ages of the young water ranged from 6–33 years (*dp*=0.01) and 4–32 years (*dp* =0.5), with fractions of 0.61–0.97 and 0.33–0.98, respectively (Table 4.4). There was no significant seasonal difference in the observed ages between the two sampling periods. The age PDF with the two *dp* values was generated and compared to provide information about the age distribution of the study area (Fig.4.10). The results show that most of the young water component (> 80%) has ages younger than 20 years, except for several wells which have ages of 40 years. In the age fraction graph, the age distribution is spread around the peak age according to the given *dp* values. A greater fraction of young groundwater was observed for the higher *dp* values in which dispersive mixing is stronger than advective mixing. There were no considerable

differences in the age distribution curves between lowland and upland wells in the LPM.

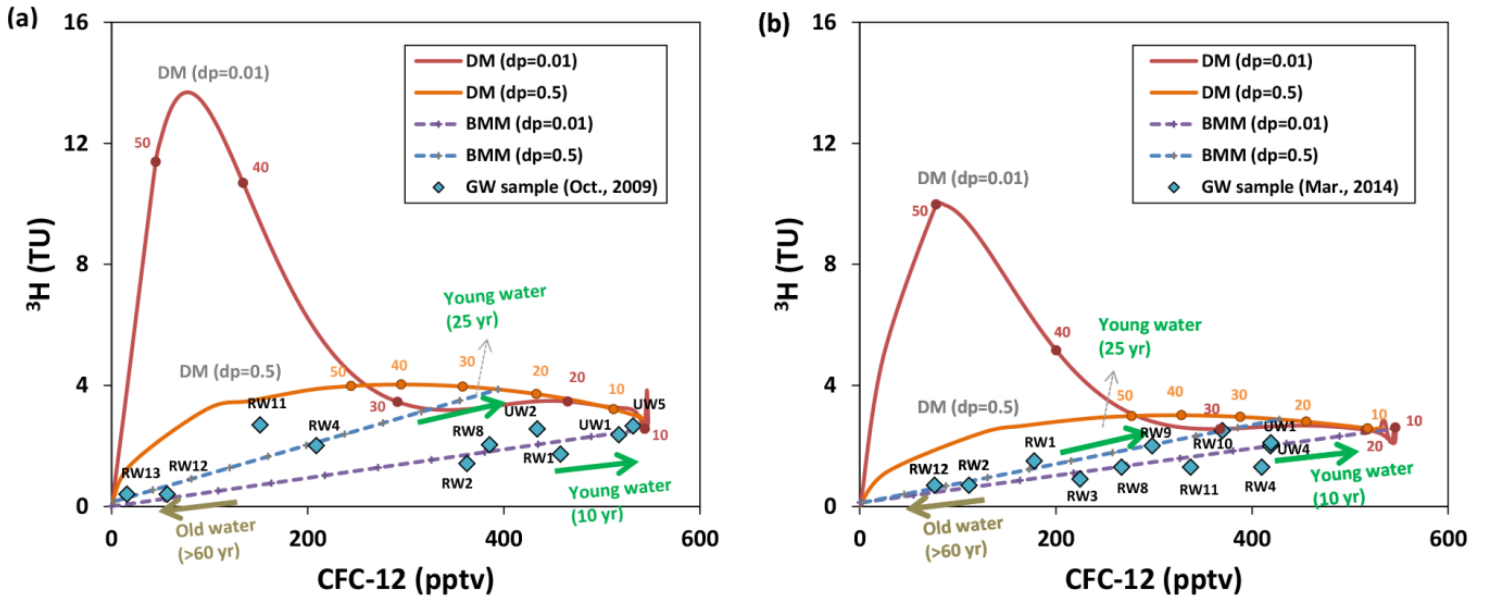

Fig.4.9. LPM-based mixing curves of CFC-12 and ^{3}H in the regional groundwater samples collected during (a) Oct., 2009 and (b) Mar., 2014.

Table 4.4. Ages and fraction of young water component derived from the lumped parameter model

Date	Well ID	^{3}H	CFC-12	NO_3-N	dp=0.01		dp=0.5	
		TU	pptv	mg/L	DM age	young fraction	DM age	young fraction
Oct., 2009	RW1	1.7	457.7	15.4	10	0.84	-	-
	RW8	2	385.5	20.8	10	0.71	4	0.71
	RW11	2.7	151.5	16.9	33	0.62	-	-
	UW1	2.4	517.2	15.7	10	0.95	4	0.96
	UW2	2.6	434.2	15.5	13	0.81	7	0.82
	UW3	2.0	208.9	17.0	27	0.61	25	0.53
	UW6	2.7	531.8	17.6	10	0.97	4	0.98
Mar., 2014	RW1	1.5	178	3.8	33	0.35	32	0.33
	RW3	0.9	224.8	8.9	7	0.41	-	-
	RW4	1.3	409.9	23.1	15	0.75	-	-
	RW8	1.3	267	9.8	20	0.33	10	0.5
	RW9	2.0	298.5	10.4	29	0.5	24	0.56
	RW10	2.5	369.9	12.0	29	0.55	24	0.7
	RW11	1.3	337.5	12.2	6	0.62	-	-
	UW1	2.1	419.3	23.5	20	0.45	8	0.79
	UW4	2.0	418.9	31.4	10	0.77	6	0.79

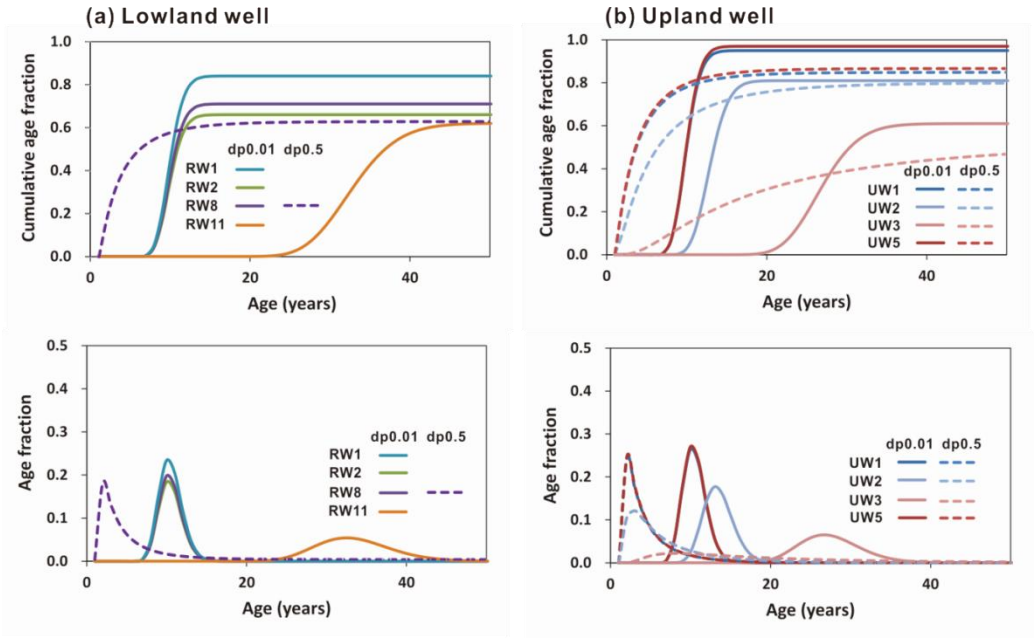

Fig.4.10. Cumulative age distributions and age distributions of the young water component derived from LPM, grouped into (a) lowland and (b) upland wells.

4.4.3. Numerical model results

Numerical model calibrations were performed for both the perched and regional aquifer, comparing the averaged heads (Perched GW, 2009–2010; Regional GW, 2001–2012) and ^{3}H values (2009, 2012, 2013, and 2014) measured in the field with the simulated ones. The calibration results, presented in Fig.4.11, show well matched values between observed and simulated heads and ^{3}H were obtained. With the calibrated model, ADE transport of the mean age and the age CDF was implemented in the two aquifers. Cross-sectional view of regional groundwater age and age CDF with time were generated in Figs.4.12a and 4.12b, respectively.

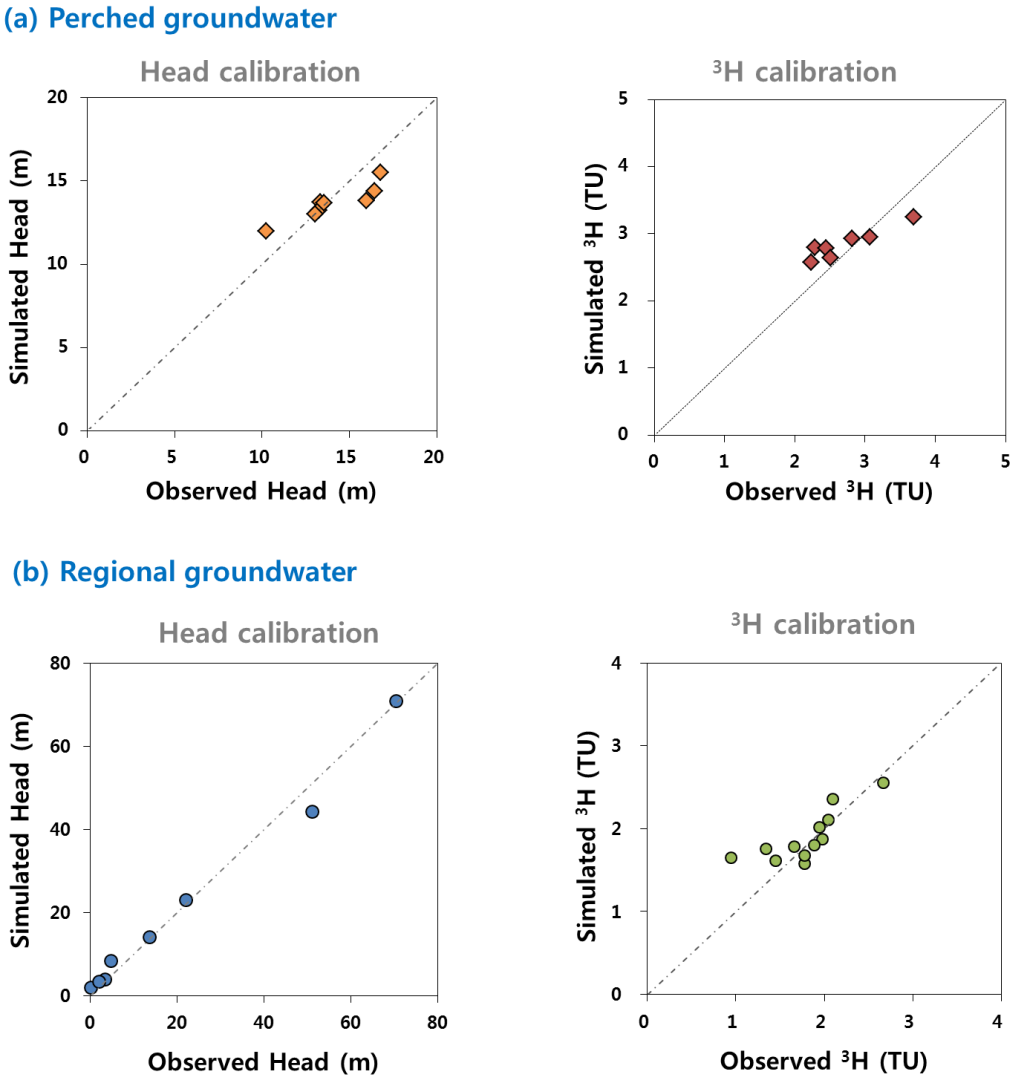

Fig.4.11. Comparison between the simulated and the observed hydraulic heads (a: Perched GW, 2009–2010; b: Regional GW, 2001–2012) and ^{3}H concentrations (2009, 2012, 2013, and 2014).

ADE transport of the mean age and the age CDF was implemented into both perched and regional aquifers using the calibrated model set-up. The simulated mean ages of the perched aquifer had a range from 1.5 to 11.65 years. Fig.4.12a and 4.12b illustrates the cross-sectional views of groundwater age and age CDF for regional aquifer, respectively. The mean age distribution (Fig.4.12a) showed that in the regional aquifer, rainwater with zero age infiltrated through the top upland area to the subsurface and moved along the groundwater flow direction with increasing age toward the coastal discharge area. In the lowland area where the clay layer blocks direct recharge from the surface, relatively old groundwater input passing through the clay layer governs the age distribution. Fig.4.12a also showed the effect of leaky well hydraulics and groundwater pumping on the mean groundwater age distribution. After introducing leaky wells and pumping effects, inflow of young perched groundwater via leaky wells was observed (bottom panel in Fig.4.12a). The figure also illustrates that groundwater pumping from the leaky well induced upward movement of old groundwater from the SGF into the leaky well.

Based on the evolution in the age CDF distribution with time, the sequential progress of groundwater recharge into the regional aquifer can be inferred (Fig.4.12b). The upland area was replenished with recharge from rainwater within a relatively short period whereas the lowland aquifer required a longer time to be replenished by perched water passing through the clay layer. The estimated CDF in some lower parts of the SGF had not reached a value close to 0.9 even after 1000 years, suggesting potential

existence of fossil groundwater over 1000 years in this area.

The age CDFs and PDFs obtained by the numerical model showed that lowland and upland wells had differently shaped age distributions from each other. In Fig.4.13a, I identified three separate flow-components that mainly influence the age distributions in the lowland wells: well leakage from the perched to the regional aquifer, upland recharge, and free-drainage of perched groundwater through the clay ("clay drainage"). The groundwater travelling through the well leakage and from upland recharge (ages less than 10 to 30 years) comprises about 23 to 56% of the age CDFs in the lowland wells. The water coming from the perched aquifer via clay drainage, having about 30 years of mean age, also takes a significant portion (40 to 55%) of the full age distribution. I also observed that these lowland wells did not reach 100% probability of CDF (or 1.0 on the y axis) in 100 years (upper panel in Fig.4.13a), which was caused by mixing with old water from SGF. The mixing ratio of old SGF water in the lowland leaky well was estimated to be less than 10% based on the obtained probability values. In the case of the upland wells (Fig.4.13b), the age distributions are mainly influenced by infiltration of surface recharge, similar to those derived from the LPM.

The mean ages of the lowland wells obtained from the age PDFs ranged from 24.7–41.2 years, which were older than those from the upland wells (9.7 to 14.5 years). The lowland region could have older groundwater ages as compared to upper zone because the mixing with old water, such as from drainage of perched groundwater through the

clay bed or from the SGF layer, could affect the age distribution of lowland wells.

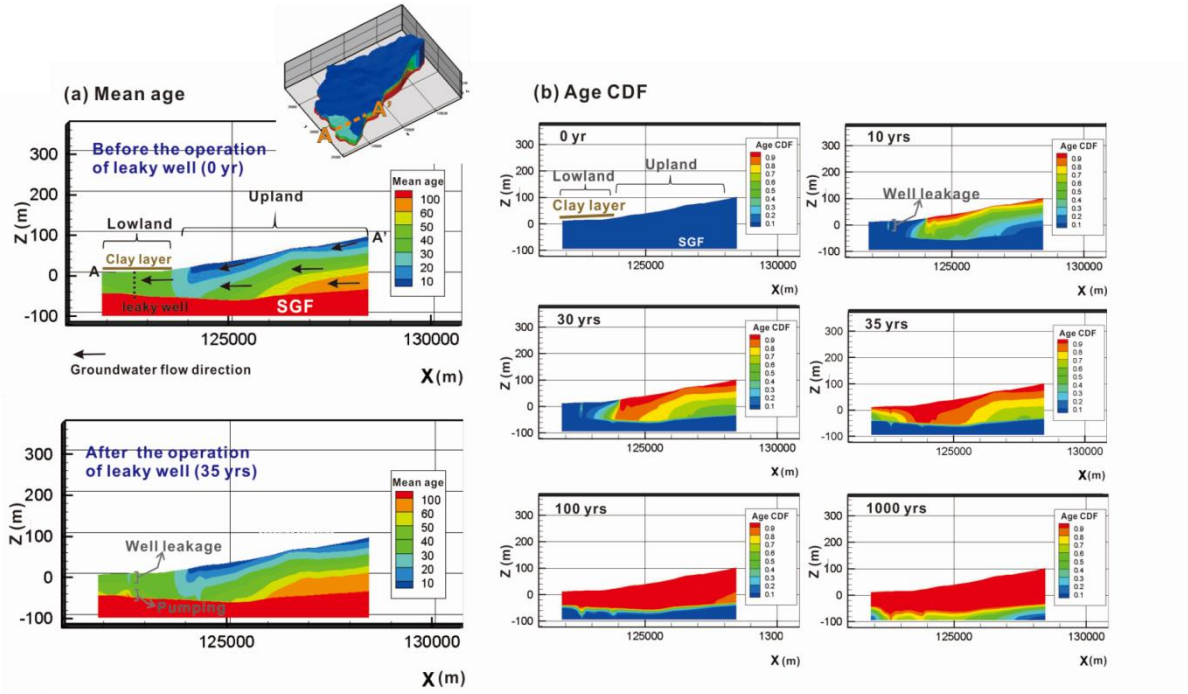

Fig.4.12. Cross-sectional view of (a) mean age distribution, and (b) sequential evolution of the age CDF obtained by the numerical simulation.

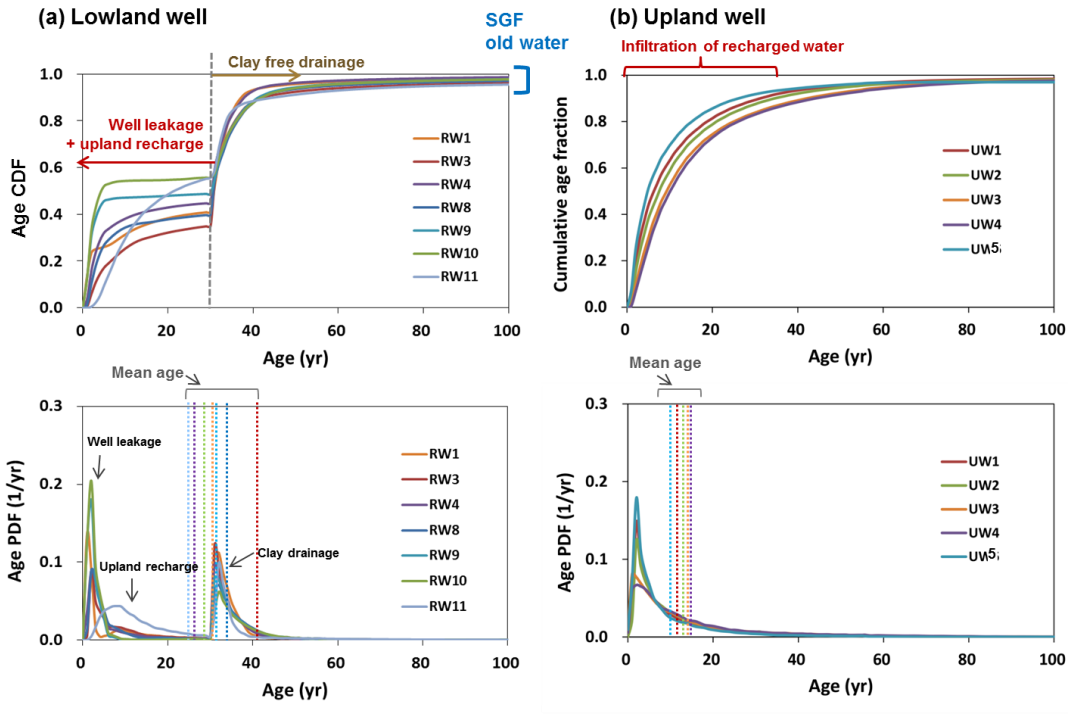

Fig.4.13. Age CDF and PDF curves for (a) lowland and (b) upland wells derived from the numerical simulation.

4.5. Discussion

4.5.1. Comparison of estimated regional groundwater ages between different models

The apparent ages (^{3}H-^{3}He, CFC-12) of the regional groundwater samples ranged from 18–61 years. The estimated apparent ages were relatively old compared to those from the numerical simulation (9.7–41.2 years). In the apparent ages, some discrepancies were observed between reconstructed initial ^{3}H and the ^{3}H input history curve (Fig.4.8). These uncertainties in the estimated tracer ages could be attributed to samples containing a fraction of prebomb water (Ekwurzel et al., 1994; Aeschbarch-Hertig et al., 1998) and to groundwater mixing process in the regional aquifer associated with various recharge sources and complex flow regimes (Bethke and Johnson, 2008). As already mentioned, the apparent age incorporates a closed aquifer system with piston flow model, in which mixing of groundwater from different pathways is not considered.

The LPM demonstrated that the groundwater ages in the study area could be explained by binary mixing between young and old water. The modelled ages of the young water components in the regional wells ranged from 4 to 33 years. Given the mixing with the old water component, the mean ages of the regional groundwater samples are expected to be older. There was no distinct difference in shapes of age PDFs between the upland and lowland wells (Fig.4.9), despite the considerable

difference in hydrogeological setting between the two regions. Several characteristics of the lowland groundwater flow regimes observed by previous studies (water drainage from perched aquifer, well leakage) were not represented in the LPM, suggesting that the model could have limitations for characterizing groundwater flow regimes in a complex hydrogeologic setting such as the study area, especially in the lowland aquifer region.

Unlike the apparent age or the LPM, the numerically computed mean ages showed a notable difference between the lowland (24.7–41.2 years) and upland (9.7–14.5 years) wells. Specifically, the age PDF/CDFs of the lowland wells showed distinctly different shapes from the LPM (Fig.4.13). It is noteworthy that the numerical model provided the full age distribution in consideration of various groundwater mixing components (well leakage, clay leakage, upland recharge, and upward flux from SGF) which contribute to the differences of the age PDFs between the lowland and upland areas. The results demonstrated that the complex mixing of groundwater with different ages and pathways can occur inside leaky wells, and can substantially influence the groundwater age distribution.

4.5.2. Estimation of time scales of NO_3-N response to historical fertilizer use

Aquifer vulnerability to nitrate contamination can be evaluated in relation to the

groundwater ages and the corresponding recharge history. Generally, groundwater with younger ages tends to show rapid response to fertilizer applications and higher vulnerability to the accidental release of contaminants at the surface (Manning et al., 2005; McMahon et al., 2008a; Visser et al., 2013). By utilizing the estimated groundwater age and the nitrate concentration data, the nitrate loading history to regional groundwater can be reconstructed and the response of the aquifer to the historical nitrate loading can be evaluated (Katz et al., 2001; Koh et al., 2006b; McMahon et al., 2008b; Green et al., 2010, 2016).

In Fig.4.14, the relationships between the estimated groundwater recharge year and the NO_3-N concentration at the time of recharge are presented together with the N-fertilizer use history (Böhlke, 2002; Koh et al., 2006b; Visser et al., 2007). I used the current NO_3-N concentrations as approximations of the NO_3-N at the time of recharge because no appreciable reduction of NO_3-N (denitrification) was observed in the regional aquifer (Koh et al., 2012). There could be some bias in the estimated nitrate loading history associated with local denitrification in the perched aquifer.

In Fig.4.14a, the apparent ^3H-^3He and CFC-12 age was used to plot the recharge year of each groundwater sample. The recharge-year corrected NO_3-N input history matched well with the adjusted fraction (F_{adj}) of 5–16% of the fertilizer use. The range of the adjusted fraction could result from heterogeneous features affecting occurrence of nitrate dissolved in the subsurface system, such as uptake of NO_3^- in the unsaturated

zone, local NO_3^- reaction processes, discharge of nitrate to the coastal area along with groundwater in the perched aquifer (McMahon et al., 2008a; Liao et al., 2012, Koh et al., 2016). Estimated recharged years from the apparent ^3H-^3He and CFC-12 ages demonstrated that the measured NO_3-N concentration showed a delayed response to the fertilizer usage history. The peak of fertilizer use in the 1990s has not yet affected most of the regional groundwater wells (Fig.4.14a). The apparent ages can have potential bias in their estimates due to the limitation of the piston flow and a closed system assumption, therefore, they require careful interpretation when applied in a regional scale assessment (Bethke and Johnson, 2008; Cornaton et al., 2011; McCallum et al., 2014).

Fig.4.14b and 4.14c show the historical N-loading history obtained from the LPM and numerical models, respectively. In Gosan, chemical fertilizers have been applied since the 1960's, therefore, the groundwater mixing components older than 60 years do not contribute to the elevated nitrate concentration in groundwater. Consequently, for reconstructing the groundwater recharge years that are responsible for nitrate contamination, only young groundwater components (<60 years) of the age PDFs were considered in the analysis. In addition, the NO_3-N concentrations in the young water component were adjusted to compensate for the mixing with old water which had very low NO_3-N concentrations.

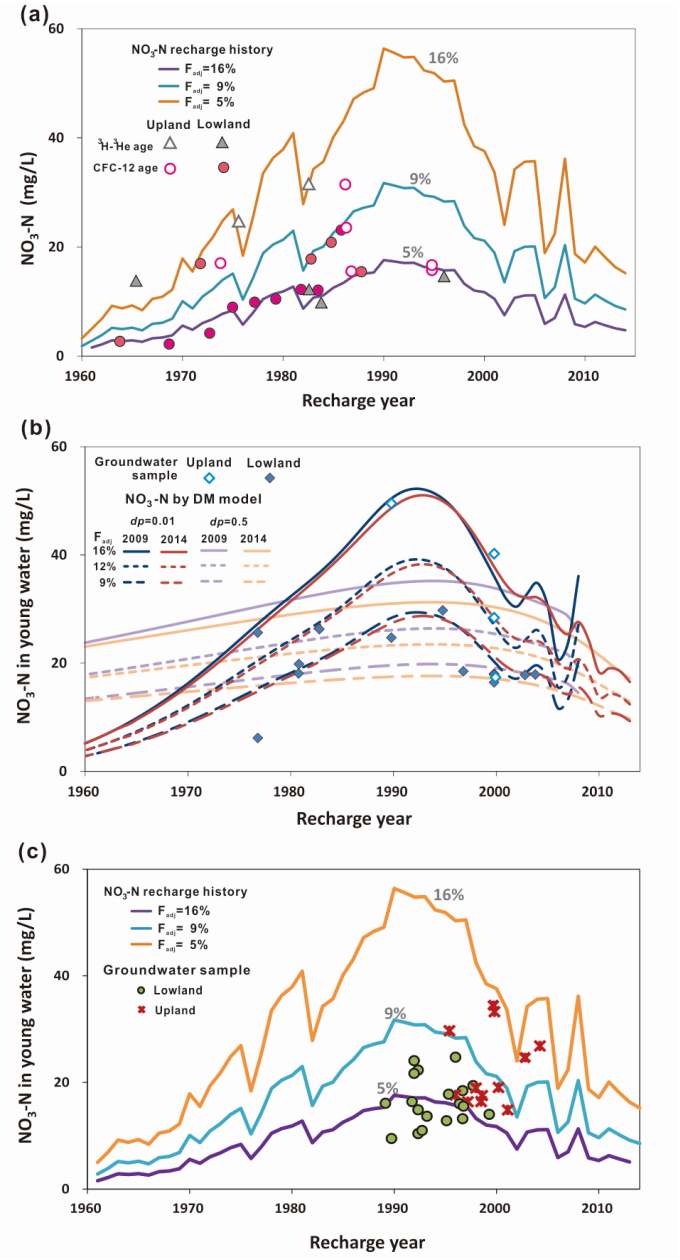

Fig.4.14. Reconstructed NO_3-N input history into the regional groundwater of Gosan based on (a) the apparent ^3H-^3He and CFC-12 ages, (b) lumped parameter model and (c) numerical simulation.

The reconstructed nitrate loading history based on the LPM demonstrated that the recalculated NO_3-N concentration in the young water showed good matches with the N-loading curves of F_{Adj}: 9–16% (Fig.4.14b). Fig.4.14b also revealed that the estimated recharge years of regional groundwater from the LPM were more recent (1977–2006) than those estimated with the apparent ages. Since the LPM considered only young water components in configuring the nitrate loading history, the recharge years of the sampled groundwater shifted to more recent values (6–24 years from the apparent age estimates). In Fig.4.14b, it can be observed that some of the regional groundwater wells have passed the highest loading of nitrate (the peak of historical fertilizer usage in Gosan) while the others have not.

Among the three age dating models, the groundwater ages (‘young component age’) obtained from the numerical model were dated as the youngest, indicating that that recharge of precipitation into the regional wells has occurred most recently, from 1989 to 2004 (Fig. 4.14c). According to the estimated groundwater ages from the numerical model, the regional aquifer of Gosan responded to the surface fertilizer more rapidly than those estimated by other models. Another interesting finding in Fig. 4.14c is that the regional groundwater samples are divided into the lowland and upland groups. The lowland wells were plotted between 1989 and 1999 along the 5 to 9% of F_{Adj} curve and they were characterized by lower NO_3-N concentrations (9.5~24.7 mg/L) and older recharge years. On the other hand, the upland wells generally showed greater NO_3-N (14.8~34.5 mg/L) and the groundwater recharge occurred more recently (1995 to 2004)

than in the lowland wells. The relatively old ages and low NO_3-N in the lowland wells were impacted by the perched aquifer above, which acted as a buffer zone of downward movement of nitrate into the regional aquifer. In Fig.4.14c, most of regional wells have passed or been passing the peak of historical fertilizer usage (the maximum loading period of nitrate into the subsurface).

Our results demonstrated that three age estimation approaches applied in this study produced markedly different shapes of age distributions. Furthermore, the reconstructed nitrate loading histories for the regional aquifer varied among methods. There are several previous studies that utilized different age dating approaches to compare the groundwater age distributions and their implications for aquifer vulnerability. Eberts et al. (2012) applied particle tracking and the LPM to four different hydrogeologic settings and observed that comparably similar age distributions were made by the two different approaches due to the well-defined conceptual model. Similarly, Green et al. (2014) found that the functional form of unimodal and bimodal LPMs (not including piston flow) did not strongly affect predictions of age or NO_3^- concentrations. However, in this study, I observed that shapes of the age PDFs could be considerably different depending on the applied age-dating models. The reconstructed and predicted NO_3-N concentrations also could vary depending on the model, especially as affected by hydrogeological complexity. Although the LPM can provide appropriate estimation of the groundwater age distribution for properly conceptualized aquifer systems, its applicability may be limited in settings with multiple and discrete

groundwater flow components, such as with the perched layer in this study. A multi-model approach can provide better estimation of age distributions to account for such complexities (Green et al., 2014; 2016), but the increased numbers of parameters in such approaches may make calibration difficult. In such cases, numerical models combined with the tracer concentration could be an alternative method to identify and characterize the multiple recharge pathways and to obtain multimodal age distributions.

4.5.3. Groundwater mixing characteristics and major pathways of nitrate in the regional aquifer

Based on the age PDFs produced from the numerical models, I conceptualized the mixing characteristics of groundwater with different ages (pathways) in the regional aquifer (Fig. 4.15a) and estimated the relative contribution of each component to the mixed groundwater age (Fig.4.15b). In the regional aquifer of Gosan, water-mixing characteristics were heavily influenced by the local aquifer geometry including recharge infiltration, drainage through the clay layer, mixing with old groundwater from the SGF as well as the artificial factor of water leakage through improperly constructed wells. From Fig.4.15, I observed that local heterogeneity could lead to considerable spatial variations in the groundwater flow dynamics. The upland region of the study site is mainly replenished by recharge infiltration from the surface, whereas the lowland aquifer is controlled by more complex flow regimes that are attributed to the various water input sources and pathways.

By combining the extracted age PDFs of the flow components and the numerically obtained nitrate concentration data (Fig.4.16) corresponding to the time of recharge, I generated NO_3-N PDF curves for the regional wells in Gosan (Fig.4.15c). Each curve shown in Figure 10c represents the portion of the well's overall NO_3-N PDF contributed by that flow component. Summing the curves for the three components yields the overall NO_3-N PDF with an integral of 1. Comparing the individual PDF components enables a quantitative demonstration of the nitrate contribution from each flow component to the regional groundwater. The generated NO_3-N PDF curves also revealed distinctive differences depending on the sources, in terms of their similarity to the groundwater age PDFs (Fig.4.15b). In the case of upland recharge infiltration (component ①), the shapes of the age PDFs did not show significant differences between flow and NO_3-N. On the other hand, the shapes of NO_3-N PDFs for well leakage and clay drainage were considerably different from the flow age PDFs. For well leakage, the contribution to NO_3-N PDFs (as estimated by the area under the curve) was noticeably greater than the contribution to the water age PDFs (component ②). For clay drainage, on the contribution to the nitrate level in the lowland wells was less than the contribution to the water age PDFs (component ③). Due to local denitrification in the perched aquifer, the level of nitrate in the perched groundwater decreases with time. Consequently, by the time that the perched groundwater enters the regional aquifer via clay drainage (about 30 years later), the nitrate concentration is significantly reduced and the clay drainage has less impact on the nitrate level in the

regional aquifer. On the other hand, groundwater travelling through the leaking wells maintains relatively constant nitrate concentrations due to the short residence time in the perched aquifer (< 6 years) and shows enhanced influence on the regional groundwater quality.

Comparison of NO_3-N PDFs between lowland and upland areas showed that at the upland wells, where direct recharge is the dominant water component, contaminant loading from the last 30 years greatly affects the water quality (Fig.4.15c). In the lowland area, the well leakage flux acts as a rapid pathway of nitrate-rich groundwater to the regional aquifer, and also as a major source of nitrate (23~74% of the total NO_3-N PDF) deteriorating the groundwater quality. Similar observations were made quantitatively by the numerical simulation of Koh et al. (2016). It is interesting that while the clay drainage comprises a large portion of the full age PDF in the lowland wells in terms of water flux, its contribution is significantly decreased (9–12%) for the NO_3-N PDF. The NO_3-N migrating from the upland area toward the lowland wells showed delayed response (7–30 years) with varying proportions (6–40%) depending on the wells. Our results demonstrated that the NO_3-N PDF can provide valuable information to quantify the impact of different nitrate pathways on the nitrate occurrence in a complex aquifer system and to identify major sources of nitrate influencing groundwater quality.

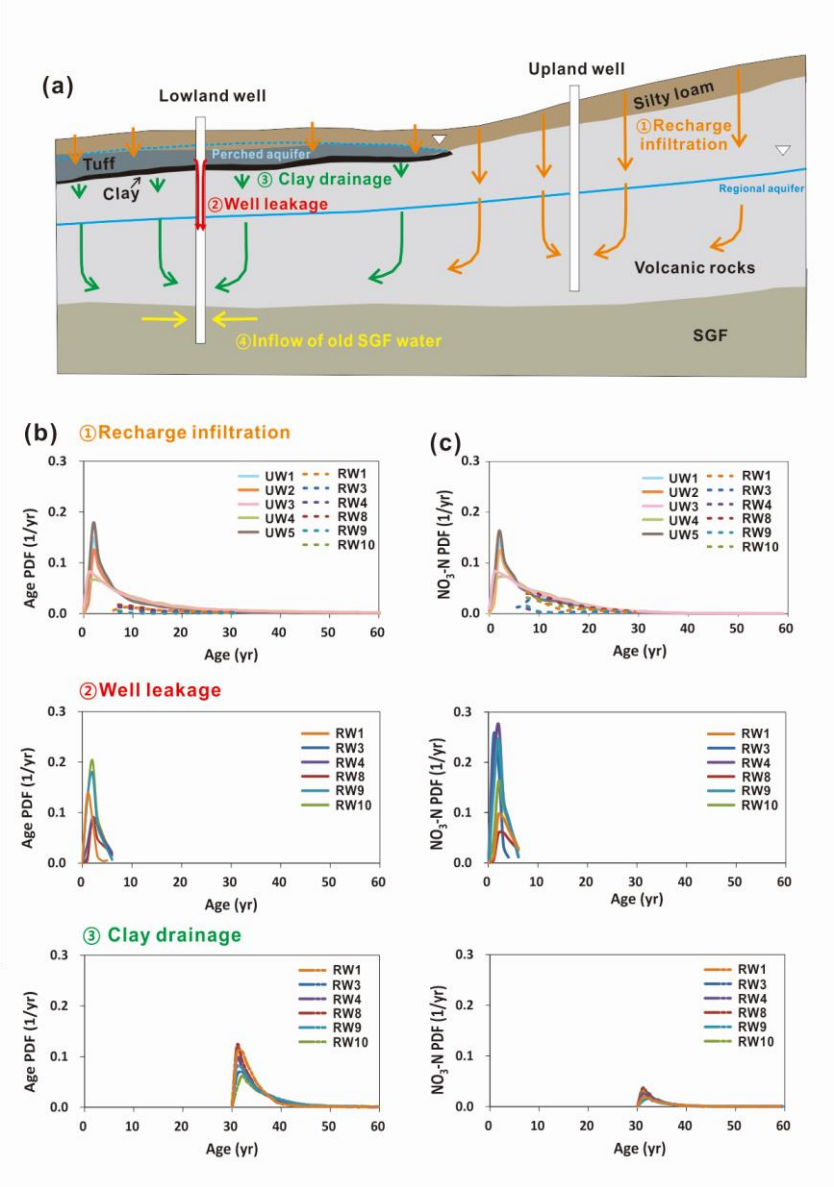

Fig.4.15. Schematic diagram showing (a) the groundwater flow regimes and the mixing characteristics of groundwater with different ages (pathways) in the regional aquifer, (b) portions of the overall age PDF contributed by each flow component, and (c) portions of the overall NO_3-N PDF contributed by each flow component.

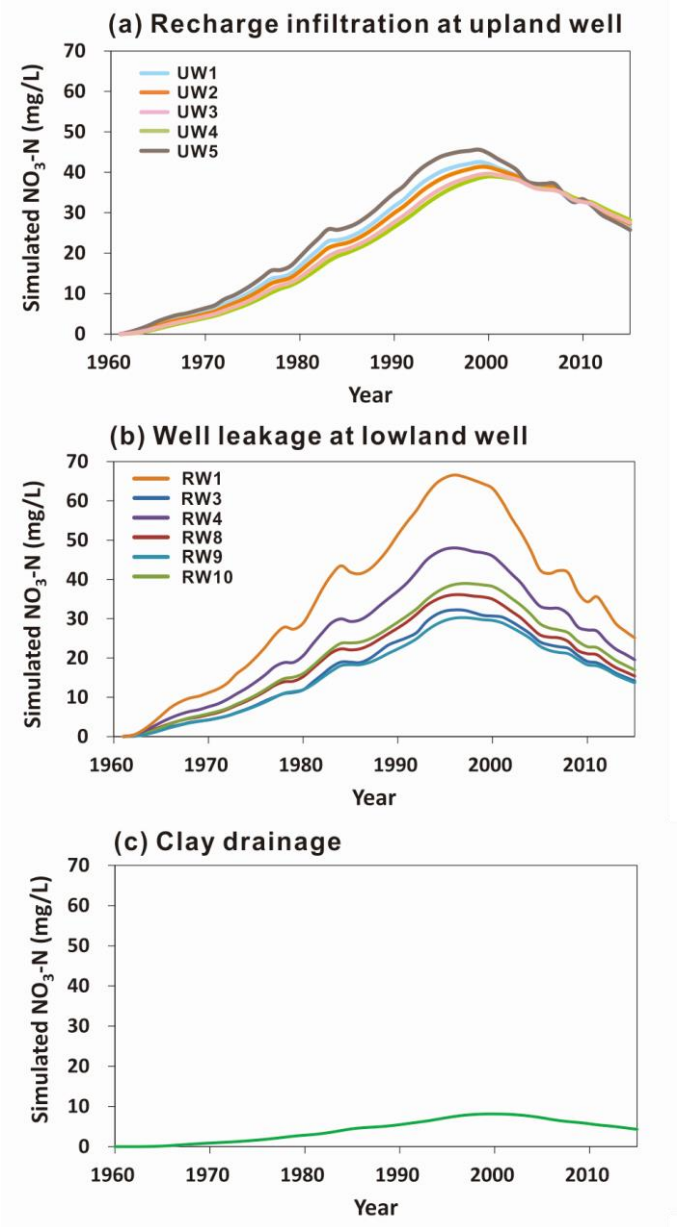

Fig.4.16. Simulated NO3-N concentrations of the water-mixing flow components from 1961 to 2014, (a) NO3-N concentrations for the upland recharge infiltration (component ① in Fig. 4.15), (b) well leakages (component ②), and (c) clay drainage (component ③).

4.5.4. Long-term groundwater management plans based on the different age dating methods

To control the nitrate contamination in the regional aquifer of the study area, management actions should be undertaken in consideration of the historical loading of the nitrate and the corresponding response time of groundwater. Variations in estimated groundwater ages and the PDFs depended on the applied age-dating models, and, thus, could suggest different groundwater management plans. In this study, I compared long-term groundwater management plans of Gosan based on the three different age estimation methods.

The apparent ages predicted the most delayed response of the regional aquifer to the nitrate loading. According to the apparent age result, the highest peak of the nitrate loading has not reached the regional aquifer yet, implying that nitrate concentration in the regional wells would increase further, reaching the maximum level in approximately 5~25 years. In this case, reduction of fertilizer usage may not be adequate to protect groundwater quality, because historical nitrate loadings would continuously increase nitrate concentration for a long period regardless of immediate fertilizer reductions. The management strategy based on the apparent ages suggests that additional mitigation methods such as bioremediation are needed to remove the residual nitrate components in the groundwater of the Gosan area.

In comparison to the apparent age, the LPM predicted relatively short response times

of regional groundwater to the fertilizer applications. In reconstructed nitrate loading history graphs, I observed that some of the wells have not passed the peak of past nitrate loading yet, implying that groundwater remediation action might be required (Fig.4.14b). Aside from these wells, nitrate concentrations in the regional aquifer will steadily decrease under proper controls on the application rates of fertilizer, and groundwater contamination of the regional aquifer will be relieved within 10 to 35 years.

The numerical model predicted that most of the regional wells have passed the maximum loading period of surface fertilizer and the levels of nitrate in groundwater will tend to decrease. The rapid response of the regional aquifer to the surface loading shown in the numerical model indicates that more attention is needed to prevent the accidental release of contaminants at the surface. Our results demonstrated that the numerical model results were particularly useful in identifying the major sources and pathways of nitrate in the study area (leaky wells in the lowland region and surface recharge in the upland area). Therefore, a concrete and specific groundwater management strategy can be established reflecting the local heterogeneity of the study area. For example, the model recommended that the management of the leaky wells in the lowland region (e.g. well sealing, re-organization of well facilities) can efficiently reduce the aquifer vulnerability to groundwater contamination, while reduction of the fertilizer usage is necessary for the upland area.

4.6. Conclusions

In this study, I compared the results of the three age dating approaches (apparent age, LPM, and numerical models) to characterize the nitrate input history and its major pathways influencing groundwater quality of the Gosan Jeju Island, and compared suitable groundwater management strategies according to the predicted groundwater ages of each approach. I observed that each age-dating method led to different results in terms of mean groundwater age (distribution) and nitrate loading history. The apparent age predicted a relatively old range of groundwater mean ages (18–61 years) and a delayed response of the water quality in the regional aquifer to the long-term use of fertilizer at the surface. The LPM indicated that groundwater age in the study area could be explained by the binary mixing of young groundwater (4-33 years) and an old water component (>60 years). The separation of the young water component in LPM suggested the response time of regional aquifer to surface fertilizer loading could be shorter than that estimated from apparent age. The numerical model demonstrated that the age distribution of the Gosan was highly dependent on the local aquifer geometry. The numerical model was useful to assess the impact of various groundwater mixing components (well leakage, clay leakage, upland recharge, and upward flux from SGF) on the age distribution and flow regimes, especially for the lowland aquifer with a more complex hydrogeological setting including a perched aquifer and leaky wells. Among the three age dating models, the groundwater ages (‘young component age’)

obtained from the numerical model were dated as the youngest (9.7-22.3 years), implying the potentially high vulnerability of the aquifer to the accidental release of surface contaminants. It also should be noted that a comparison of the contributions of each flow component to the NO_3-N PDF provided detailed information to better characterize nitrate transport with respect to the local heterogeneity of the subsurface system, and hence this approach is helpful in establishing a more specific and concrete groundwater management strategy.

Our study highlights that the different age estimation methods lead to variations in the estimated contaminant loading history, and accordingly, different groundwater management strategies. The discrepancy in the age estimation produced by different models was more prominently observed in the complex hydrogeologic system. This result implies that in order to establish a proper groundwater management plan against aquifer contamination, it is necessary to apply multiple age estimation methods and compare the results based on interpretation of the full age distributions. In a complex hydrogeological system like the study area, numerical models combined with tracer data can provide the benefit of identifying the existing and historical sources of nitrate and the major transport pathways that are responsible for the groundwater contamination.

Chapter 5. Concluding remarks

On Jeju Island, where the groundwater is an invaluable water resource, the aquifer is highly vulnerable to surface contaminants due to its hydrogeological features. As historical agricultural activities since the 1960s in the island, chemical fertilizers have long deteriorated the water quality through nitrate contamination. In the complex aquifer system formed by multiple volcanic eruptions on the island, factors the links between the fate of nitrate and their transport in the subsurface groundwater has scarcely been evaluated with regard to the effects of these factors on nitrate contamination. Previous works which undertook assessments of the degree of nitrate contamination on the island focused mainly on qualitative evaluation approaches such as source identification, spatial and temporal variations, and estimations of the history of contamination on the island. These types of qualitative evaluations are limited in that they cannot fully provide exact information related to changes, the magnitude, and the timing of effects on nitrate contamination on the island. These factors should be known before proper and efficient management plans to protect the groundwater resources against nitrate contamination on Jeju Island can be formulated.

This study utilizes combined approaches involving simple statistical trend analysis, a numerical modeling scheme, and age-dating methods to assess the nitrate contamination dynamics on Jeju Island fully throughout the three chapters (Fig. 5.1). The spatial and temporal changes in the NO_3-N and Cl concentrations were identified

on the scale of a regional island with massive amounts of water quality data (more than 16,000 data points). Based on the determined trends pertaining to NO_3-N, groundwater contamination by NO_3-N has occurred across the island and in some places was fond to increase, whereas the concentrations of Cl did not increase. Like the successful groundwater management plans which have controlled enriched Cl concentrations in the eastern region, additional management actions to relieve nitrate contamination in the western agricultural lands should be retained on the basis of a full understanding of the nitrate contamination characteristics.

Based on the results determined here, an intensified study related to the nitrate contamination in the heavily cultivated land of the western Gosan area is undertaken in an effort to propose a quantitative evaluation of the major contamination pathways as well leakage flux characteristics in the layered aquifer system present in the area. To accomplish the study objectives, a double-domain integration approach was adopted as an alternative method to represent the nitrate migration process in the multi-layered aquifer system. The simulation results clearly indicated that leaky wells facilitated the downward migration of nitrate-rich perched groundwater, resulting in contamination of the underlying regional aquifer. Based on a simulation of nitrate management scenarios, sealing the leaky wells would effectively lower the elevated concentrations of NO_3-N as compared to reducing the amounts of fertilizer used, which would likely not be deemed acceptable by farmers.

To determine the impacts on the nitrate loading history by various water mixing components in the Gosan multi-layered aquifer system, several groundwater age-dating techniques were utilized. The groundwater age estimations conducted as part of this study initially compared the findings by three age-dating methods (an environmental tracer age method, a lumped parameter model, and a numerical model), all of which determine contaminant loading histories differently. In the complex aquifer system of the area (a layered aquifer penetrated by well leakage), the environmental tracer age estimation and the lumped parameter model, widely used in previous studies, showed a limitation when used to present a full description of the various age-mixing processes. With the numerical age model, multiple components in the groundwater can be properly identified and found to have various magnitudes of influence on the nitrate response history depending on the mixing origin. To establish a proper management plan against groundwater contamination, the use of multiple age-dating methods and a comparison of the results based on an interpretation of the full age distributions are recommended.

This study provides a systematic procedure for characterizing and managing nitrate contamination in a complex aquifer system. The hydrogeological and anthropogenic impacts on the contamination can be effectively quantified by means of multiple methods with field measurement data. Proper identification of the nitrate transport pathways can be achieved with the combined approaches proposed in this study, and overall the methods presented here would be helpful for the establishment of

sustainable groundwater protection plans, especially for site-specific hydrogeological features.

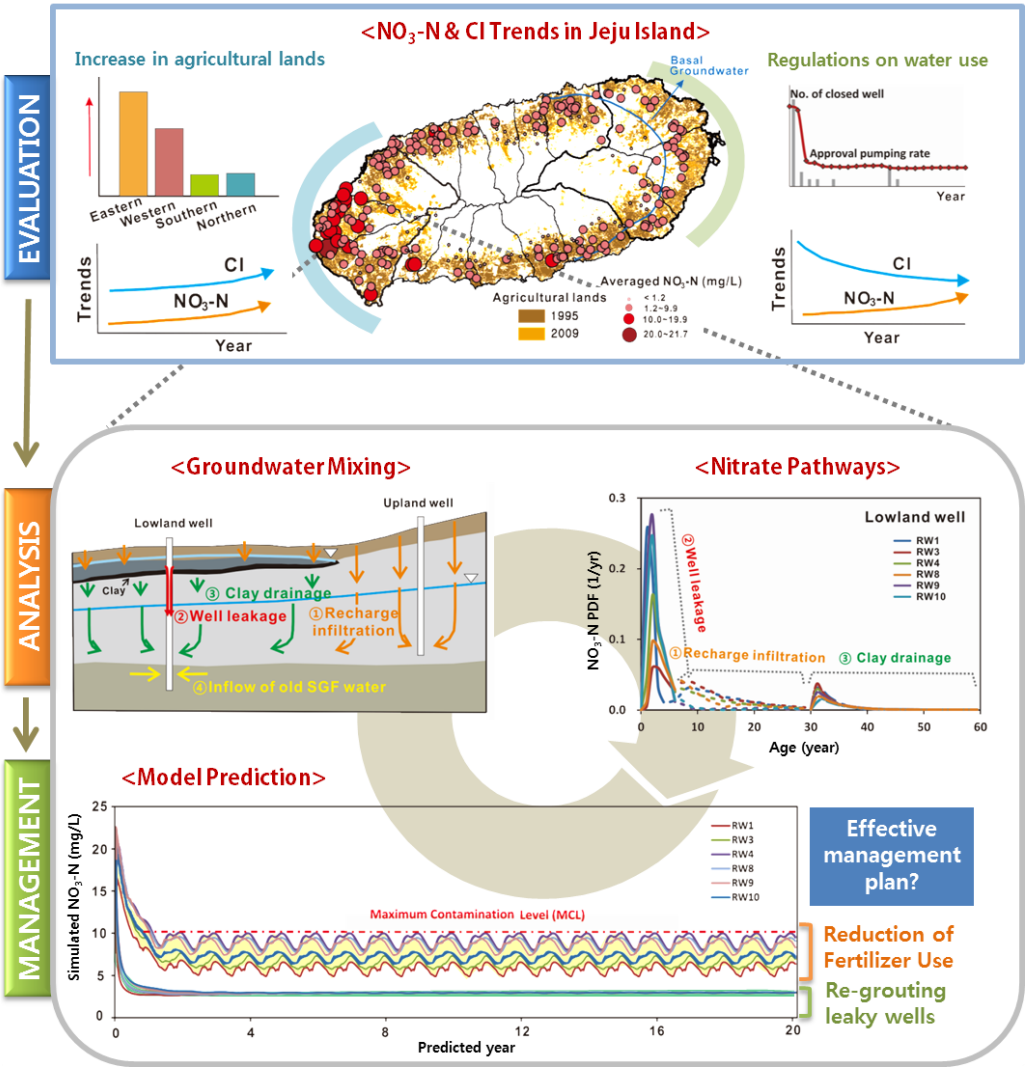

Fig. 5.1. Schematic diagram discriminating results of this study.

References

Aeschbach-Hertig, W., F. Peeters, U. Beyerle, and R. Kipfer. 1999. Interpretation of dissolved atmospheric noble gases in natural waters. *Water Resour. Res.*, 35, 2779-2792.

Aeschbach-Hertig, W., P. Schlosser, M. Stute, H. J. Simpson, A. Luding, and J. F. Clark. 1998. A $^{3}H/^{3}He$ study of ground water flow in a fractured bedrock aquifer. *Ground Water*, 36(4), 661-670.

Aguilar, J. B., P. Orban, A. Dassargues, and S. Brouyère. 2007. Identification of groundwater quality trends in a chalk aquifer threatened by intensive agriculture in Belgium. Hydrogeol. J. 15:1615-1627.

Alikhani, J., A. Deinhart, A. Visser, R. Bibby, R. Purtshert, J. Moran, A. Massoudieh, and B. Esser. 2016. Nitrate vulnerability projections from Bayesian inference of multiple groundwater age tracers. *J. Hydrol.*, 543, 167-181.

Almasri, M. and J. J. Kaluarachchi. 2005. Multi-criteria decision analysis for the optimal management of nitrate contamination of aquifers. Journal of Environ. Manage. 74, 365–381.

Avci, C. B. 1992. Flow occurrence between confined aquifers through improperly plugged boreholes. J. Hydrol. 139, 97–114.

Babiker I. S., M. A. A. Mohamed, H. Terao, K. Kato, and K. Ohta. .2004. Assessment of groundwater contamination by nitrate leaching from intensive vegetable cultivation using geographical information system. Environ. Int., 29: 1009-1017.

Bakari, S. S., P. Aagaard, R. D. Vogt, F. Ruden, I. Johansen, and S. A. Vuai. 2012. Delineation of groundwater provenance in a coastal aquifer using statistical and

isotopic methods, Southeast Tanzania. Environ. Earth Sci., 66: 889-902.

Baram, S., D. Kurtzman, Z. Ronen, A. Peeters, and O. Dahan. 2014. Assessing the impact of dairy waste lagoons on groundwater quality using a spatial analysis of vadose zone and groundwater information in a coastal phreatic aquifer. J. Environ. Manage, 132: 135-144.

Barlow, P. M. 2003. Ground water in freshwater–saltwater environments of the Atlantic coast. U.S. Geological Survey. Circular 1262. Reston, Virginia.

Batu, V. 1998. Aquifer hydraulics: a comprehensive guide to hydrogeologic data analysis. John Wiley and Sons, LNC.

Bear, J, A. H. D. Cheng, S. Sorek, D. Ouazar, and I. Herrera. 1999. Seawater intrusion in coastal aquifers—concepts, methods, and practices. Kluwer Academic Publishers, Dordrecht, Netherlands.

Benson, V. S., J. A. VanLeeuwen, J. Sanchez, I. R. Dohoo, and G.H. Somers. 2006. Spatial analysis of land use impacts on ground water nitrate concentrations. J. Environ. Qual., 23(2), 421-432.

Bethke, C. M. and T. M. Johnson. 2008. Groundwater age and groundwater age dating. Ann. Rev. Earth Planet. Sci., 36, 121-152.

Böhlke, J. K. 2002. Groundwater recharge and agricultural contamination. Hydrogeol. J., 10, 153-179.

Böhlke, J. K. and J. M. Denver. 1995. Combined use of groundwater dating, chemical, and isotopic analyses to resolve the history and fate of nitrate contamination in two agricultural watersheds, Atlantic coastal plain, Maryland. Water Reour. Res., 31(9), 2319-2339.

Bonton, A., A. Rouleau, C. Bouchard, and M. J. Rodriquez. 2011. Nitrate transport modeling to evaluate source water protection scenarios for a municipal well in an agricultural area. Agric. Syst., 104(5), 429–439.

Booh S. A. and G. C. Jeong. 2000. Saline water intrusion into fresh groundwater aquifer of eastern area, the Cheju Island. (In Korean, with English abstract.) J. Eng. Geo., 10(2), 115-130.

Böttcher, J., O. Strebel, S. Voerkelius, and H. L. Schmidt. 1990. Using isotope fractionation of nitrate-nitrogen and nitrate-oxygen for evaluation of microbial denitrification in a sandy aquifer. J. Hydrol., 114, 413–424.

Bouraoui F. and B. Grizzetti. 2014. Modelling mitigation options to reduce diffuse nitrogen water pollution from agriculture. Sci Total Environ., 468-469, 1267-1277.

Brunner, P. and C. T. Simmons. 2012. HydroGeoSphere: a fully integrated, physically based hydrological model. Ground Water, 50(2), 170–176.

Bu, X. and M. J. Warner. 1995. Solubility of chlorofluorocarbon 113 in water and seawater. Deep-Sea Res., 42(7), 1151-1161.

Burkart, M. R. and D.W. Kolpin. 1993. Hydrologic and land use factors associated with herbicides and nitrates in near-surface aquifers. J. Environ. Qual., 22, 646–656.

Burow, K., N. Dubrovsky, and J. Shelton. 2007. Temporal trends in concentrations of DBCP and nitrate in groundwater in the eastern San Joaquin Valley, California, USA. Hydrogeol. J., 15(5), 991–1007.

Burow, K. R., S. Y. Panshin, N. M. Dubrovsky, D. VanBrocklin, and G. E. Fogg. 1999. Evaluation of processes affecting 1,2-dibromo-3-chloropropane (DBCP) concentrations in ground water in the eastern San Joaquin Valley, California: Analysis of chemical data and ground-water flow and transport simulations. U.S. Geol. Surv.

Water Resour. Invest., 99-4059.

Busenberg, E. and L. N. Plummer. 1992. Use of chlorofluorocarbons (CCl3F and CCl2F2) as hydrologic tracers and age-dating tools: the alluvium and terrace system of central Oklahoma. Water Resour. Res., 28, 2257-2283.

Busenberg, E. and L. N. Plummer. 2000. Dating young groundwater with sulfur hexafluoride: natural and anthropogenic sources of sulfur hexafluoride. Water Reour. Res., 36(10), 3011-3030.

Calvache M. L. and A. Pulido-Bosch. 1997. Effects of geology and human activity on the dynamics of salt-water intrusion in three coastal aquifers in southern Spain. Environ Geol., 30(3/4), 215-223.

Carrera, J., E. Vázquez-Suñé, O. Castillo, and X. Sánchez-Vila. 2004. A methodology to compute mixing ratios with uncertain end-members. Water Resour. Res., 40, W12101.

Castro, M. C., M. Stute, and P. Schlosser. 2000. Comparison of 4He ages and 14C ages in simple aquifer systems: implications for groundwater flow and chronologies. Appl. Geochem., 15, 1137-1167.

Cerro, I., I. Antigüedad, R. Srinavasan, S. Sauvage, M. Volk, and J. M. Sanchez-Perez. 2011. Simulating land management options to reduce nitrate pollution in an agricultural watershed dominated by an alluvial aquifer. J. Environ. Qual., 43(1), 67–74.

Cey, E. E., D. L. Rudolph, R. Aravena, and G. Parkin. 1999. Role of the riparian zone in controlling the distribution and fate of agricultural nitrogen near a small stream in southern Ontario. J. Contam. Hydrol., 37, 45–67.

Chang, H. 2008. Spatial analysis of water quality trends in the Han River basin, South

Korea. Water Res., 42, 3285-3304.

Chen, W. F. and T. K. Liu. 2003. Dissolved oxygen and nitrate of groundwater in Choshui Fan-Delta, western Taiwan. Environ Geol., 44, 731-737.

Choi, S. H. and Y. K. Kim. 1989. Geochemical characteristics of groundwater in Cheju Island. (In Korean with English abstract.) J. Geol. Soc. Korea, 25(3), 230-238.

Choi, H. M., J. Y. Lee, K. Ha, and G. P. Kim. 2011. The study on time series analysis of groundwater data and groundwater recharge in Jeju Island. (In Korean with English abstract.) J. Eng. Geol., 21(4), 337-348.

Choung, S. W., N. C. Woo, and K. S. Lee. 2004. Temporal & spatial variations of groundwater quality in Hanlim, Jeju Island. (In Korean, with English abstract.) J. Geol. Soc. Korea, 40(4), 537-558.

Church, P. E. and G. E. Granato. 1996. Bias in ground-water data caused by well-bore flow in long-screen wells. Ground Water, 34(2), 262–273.

Clark, I. and P. Fritz. 1997 Environmental isotopes in hydrogeology, 171-195, Lewis, Boca Raton, FL.

Cloutier, V., R. Lefebvre, R. Therrien, and M. Savard. 2008. Multivariate statistical analysis of geochemical data as indicative of the hydrogeochemical evolution of groundwater in a sedimentary rock aquifer system. J. Hydrol. 353, 294–313.

Constantin, J., B. Marry, F. Laurent, G. Aubrion, A. Fontaine, P. Kerveillant, and N. Beaudoin. 2010. Effects of catch crops, no till and reduced nitrogen fertilization on nitrogen leaching and balance in three long-term experiments. Agric. Eco Environ., 135, 268-278.

Cook, P. G. and J. K. Böhlke. 2000. Determining timescales for groundwater flow and

solute transport, in Environmental Tracers in Subsurface Hydrology, edited by P. G. Cook, and A. L. Herczeg, 1-30, Kluwer Academic Publishers, Boston, Mass.

Cornaton, F. J., Y. J. Park, and E. Deleersnijder. 2011. On the biases affecting water ages inferred from isotopic data. J. Hydrol., 410(3), 217-225.

Cornaton, F. J., and P. Perrochet. 2006. Groundwater age, life expectancy and transit time distributions in advective–dispersive systems: 1. Generalized reservoir theory. Adv. Water Resour., 29, 1267–1291.

Cunnold, D. M., P. J. Fraser, R. F. Weiss, R. G. Prinn, P. G. Simmonds, B. R. Miller, F. N. Alyea, and A. J. Crawford. 1994. Global trends and annual releases of CCl3F and CCl2F2 estimated from ALE/GAGE and other measurements from July 1978 to June 1991. J. Geophys. Res., 99, 1107-1126.

Dragon, K., J. Gorski, M. Marciniak, and D. Kasztelan. 2009. Use of mathematical modeling to investigate inter-aquifer contamination by organic-rich water through an unplugged well (central Wielkoposka, Poland). Hydrogeol. J., 17, 1257–1564.

Dunkle, S. A., L. N. Plummer, E. Busenberg, P. J. Phillips, J. M. Denver, P. A. Hamilton, R. L. Michel, and T. B. Coplen. 1993. Chlorofluorocarbons (CC13F and CC12F2) as dating tools and hydrologic tracers in shallow groundwater of the Delmarva Peninsula, Atlantic Coastal Plain, United States. Water Resour. Res., 29(12), 3837-3860.

Eberts, S. M., J. K. Böhlke, L. J. Kauffman, and B. C. Jurgens. 2012. Comparison of particle-tracking and lumped-parameter age-distribution models for evaluating vulnerability of production wells. Hydrogeol. J., 20, 263-282.

Eckhardt, D. A. and P. E. Stackelberg. 1995. Relations of ground-water quality to land use on Long Island, New York. Ground Water, 33(6), 1019-1033.

Ekwurzel, B., P. Schlosser, W. M. Smethie Jr., L. N. Plummer, E. Busenberg, R. L. Michel, R. Weppernig, and M. Stute. 1994. Dating of shallow groundwater: Comparison of the transient tracers 3H/3He, chlorofluorocarbons, and 85Kr. Water Resour. Res., 30, 1693-1708.

Elci, A., F. J. Molz III, and W. R. Waldrop. 2001. Implications of observed and simulated ambient flow in monitoring wells. Ground Water, 39 (6), 853–862.

Engdahl, N. B. and R. M. Maxwell. 2015. Quantifying changes in age distributions and the hydrologic balance of a high-mountain watershed from climate induced variations in recharge. J. Hydrol., 522, 152-162.

Environmental Protection Agency (EPA). 2010. No.1. Nitrate in drinking water. Joint Position Paper.

Erisman J. W., M. A. Sutton, J. Galloway, Z. Kilmont, and W. Winiwarter. 2008. How a century of ammonia synthesis changed the world. Nat. Geosci., 1, 636-639.

ESRI. 2011. ArcGIS Desktop: Release 10.0. ESRI, Inc., Redlands, CA.

FAO (Food and Agriculture Organization). 1997. Seawater intrusion in coastal aquifers: Guidelines for study, monitoring and control. FAO Water Reports, ISBN 92-5-103986-0, Rome, Italy.

Frapporti, G. and S.P. Vriend. 1993. Hydrogeochemistry of the shallow Dutch groundwater: interpretation of national groundwater quality monitoring network. Water Resour., 29, 2993–3004.

Gardner, K. K. and R. M. Vogel. 2005. Predicting ground water nitrate concentration from land use. Ground Water, 43(3), 343-352.

Gass, T. E., J. E. Lehr, and H. W. Heiss Jr. 1977. Impact of abandoned wells on ground

water. EPA Rep. 600/3-77-095. U.S. Gov. Print. Office, Washington, D.C.

Gelhar, L.W. 1986. Stochastic subsurface hydrology from theory to application. Water Resour. Res., 22 (1), 161–180.

Gheysari, M., S. M. Mirlatifi, M. Homaee, M. E. Asadi, and G. Hoogenboom. 2009. Nitrate leaching in a silage maize field under different irrigation and nitrogen fertilizer rates. Agric. Water Manage, 96, 946-954.

Goderniaux, P., S. Brouyère, S. Wildemeersch, R. Therrien, and A. Dassargues. 2015. Uncertainty of climate change impact on groundwater reserves – Application to a chalk aquifer. J. Hydrol., 528, 108–121.

Goodchild, R. G. 1998. EU policies for the reduction of nitrogen in water: the example of the Nitrate Directive. Environ. Pollut., 102(S1), 737-740.

Goode, D. J. 1996. Direct simulation of groundwater age. Water Resour. Res., 32(2), 289-296.

Grath J., A. Scheidleder, S. Uhlig, K. Weber, M. Kralik, and T. Keimel. 2001. The EU Water Framework Directive: statistical aspects of the identification of groundwater pollution trends, and aggregation of monitoring results. Final Report. Austrian Federal Ministry of Agriculture and Forestry, Environment and Water Management, European Commission, Vienna.

Green, C. T., B. A. Bekins, S. J. Kalkhoff., R. M. Hirsch, L. Liao, and K. K. Barnes. 2014. Decadal surface water quality trends under variable climate, land use, and hydrogeochemical setting in Iowa, USH. Water Resour. Res., 50, 2425-2443.

Green, C. T., J. K. Böhlke, B. A. Bekins, and S. P. Phillips. 2010. Mixing effects on apparent reaction rates and isotope fractionation during denitrification in a heterogeneous aquifer. Water Resour. Res., 46, W08525.

Green, C. T., B. C. Jurgens, Y. Zhang, J. J. Starn, M. J. Singelton, and B. K. Esser. 2016. Regional oxygen reduction and denitrification rates in groundwater from multi-model residence time distributions, San Joaquin Valley, USA. J. Hydrol., 543(A), 155-166.

Green, C. T., Y. Zhang, B. C. Jurgens, J. J. Starn, and M. K. Landon. 2014. Accuracy of travel time distribution (TTD) models as affected by TTD complexity, observation errors, and model and tracer selection. Water Resour. Res., 50(7), 6191-6213.

Ha, K., W. B. Park, and D. Moon. 2009. Estimation of direct runoff variation according to land use change in Jeju Island. Econ. Environ. Geol., 43(4), 343-356.

Hahn, J., K. Hahn, C. Kim, N. Kim, and C. Hahn. 1994. Sustainable yield of groundwater resources of the Cheju Island. (In Korean with English abstract.) J. Geol. Soc. Korea, 1(1), 33-50.

Han, D., G. Cao, J. McCallum, and X. Song. 2015. Residence times of groundwater and nitrate transport in coastal aquifer systems: Daweijia area, northeastern China. Sci. Total Environ., 538, 539-554.

Han K. E. and H. S. Shin. 2000. The study of high chloride in the coastal area of Cheju Island. (In Korean with English abstract.) J. Eng. Geol., 10(2), 150-171.

Han, D. M., X. F. Song, M. J. Currell, J. L. Yang, and G. Q. Xiao. 2014. Chemical and isotopic constraints on evolution of groundwater salinization in the coastal plain aquifer of Laizhou Bay, China. J. Hydrol., 508, 12-27.

Hansen, B., L. Thorling, T. Dalgaard, and M. Erlandsen. 2011. Trend reversal of nitrate in Danish groundwater – a reflection of agricultural practices and nitrogen surpluses since 1950. Environ. Sci. Technol., 45, 228-234.

Harter, T. 2003. Water well design and construction. the Farm Water Quality Planning

(FWQP), University of California.

Helena, B., R. Pardo, M. Vega, E. Barrado, J.M. Fernandez, and L. Fernandez. 2000. Temporal evolution of groundwater composition in an alluvial aquifer (Pisuerga River, Spain) by principal component analysis. Water Research, 34(3), 807–816.

Helsel, D. R. and R. M. Hirsch. 2002. Statistical methods in water resources. U.S. Geological Survey.

Hibberd, J. 1992. Abandoned well survey of Denmark Township, Washington Country, Minnesota. J. Environ. Health, 54(6), 18–21.

Hirsch, R. M., R. B. Alexander, and R. A. Smith. 1991. Selection of methods for the detection and estimation of trends in water quality. Water Resour. Res., 27(5), 803-813.

Hodnett, M.G. and Tomasella, J. 2002. Marked differences between van Genuchten soil water-retention parameters for temperate and tropical soils: a new water-retention pedo-transfer functions developed for tropical soils. Geoderma., 108, 155–180.

Hyun, G. T., S. T. Song, D. H. Joa, and Y. H. Ko. 2010. Characteristics of groundwater and soil contamination in Hallim area of Jeju Island. (In Korean with English abstract.) J. Kor. Soc. Soil and Groundwater Env., 15(3), 44-51.

Institute of Water Resource. 2013 Monitoring data of groundwater levels. Information of water resource in Jeju Island. Institute of Water Resource, Jeju Special Self-Governing Province, http://www.jejuwater.go.kr.

Jejudo. 1997. Report on the general investigation of the mid-mountainous area in Jeju Island. (In Korean.) Jeju Provincial Government, Jeju Island.

Jejudo. 2003. Report on the overall investigation of hydrogeology and the groundwater resource in Jeju Island (Ⅲ). (In Korean.) Jeju Provincial Government, Jeju Island.

Jeju Special Self-Governing Province. 2009. Jeju statistics yearbook. (In Korean.) Jeju Special Self-Governing Province, Korea.

Jeju Special Self-Governing Province. 2013a. Supply of fertilizers. Statistics annual report. Jeju Special Self-Governing Province, http://www.jeju.go.kr.

Jeju Special Self-Governing Province. 2013b. Comprehensive plans for managing water resources in Jeju (2013-2022). (In Korean.) Jeju Special Self-Governing Province, Jeju Island.

Jeju Special Self-Governing Province. 2015. Jeju Statistical Yearbooks, http://www.jeju.go.kr.

Jeju Special Self-Governing Province and JDI (Jeju Development Institute). 2012. Fifty years of water supply in Jeju. (In Korean.) Jeju Special Self-Governing Province, Jeju Island.

Jeju Water Resources Management Office. 2001. Data collection book of geological logs of Jeju Island. (In Korean.) Jeju Special Self-Governing Province, Korea.

Jeju Water Resources Management Office. 2013, http://www.jejuwater.go.kr/.

Jeong, S. W., N. C. Woo, and K. S. Lee. 2004. Temporal & spatial variations of groundwater quality in Hanlim, Jeju Island. (In Korean, with English abstract.) J. Geol. Soc. Korea, 40(4), 537–558.

Jiménez-Martínez, J., R. Aravena, and L. Candela., 2011. The role of leaky boreholes in the contamination of a regional confined aquifer. A case study: the Campo de Cartagena region, Spain. Water Air Soil Pollut., 215, 311–327.

Jung, H. W., S. T. Yun, K. H. Kim, S. S. Oh, and K. G. Kang. 2014. Role of an impermeable layer in controlling groundwater chemistry in a basaltic aquifer beneath

an agricultural field, Jeju Island, South Korea. Appl. Geochem., 45, 82-93.

Jurgens, B. C., J. K. Böhlke, and S. M. Eberts. 2012. TracerLPM (Version 1): An Excel® workbook for interpreting groundwater age distributions from environmental tracer data, United States Geological Survey Techniques and Methods Report 4-F3, 60. Reston, Virginia, USA.

Jurgens, B. C., J. K. Böhlke, L. J. Kauffman, K. Belitz, and B. K. Esser. 2016. A partial exponential lumped parameter model to evaluate groundwater age distributions and nitrate trends in long-screened wells, J. Hydrol., 543, 109-126.

Kanfi, Y., D. Ronen, and M. Magaritz. 1983. Nitrate trends in the coastal-plain aquifer of Israel. J. Hydrol., 66, 331-341.

Kang, B. K. and C. K. Song. 2001. Crop growth and nutrient leaching from soil with application of urea and compost in volcanic ash soil. Korean J. Organic Agric., 9(2), 101-115.

Kaown, D., Y. Hyun, G. O. Bae, and K. K. Lee. 2007. Factors affecting the spatial pattern of nitrate contamination in shallow groundwater. J Environ. Qual., 36, 1479-1487.

Kaown, D., D. C. Koh, B. Mayer, and K. K. Lee. 2009. Identification of nitrate and sulfate sources in groundwater using dual stable isotope approaches for an agricultural area with different land use (Chuncheon, mid-eastern Korea). Agric. Ecosyst. Environ., 132, 223-231.

Katz, B. G., J. K. Böhlke, and H. D. Hornsby. 2001. Timescales for nitrate contamination of spring waters, northern Florida, USA. Chem. Geol., 179, 167-186.

Katz, B. G., A. R. Chelette, and T. R. Pratt. 2004. Use of chemical and isotopic tracers to asses nitrate contamination and groundwater age, Woodville Karst plain, USA. J.

Hydrol., 289, 36-61.

Kay, P., R. Grayson, M. Philips, K. Stanley, A. Dodsworth, A. Hanson, A. Walker, M. Foulger, I. McDonnell, and S. Taylor. 2012. The effectiveness of agricultural stewardship for improving water quality at the catchment scale: experiences from an NVZ and ECSFDI watershed. J. Hydrol., 422–423, 10–16.

Kendall, M. G. 1948. Rank correlation methods, Charles Griffin, London.

Kent, R. and M. K. Landon. 2013 Trends in concentrations of nitrate and total dissolved solids in public supply wells of the Bunker Hill, Lytle, Rialto, and Colton groundwater subbasins, San Bernardino County, California: Influence of legacy land use. Sci. Total Environ., 452-453, 125-136.

KIGAM. 2011. Assessment of the sustainable yield on groundwater in Jeju and discovery of the functional groundwater. (In Korean.) Korea Institute of Geoscience and Mineral Resources.

Kim, G. B., J. W. Kim, J. H. Won, and G. W. Koh. 2007. Regional trend analysis for groundwater quality in Jeju Island: Focusing on chloride and nitrate concentrations. (In Korean, with English abstract.) J. Kor. Water Res., 40(6), 469-483.

Kim, Y., K. S. Lee, D. C. Koh, D. H. Lee, S. G. Lee, W. B. Park, G. W. Koh, and N. C. Woo. 2003. Hydrogeochemical and isotopic evidence of groundwater salinization in a coastal aquifer: a case study in Jeju volcanic island, Korea. J. Hydrol., 270, 282-294.

Kim, C. K., B. H. Rho, and K. J. Lee (1998), Environmental tritium in the areas adjacent to the Wolsong Nuclear Power Plant, *J. Environ. Radioact.*, 41(2), 217-231.

Ko, K. S., Y. Kim, D. C. Koh, K. S. Lee, S. G. Lee, C. H. Kang, H. J. Seong, and W. B. Park. 2005. Hydrogeochemical characterization of groundwater in Jeju Island using principal component analysis and geostatistics. (In Korean, with English abstract.)

Econ. Environ. Geol., 38(4), 435-450.

Koh, G. W. 1997 Characteristics of the groundwater and hydrogeologic implication of the Seoquipo formation in Cheju Island. (In Korean, with English abstract.) Ph.D. Thesis, Busan National University, Korea.

Koh, G. W. 2006a. Characteristics of groundwater and water resource management in Jeju Island (III). (In Korean.) J. Kor. Water Res., 39(8), 80-89.

Koh, D. C., H. W. Chang, K. S. Lee, K. S. Ko, Y. J. Kim, and W. B. Park. 2005. Hydrogeochemistry and environmental isotopes of groundwater in Jeju volcanic island, Korea: implications for nitrate contamination. Hydrol. Processes, 19, 2225-2245.

Koh, D. C., and B. R. Kang. 2011. Estimation of groundwater ages by using CFCs and 3H environmental tracers, (In Korean.) in Research of technique for preventing nitrate-nitrogen contamination. Jeju special self-governing province.

Koh, E. H., D. Kaown, B. Mayer, B. R. Kang, H. S. Moon, and K. K. Lee. 2012. Hydrogeochemistry and isotopic tracing of nitrate contamination of two aquifer systems on Jeju Island, Korea. J. Environ. Qual., 41, 1835-1845.

Koh, D. C., K. S. Koh, Y. Kim, S. G. Lee, and H. W. Chang. 2007. Effect of agricultural land use on the chemistry of groundwater from basaltic aquifers, Jeju Island, South Korea. Hydrogeol. J., 15, 727-743.

Koh, E. H., S. H. Lee, D. Kaown, H. S. Moon, E. Lee, K. K. Lee, and B. R. Kang. 2017. Impacts of land use change and groundwater management on long-term nitrate-nitrogen and chloride trends in groundwater of Jeju Island, Korea. Environ. Earth Sci., 76, 176.

Koh, E. H., E. Lee, and K. K. Lee. 2016. Impact of leaky wells on nitrate cross-contamination in a layered aquifer system: Methodology for and demonstration of

quantitative assessment and prediction. J. Hydrol., 541, 1133-1144.

Koh, D. C., L. N. Plummer, D. K. Solomon, E. Busenberg, Y. J. Kim, and H. W. Chang. 2006b. Application of environmental tracers to mixing, evolution, and nitrate contamination of ground water in Jeju Island, Korea. J. Hydrol., 327, 258–275.

Kolbe, T., J. Marçais, Z. Thomas, B. W. Abbott, J-R. de Dreuzy, P. Rousseau-Gueutin, L. Aquilina, T. Labasque, and G. Pinay. 2016. Coupling 3D groundwater modeling with CFC-based age dating to classify local groundwater circulation in an unconfined crystalline aquifer. J. Hydrol., 14, 880-893

Konikow, L. F. and G. Z. Hornberger. 2006. Modeling effects of multi-node wells on solute transport. Ground Water, 44(5), 648–660.

Korea Meteorological Administration. 2014, http://www.kma.go.kr.

Korea Meteorological Administration. 2015, http://www.kma.go.kr.

Kurtzman, D. and B. R. Scanlon. 2011. Groundwater recharge through vertisols: irrigated cropland vs. natural land, Israel. Vadose Zone J., 10, 662-674.

Kurtzman, D., R. Shapira, A. Bar-Tal, P. Fine, and D. Russo. 2013. Nitrate fluxes to groundwater under citrus orchards in Mediterranean climate: observations, calibrated models, simulations and agro-hydrological conclusions. J. Contam. Hydrol., 151, 93-104.

Lacombe, S., E. A. Sudicky, S. K. Frape, and A. J. A. Unger. 1995. Influence of leaky boreholes on cross-formational groundwater flow and contamination transport. Water Resour., 31(8), 1871–1882.

Landon, M. K., B. C. Jurgens, B. G. Katz, S. M. Eberts, K. R. Burow, and C. A. Crandall. 2010. Depth-dependent sampling to identify short-circuit pathways to public-

supply wells in multiple aquifer settings in the United States. Hydrogeol. J., 18, 577–593.

Lee, E., Y. Hyun, and K. K. Lee. 2010. Numerical modeling of groundwater flow into a radial collector well with horizontal arms. Geosci. J., 14(4), 403–414.

Lee, J. H., Y. G .Kim, and H. S. Ryu. 2003. Effect of soil quality and nitrogen fertilizer method on nitrogen leaching in tea garden of Jeju Island area. (In Korean.) Korean Tea Society, 9(1), 91-102.

Lee, J. Y., G. S. Lee, and S. H. Song. 2007. An interpretation of changes in groundwater level and electrical conductivity in monitoring wells in Jeju Island. J. Korean Earth Science Society, 28(7), 925-935.

Lee, C. S., Y. H. Park, J. Y. Lee, and S. K. Lee. 1996. Studies on recommendation of N fertilizer rates for vegetable crops in vinyl house soil. (In Korean with English abstract.) RDA. J. Agri. Sci., 38(1), 402–409.

Lemieux, J. M. and E. A. Sudicky. 2010. Simulation of groundwater age evolution during the Wisconsinian glaciation over the Canadian landscape. Envrion. Fluid Mech., 10, 91-102.

Li, Q., A. J. A. Unger, E. A. Sudicky, D. Kassenaar, E. J. Wexler, and S. Shikaze. 2008. Simulating the multi-seasonal response of a large-scale watershed with a 3D physically-based hydrologic model. J. Hydrol., 357, 317–336.

Liao, L., C. T. Green, B. A. Bekins, and J. K. Böhlke. 2012. Factors controlling nitrate fluxes in groundwater in agricultural areas. Water Resour. Res., 48, W00L09.

MAFRA (Ministry of Agriculture, Food and Rural Affairs). 2001. Studies on improvement of soil environment and investigation for unnormal defolication in citrus orchard.

Maloszewski, P., W. Stichler, and A. Zuber. 2004. Interpretation of environmental tracers in groundwater systems with stagnant water zones. Isot. Environ. Health Studies, 40(1), 21-33.

Maloszewski, P. and A. Zuber. 1982. Determining the turnover time of groundwater systems with the aid of environmental tracers: 1. Models and their applicability. J. Hydrol., 57(3-4), 207-231.

Mann, H. B. 1945. Nonparametric tests against trend. Econometrica, 13, 245-259.

Mann. H. B. and D. R. Whitney. 1947. On a test of whether one of two random variables is stochastically larger than the other. Ann. Math Statist., 18(1), 50-60.

Manning, A. H., D. K. Solomon, and S. A. Thiros. 2005. 3H/3He age data in assessing the susceptibility of wells to contamination. Ground Water, 43, 353-367.

Mamyrin, B. A. and I. N. Tolstikhin. 1984. Helium isotopes in nature, Elsevier, Amsterdam.

McCallum, J. L., P. G. Cook, C. T. Simmons, and A. D. Werner. 2014. Bias of apparent tracer ages in heterogeneous environments. Ground Water, 52(2), 239-250.

McMahon, P. B., J. K. Böhlke, L. J. Kauffman, K. L. Kipp, M. K. Landon, C. A. Crandall, K. R. Burow, and C. J. Brown. 2008a. Source and transport controls on the movement of nitrate to public supply wells in selected principal aquifers of the United States. Water Resour. Res., 44, W04401.

McMahon, P. B., K. R. Burow, L. J. Kauffman, S. M. Eberts, J. K. Böhlke, and J. J. Gurdak. 2008b. Simulated response of water quality in public supply wells to land use change. Water Resour. Res., 44, W00A06.

Melloul, A. and M. Collin. 1992. The ‘principal components’ statistical method as a

complementary approach to geochemical methods in water quality factor identification; application to the Coastal Plain aquifer of Israel. J. Hydrol., 140, 49–73.

Ministry of Environment (ME). 2014. Regulations for water quality criteria and examination, Republic of Korea.

Mishima, Y., M. Takada, and R. Kitagawa. 2011/ Evaluation of intrinsic vulnerability to nitrate contamination of groundwater: appropriate fertilizer application management. Environ. Earth Sci., 63, 571-580.

Mohamed, A. and K. Rushton. 2006. Horizontal wells in shallow aquifers: Field experiment and numerical model. J. Hydrol., 329, 98–109.

Molénat, J. and C. Gascuel-Odoux. 2002. Modelling flow and nitrate transport in groundwater for the prediction of water travel times and of consequences of land use evolution on water quality. Hydrol. Processes, 16(2), 479–492.

Molson, J. W. and E. O. Frind. 2012. On the use of mean groundwater age, life expectancy and capture probability for defining aquifer vulnerability and time-of-travel zones for source water protection. J. Contaminant Hydrology., 127, 76-87.

Mtoni, Y., I. C. Mjemah, C. Bakundukize, M. V. Camp, K. Martens, and K. Walraevens. 2013. Saltwater intrusion and nitrate pollution in the coastal aquifer of Dar es Salaam, Tanzania. Environ. Earth Sci., 70, 1091-1111.

Nolan, B. T. and J. D. Stoner. 2000. Nutrients in groundwaters of the conterminous United States, 1992–1995. Environ. Sci. Technol., 34, 1156-1165.

Oh, S. S., I. H. Hyun, Y. C. Song, S. M. Kim, S. J. Kim, and B. R. Kang. 2010. Effect of surplus nitrate-nitrogen in the farm on the groundwater quality. (In Korean, with English abstract.) In: Environ. Resour. Res, Editor, 21th Report of J. I. H. E. Jeju Special Self-Governing Province, Korea, 135-155.

O’Leary, D. R., J. A. Izbicki, and L. F. Metzger. 2015. Sources of high-chloride water and managed recharge in an alluvial aquifer in California, USA. Hydrogeolo. J., 23, 1515-1533.

Panno, S. V., K. C. Hackley, H. H. Hwang, S. E. Greenberg, I. G. Krapac, S. Landsberger, and D. J. O'Kelly. 2006. Characterization and identification of Na-Cl sources in ground water. Ground Water, 44(2), 176-187.

Park, Y. J., F. J. Cornaton, S. D. Normani, J. F. Sykes, and E. A. Sudicky. 2008. Use of groundwater lifetime expectancy for the performance assessment of a deep geologic radioactive waste repository: 2. Application to a Canadian Shield environment. Water Resour. Res., 44, W04407.

Park, H. Y., K. Jang, J. W. Ju, and I. W. Yeo. 2012. Hydrogeological characterization of seawater intrusion in tidally forced coastal fractured bedrock aquifer. J. Hydrolo., 446-477, 77-89.

Pejman, A. H., G. N. Bidhendi, A. R. Karbassi, N. Mehrdadi, and M. E. Bidhendi. 2009. Evaluation of spatial and seasonal variations in surface water quality using multivariate statistical techniques. Int. J. Environ. Sci. Technol., 6 (3), 467-476.

Peleg, N. and H. Gvirtzman. 2010. Groundwater flow modelling of two-levels perched karstic leaking aquifers as a tool for estimating recharge and hydraulic parameters. J. Hydrol., 388, 13–27.

Peñe-Haro, S., C. Llopis-Albert, M. Pulido-Velazquez, and D. Pulido-Velazquez. 2010. Fertilizer standards for controlling groundwater nitrate pollution from agriculture: El Salobral-Los Llanos case study, Spain. J. Hydrol., 392, 174–187.

Plummer, L. N. and E. Bunsenberg. 2000. Chlorofluorocarbons, in Environmental Tracers in Subsurface Hydrology, edited by P. G. Cook, and A. L. Herczeg, 441-478,

Kluwer Academic Publishers, Boston, Mass.

Plummer, L. N., R. L. Michel, E. M. Thurman, and P. D. Glynn. 1993. Environmental tracers for age dating young ground water, in Regional Ground-Water Quality, edited by W. M. Alley, 255-294, Van Nostrand Reinhold, New York.

Plummer, L.N., M.G. Rupert, E. Busenberg, and P. Schlosser. 2000. Age of irrigation water in ground water from the eastern Snake River plain aquifer, South-Central Idaho. Ground Water 38, 264–283.

Pokhrel, Y. N., N. Hanasaki, P. J.-F. Yeh, T. J. Yamada, S. Kanae, and T. Oki. 2012. Model estimates of sea-level change due to anthropogenic impacts on terrestrial water storage, Nat. Geosci., 5, 389–392.

Postma, D., C. Boesen, H. Kristiansen, and F. Larsen. 1991. Nitrate reduction in an unconfined aquifer: water chemistry, reduction processes, and geochemical modeling. Water Resour., 27, 2027–2045.

Powers, J.P. 1992. Construction dewatering: New methods and applications. John Wiley & Sons, INC.

Puckett, L. J. and T. K. Cowdery. 2002. Transport and fate of nitrate in a glacial outwash aquifer in relation to ground water age, land use practice, and redox processes. J. Environ. Qual., 31, 782–796.

Reilly, T. E., O. L. Franke, and G. D. Bennett. 1989. Bias in groundwater samples caused by wellbore flow. J. Hydraul. Eng., 115, 270–276.

Richards, L. A. 1931. Capillary condition of liquids through porous mediums. Physics 1(5), 318–333.

Robertson, W. M. and J. M. Sharp Jr. 2013. Variability of groundwater nitrate

concentration over time in arid basin aquifers: sources, mechanisms of transport, and implications for conceptual models. Environ. Earth Sci., 69, 2415-2426.

Saffigna, P. G. and D. R. Keeney. 1977. Nitrate and chloride in ground water under irrigated agriculture in central Wisconsin. Ground Water, 15(2), 170-177.

Santi, P. M., J. E. McCray, and J. L. Martens. 2006. Investigating cross-contamination of aquifers. Hydrogeol. J., 14, 51–68.

Schlosser, P., M. Stute, C. Sonntag, and K. O. Munnich. 1989. Tritiogenic 3He in shallow groundwate. Earth Planet. Sci. Lett., 94, 245-256.

Schot, P. P. and J. van der Wal. 1992. Human impact on regional groundwater composition through intervention in natural flow patterns and changes in land use. J. Hydrol., 134, 297–313.

Silva, I. and D. D. Williams. 2001. Buffer zone verses whole catchment approaches to studying land use impact on river water quality. Water Res., 35, 3462-3472.

Šimůnek, J., N. J. Jarvisb, M. T. van Genuchten, and A. Gärdenä. 2003. Review and comparison of models for describing non-equilibrium and preferential flow and transport in the vadose zone. J. Hydrol., 272, 14–35.

Smethie Jr., W. M., D. W. Chipman, J. H. Swift, and K. P. Koltermann. 1988. Chlorofluoromethanes in the Arctic Mediterranean seas: Evidence for formation of bottom water in the Eurasian Basin and deep-water exchange through Fram Strait. Deep Sea Res., 35, 347-369.

Smith, J. T., R. T. Clarke, and M. J. Bowes. 2010. Are groundwater nitrate concentrations reaching a turning point in some chalk aquifers?. Sci. Total Environ., 408, 4722-4732.

Solomon, D. K. and P. G. Cook. 2000. 3H and 3He. In Environmental Tracers in Subsurface Hydrology, edited by P. G. Cook and A. Herczeg, 397-424, Kluwer Academic Publishers, Boston, Mass.

Solomon, D. K. and E.A. Sudicky. 1991. Tritium and Helium 3 Isotope Ratios for Direct Estimation of Spatial Variations in Groundwater Recharge. Water Resour. Res., 27(9), 2309-2319.

Song, S. H. and K. J. Choi. 2012. An appropriate utilization of agricultural water resources of Jeju Island with climate change (1). J. Soil & Groundwater Environ., 17(2), 62-70.

Song, S. J., T. W. Kang, W. B. Park, and B. L. Kang. 2003. Groundwater quality in western parts of Jeju Island and agricultural practice ways for preventing contamination. Paper presented at: Assets of Jeju: water of Jeju and the world. Celebrating the World Day for Water, 11th Academic Seminar, Jeju Isalnd, Korea. 18 Mar. 89-131.

Song, Y. S., H. K. Kwak, B. Y. Yeon, C. S. Lee, J. H. Yoon, D. Y. Moon, and S. C. Lee. 2002. Recommendation of optimum amount of fertilizer nitrogen based on soil organic matter for Chinese cabbage and cabbage in volcanic ash soils of Cheju Island. (In Korean with English abstract.) Korean J. Organic Agri., 9(2), 103–117.

Spalding, R. F. and M. E. Exner. 1993. Occurrence of nitrate in groundwater—a review. J. Environ. Qual., 22, 392-402.

Spalding, R. F., Z. K. U, S. W. Hyun, G. E. Martin, M. E. Burbach, SII. Yang, M. Kim, M. E. Exner, and S. J. Song. 2001. Source identification of nitrate on Cheju Island, South Korea. Nutr. Cycling Agroecosyst, 61, 237-246.

Stadler, S., K. Osenbrück, K. Knöller, A. Suckow, J. Sültenfuß, H. Oster, T.

Himmelsbach, and H. Hötzl. 2008. Understanding the origin and fate of nitrate in groundwater of semi-arid environments. J. Arid Environ., 72, 1830–1842.

Starn, J. J., C. T. Green, S. R. Hinkle, A. C. Bagtzoglou, and B. J. Stolp. 2014. Simulating water-quality trends in public-supply wells in transient flow systems. Ground Water, 52 (S1), 53-62.

Steinhorst, R. K. and R. E. Williams. 1985. Discrimination of groundwater sources using cluster analysis, MANOVA, canonical analysis and discriminant analysis. Water Resour. Res., 21, 1149–1156.

Stites, W. and G. J. Kraft. 2001. Nitrate and chloride loading to groundwater from an irrigated north–central U.S. sand–plain vegetable field. J. Environ. Qual., 30, 1176-1184.

Stuart, M. E., P. J. Chilton, D. G. Kinniburgh, and D. M. Cooper. 2007. Screening for long-term trends in groundwater nitrate monitoring data. Q. J. Eng. Geol. Hydroge., 40(4), 361-376.

Stute, M., J. Deák, K. Révész, J. K. Böhlke, É. Deseö, R. Weppernig, and P. Schlosser. 1997. Tritium/3He dating of river infiltration: An example from the Danube in the Szigetkös area, Hungary. Ground Water, 35(5), 905-911.

Stute, M., C. Sonntag, J. Deak, and P. Schlosser. 1992. Helium in deep circulating groundwater in the Great Hungarian Plain: Flow dynamics and crustal and mantle helium fluxes. Geochim. Cosmochim. Acta, 56, 2051-2067.

Suckow, A. 2014. The age of groundwater – Definitions, models and why we do not need this term. Appl. Geochem., 50, 222-230.

Therrien, R., R. G. McLaren, E. A. Sudicky, and S. M. Panday. 2010. Hydrogeosphere-a three-dimensional numerical model describing fully-intergrated subsurface and

surface flow and solute transport. University of Waterloo and Université Laval, Canada.

Thompson, G. M. and J. M. Hayes. 1979. Trichloromethane in groundwater: A possible tracer and indicator of groundwater age. Water Resour. Res., 15, 546-554.

Tilman, D., J. Fargione, B. Wolff, C. D'Antonio, A. Dobson, R. Howarth, D. Schindler, W. H. Schlesinger, D. Simberloff, and D. Swackhamer. 2001. Forecasting agriculturally driven global environmental change. Science, 292, 281–284.

Tolstikhin, I. N. and I. L. Kamensky. 1969. On the possibility of tritium-helium-3 dating of underground waters. (in Russian.) Geokhimiya, 8, 1027-1029.

Trudell, M. R., R.W. Gillham, and J. A. Cherry. 1986. An in-situ study of the occurrence and rate of denitrification in a shallow unconfi ned sand aquifer. J. Hydrol. 83, 251–268.

Turnadge, C. and B. D. Smerdon. 2014. A review of methods for modelling environmental tracers in groundwater: Advantages of tracer concentration simulation. J. Hydrol., 519, 3674-3689.

Tziritis, E. P. 2010. Assessment of NO_3^- contamination in a karstic aquifer, with the use of geochemical data and spatial analysis. Environ. Earth Sci., 60, 1381-1390.

United Nations Development Programme (UNDP) and Food and Agriculture Organization (FAO) The United Nations. 1972. Tube Well Irrigation Project, Republic of Korea: Groundwater Resources of Selected Area of Cheju Island and the Mainland, Volume I: Text, UNDP Technical Rep. DP/ROK/68/524. Republic Korea Gov.

Van Genuchten, M. Th. 1980. A closed-form equation for predicting the hydraulic conductivity of unsaturated soils. Soil Sci. Soc. Am. J., 44, 892–989.

Varni, M. and J.Carrera. 1998. Simulation of groundwater age distributions. Water

Resour. Res., 34, 3271-3281.

Vengosh, A., A. J. Spivack, Y. Artzi, and A. Ayalon. 1999. Geochemical and boron, strontium, and oxygen isotopic constraints on the origin of the salinity in groundwater from the Mediterranean coast of Israel. Water Resour. Res., 35(6), 1877-1894.

Visser, A., H. P. Broers, B. van der Grift, and M. F. P Bierkens. 2007. Demonstrating trend reversal of groundwater quality in relation to time of recharge determined by $^{3}H/^{3}He$. Envrion Pollut., 148, 797-807.

Visser, A., H. P. Broers, R. Purtschert, J. Sültenfuß, and M. Jonge. 2013. Groundwater age distributions at a public drinking water supply well field derived from multiple age tracers (85Kr, 3H/3He, and 39Ar). Water Resour. Res., 49(11), 7778-7796.

Warner, M. J. and R. F. Weiss. 1985. Solubilities of chlorofluorocarbons 11 and 12 in water and seawater. Deep-Sea Res., 32, 1485-1497.

Weiss, W., J. Bullacher, and W. Roether. 1979. Evidence of pulsed discharges of tritium from nuclear energy installations in central European precipitation. Behaviour of Tritium in the Environment, 17-30. IAEA, Vienna.

Weiss, M. and H. Gvirtzman. 2007. Estimating ground water recharge using flow models of perched karstic aquifers. Ground Water, 45, 761–773.

Weissmann, G. S., Y. Zhang, E. M. LaBolle, and G. E. Fogg. 2002. Dispersion of groundwater age in an alluvial aquifer system. Water Resour. Res., 38(10), 1198.

Widory, D., W. Kloppmann, L. Chery, J. Bonnin, H. Rochdi, and J.-L. Guinamant. 2004. Nitrate in groundwater: an isotopic multi-tracer approach. J. Contam. Hydrol., 72, 165–188.

Wolfe, A. H. and J. A. Patz. 2002. Reactive nitrogen and human health: acute and long-

term implications. Ambio., 31(2), 120-125.

Won, J. H., J. W. Kim, G. W. Koh, and J. Y. Lee. 2005. Evaluation of hydrogeological characteristics in Jeju Island, Korea. Geosci. J., 9(1), 33-46.

Won, J. H., J. Y. Lee, J. W. Kim, and G. W. Koh. 2006. Groundwater occurrence on Jeju Island, Korea. Hydrogeol. J., 14, 532-547.

Woo, N. C., H. D. Kim, K. S. Lee, W. B. Park, G. W. Koh, and Y. S. Moon. 2001. Interpretation of groundwater system and contamination by water-quality monitoring in the Daejung watershed, Jeju Island. (In Korean, with English abstract.) Econ. Environ. Geol., 34(5), 485-498.

World Health Organization (WHO). 2002. Chloride in drinking-water, background document for development WHO guidelines for drinking-water quality.

World Health Organization (WHO). 2011. Nitrate and nitrite in drinking-water: Background document for development of WHO Guidelines for Drinking-water Quality. WHO Press, Switzerland.

Xu, Y., L. A. Baker, and P. C. Johnson. 2007. Trends in ground water nitrate contamination in the Phoenix, Arizona, region. Ground Water Monit. R., 27(2), 49-56.

Yi, M. J., J. Y. Lee, J. G. Mok, I. W. Yeo, K. K. Lee, Y. C. Park, K. H. Ahn, and J. H. Won. 2007. Evaluation of groundwater contamination through abandoned wells by multiple tracer tests. (In Korean, with English abstract.) J. Geol. Soc. Korea, 43(2), 241–252.

Yoon, Y. Y., S. Y. Cho, C. K. Lee, and Y. Kim. 2007. Low level tritium analysis using liquid scintillation counter. Anal. Sci. Tech., 20, 419-423.

Youn, J. S., G. P. Kim, and C. Y. Jung. 2003. A hydrogeological study on high saline

groundwater of Handong-ri in the eastern part of Jeju Island, Korea. (In Korean, with English abstract.) J. Geol. Soc. Korea, 39(1), 115-131.

Zhang, H. and K. M. Hiscock. 2010. Modelling the impact of forest cover on groundwater resources: A case study of the Sherwood Sandstone aquifer in the East Midlands, UK. J. Hydrol., 392, 136–149.

Zuber, A., K. Różański, J. Kania, and R. Purtschert. 2011. On some methodological problems in the use of environmental tracers to estimate hydrogeologic parameters and to calibrate flow and transport models. Hydrol. J., 19, 53-69.

Zuber, A., S. Witczak, K. Różański, I. Śliwka, M. Opoka, P. Mochalski, T. Kuc, J. Karlikowska, J. Kania, M. Jackowicz-Korczyński, and M. Duliński. 2005. Groundwater dating with 3H and SF6 in relation to mixing patterns, transport modelling and hydrochemistry. Hydrol. Process., 19, 2247-2275.

Abstract in Korean

다양하게 발생하는 지하수 오염 중에서, 질산염에 의한 지하수 오염은 많은 나라에서 큰 문제점으로 대두되고 있다. 증가하는 인간 활동으로 인해서 질산염 오염에 대한 대수층의 취약성은 향후 높아질 가능성이 있다. 따라서, 지하의 대수층 시스템에서 질산염 오염 거동을 제어하는 요인을 고려한 적절한 오염 관리 방안을 세울 필요가 있다.

지하수가 유일한 수자원인 제주도 지역에서도 질산염에 의한 지하수 오염이 심각한 상황이다. 제주도는 복잡한 수리지질 시스템과 함께 다양한 인위적 활동이 나타나고 있어서, 지하수 오염 관리 대책을 마련하기에 앞서서 복합적인 질산염 거동 특성화를 위한 체계적 평가 연구가 우선적으로 필요하다. 따라서, 본 연구에서는 제주도 지역의 질산염 오염의 메커니즘을 파악하기 위해 다양한 연구 접근법을 통합하여 질산염 오염에 관여하는 요인들의 영향을 정량화하고자 하였다.

우선적으로, 제주도 지하수의 주요 오염 성분인 질산염과 염소 농도의 제주도 전역에 걸친 시·공간적인 분포 특성을 파악하였다. 두 수질 성분의 시간적 추세를 갖고 토지이용 변화와 지하수 관리 방안이 지하수 수질 오염에 주는 영향을 평가하였다. 연구 결과, 질산성질소의 증가 추세는 농경지

면적의 증가와 관계가 있는 반면에, 염소 이온의 추세는 해수 침투에 의한 고염분 지하수 발생을 억제하기 위해 수행된 지하수 사용량 관리에 의해 영향을 받는 것으로 판단되었다. 향후 제주도 지역에서는 질산염에 의한 지하수 오염이 지속적으로 발생할 것으로 예측되며, 특히 서부지역에 대한 질산염 오염을 관리할 필요가 있다.

추세분석 결과를 바탕으로 하여, 제주도 지하수 수질을 지속적으로 저하시킬 가능성이 높은 질산성질소 오염에 대한 핵심 연구를 제주도 서부의 고산 농경지를 대상으로 수행하였다. 이를 위해서, 수치해석 모델과 지하수 연령 산정 기법을 결합하는 연구 기법을 적용하였다. 고산 연구지역에서는 분리된 층상 대수층 시스템이 불량 시공된 관정에 의해 수리적 연결되는 현상이 관찰되었다. 따라서, 층상 대수층을 통한 질산염의 교차 오염 현상을 모의하기 위해서 누수 관정 모듈과 이중 도메인 결합 접근법을 활용하여 누수 관정에 의한 질산염 오염 영향을 정량화하였다. 수치 모델 결과, 심부 지하수 관정에서의 누수 현상은 천층의 고농도의 질산염을 포함하는 부유 지하수가 하부의 심부 대수층으로 직접적으로 이동하여 수질을 빠르게 저해하고 있음이 파악되었다. 심부 지하수 관정에서의 질산성질소 농도를 저감하는 예측 모델을 수행한 결과, 비료 사용량만을 줄이는 경우에는 현 비료 사용량의 45%~65%로 감소해야 하는 반면에, 누수 현상이 발생하는 심부 지하

수 관정을 재시공할 경우에는 비료 사용량을 줄이지 않고도 질산성 질소 오염이 즉각적으로 저감됨이 나타났다.

고산 지역의 복잡한 수리지질구조에 의해서 여러 경로를 갖는 물의 유동으로 인한 지하수 연령이 혼합현상이 예상된다. 따라서, 본 연구에서는 세 가지의 지하수 연령 기법 (환경추적자, lumped parameter 모델과 수치 모델)을 적용하여서 지하수 연령을 추정하였고, 또한 질산염 오염 이력을 구축하고 지하수 수질에 영향을 주는 주요 오염 경로를 결정하고자 하였다. 또한, 세 가지의 연령 산정 기법으로 예측된 지하수 연령을 바탕으로 하여 각기 다른 지하수 관리 방안을 제한하고자 하였다. 그 결과, 다른 연령 산정 기법들은 각기 다른 오염 부하 이력을 도출하였고, 이로 인해 오염 관리 방안이 다르게 나타났다. 이러한 지하수 연령 산정 결과의 차이는 지하수 혼합현상이 지배적인 복잡한 수리지질 구조에서 우세하게 예측되었다. 따라서, 다양한 대수층 구조에 맞는 효과적인 지하수 오염 관리 방안을 마련하기 위해서는, 복합 연령 산정 기법 도입과 완전한 연령 분포 해석 결과 비교를 통해 주요 오염 경로를 파악하는 연구가 우선적으로 수행되어야 할 것이다.

주요어: 지하수, 지하수 오염, 질산염 오염, 제주도, 농업 활동, 추세 분석, 수치 모델, 지하수 연령

학번: 2011-30113